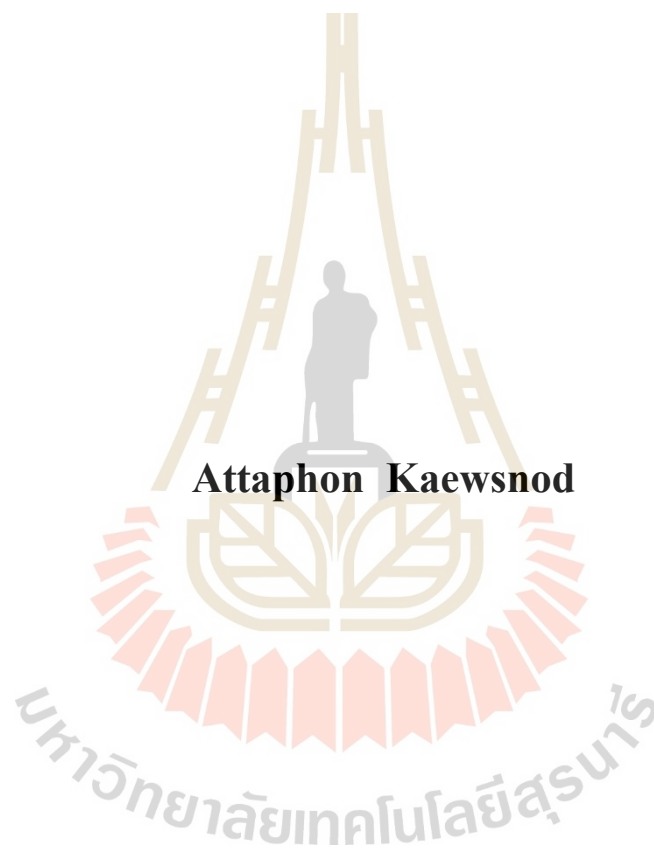


**INVESTIGATION OF INTERNAL STRUCTURE OF
LOW-LYING BARYONS VIA HELICITY AMPLITUDES**



Attaphon Kaewsnod

**A Thesis Submitted in Partial Fulfillment of the Requirements for the
Degree of Doctor of Philosophy in Physics**

Suranaree University of Technology

Academic Year 2020

การสืบเสาะโครงสร้างภายในของแบรียออนพลังงานต่ำผ่านแอมพลิจูดเฮลิซิติ



วิทยานิพนธ์นี้เป็นส่วนหนึ่งของการศึกษาตามหลักสูตรปริญญาวิทยาศาสตรดุษฎีบัณฑิต
สาขาวิชาฟิสิกส์
มหาวิทยาลัยเทคโนโลยีสุรนารี
ปีการศึกษา 2563

**INVESTIGATION OF INTERNAL STRUCTURE
OF LOW-LYING BARYONS VIA HELICITY AMPLITUDES**

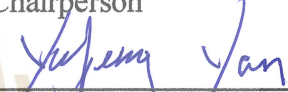
Suranaree University of Technology has approved this thesis submitted in partial fulfillment of the requirements for the Degree of Doctor of Philosophy.

Thesis Examining Committee



(Assoc. Prof. Dr. Panomsak Meemon)

Chairperson



(Prof. Dr. Yupeng Yan)

Member (Thesis Advisor)



(Assoc. Prof. Dr. Sorakrai Srisuphaphon)

Member



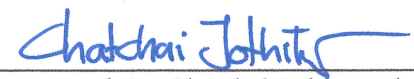
(Asst. Prof. Dr. Ayut Limphirat)

Member



(Asst. Prof. Dr. Khanchai Khosonthongkee)

Member



(Assoc. Prof. Dr. Chatchai Jothityangkoon)

Vice Rector for Academic Affairs
and Quality Assurance



(Prof. Dr. Santi Maensiri)

Dean of Institute of Science

อรรถพล แก้วโสนด : การสืบเสาะโครงสร้างภายในของแบรีออนพลังงานต่ำผ่านแอมพลิจูดเฮลิซิตี (INVESTIGATION OF INTERNAL STRUCTURE OF LOW-LYING BARYONS VIA HELICITY AMPLITUDES) อาจารย์ที่ปรึกษา : ศาสตราจารย์ ดร.ยูเป็ง แยน, 89 หน้า

งานวิจัยนี้ศึกษากระบวนการผลิตอนุภาคด้วยแสงของอนุภาคเรโซแนนซ์ $N(1440)$ $N(1520)$ และ $N(1535)$ จากกระบวนการ $py^* \rightarrow N^*$ ในแบบจำลองควาร์ก โดยสมมติให้ $N(1440)$ มีสถานะกระตุ้นเชิงรัศมีที่หนึ่งของนิวคลีออนโดยมีสถานะแบริตีเป็นค่าบวก ขณะที่ $N(1520)$ และ $N(1535)$ มีสถานะแบริตีเป็นค่าลบและมีพลังงานต่ำที่สุดภายใต้ระบบควาร์กสามตัว นอกจากนี้ยังได้นำผลการคำนวณทางทฤษฎีมาเปรียบเทียบกับข้อมูลจากการทดลองของแอมพลิจูดเฮลิซิตีตามขวางและตามยาว อีกทั้งยังวิเคราะห์ฟังก์ชันคลื่นของอนุภาคเรโซแนนซ์ $N(1440)$ $N(1520)$ และ $N(1535)$ ซึ่งพบว่าอนุภาคเรโซแนนซ์ $N(1440)$ มีองค์ประกอบหลักคือสถานะควาร์กสามตัวที่อยู่ในสถานะกระตุ้นเชิงรัศมีที่หนึ่ง อีกทั้งยังมีองค์ประกอบอื่นปนอยู่เล็กน้อย ขณะที่อนุภาคเรโซแนนซ์ $N(1520)$ และ $N(1535)$ อาจมีองค์ประกอบของเพนตะควาร์กปะปนอยู่

มหาวิทยาลัยเทคโนโลยีสุรนารี

สาขาวิชาฟิสิกส์
ปีการศึกษา 2563

ลายมือชื่อนักศึกษา Attaphon Kaensrod
ลายมือชื่ออาจารย์ที่ปรึกษา Yupung Yan
ลายมือชื่ออาจารย์ที่ปรึกษารวม Sornkrin S.

ATTAPHON KAEWSNOD : INVESTIGATION OF INTERNAL
STRUCTURE OF LOW-LYING BARYONS VIA HELICITY
AMPLITUDES. THESIS ADVISOR : PROF. YUPENG YAN, Ph.D.
89 PP.

GROUP THEORY/CONSTITUENT QUARK MODEL/HELICITY
AMPLITUDE/FORM FACTOR

We study the photoproduction of $N(1440)$, $N(1520)$, and $N(1535)$ resonances in $\gamma^*p \rightarrow N^*$ processes in quark models, assuming that the $N(1440)$ is the first radial excitation of the nucleon with a positive parity while the $N(1520)$ and $N(1535)$ are the lowest negative parity q^3 states. The comparison between the theoretical results and experimental data on the helicity amplitudes $A_{1/2}$ and $S_{1/2}$ and the analysis of the spatial wave function of the $N(1440)$, $N(1520)$ and $N(1535)$ resonances reveal that the $N(1440)$ resonance is mainly the q^3 first radial excitation but may have a small component of others while the $N(1520)$ and $N(1535)$ resonances may have a considerable pentaquark component or others.

School of Physics

Academic Year 2020

Student's Signature Attaphon Kaewsnod

Advisor's Signature Yupeng Yan

Co-Advisor's Signature Sorakorn S.

ACKNOWLEDGEMENTS

Foremost, I would like to express my deep and sincere gratitude to my thesis advisor Prof. Dr. Yupeng Yan and co-advisor Assoc. Prof. Dr. Sorakrai Srisuphaphon for the continuous support of my Ph.D. study and research, for their patience, motivation, enthusiasm, and immense knowledge. Their guidance helped me in all the time of research and writing of this thesis. I could not have imagined having a better advisor and mentor for my Ph.D. study.

Besides my advisor, I would like to thank the rest of my thesis committee: Assoc. Prof. Dr. Panomsak Meemon, Asst. Prof. Dr. Ayut Limphirat, and Asst. Prof. Dr. Khanchai Khosonthongkee, for their encouragement, insightful comments.

I thank my teachers and my friends in the Nuclear and Particle Physics group, especially: Dr. Kai Xu, Mr. Thanat Sangkhakrit, and Mr. Zheng Zhao, for the sleepless nights we were working together before deadlines, and for all the fun we have had in the daily life of the Ph.D. student.

I would like to thank for the support of the Thailand Science Research and Innovation (TSRI) for their support through the Royal Golden Jubilee Ph.D. (RGJ-PHD) Program (Grant No. PHD/0242/2558) and Suranaree University of Technology under SUT-OROG scholarship (contract no. 46/2558).

Last but not least, I would like to thank my parents and my family for their love, understanding, encouragement and supporting me spiritually throughout my life. My most heartfelt thanks.

Attaphon Kaewsnod

CONTENTS

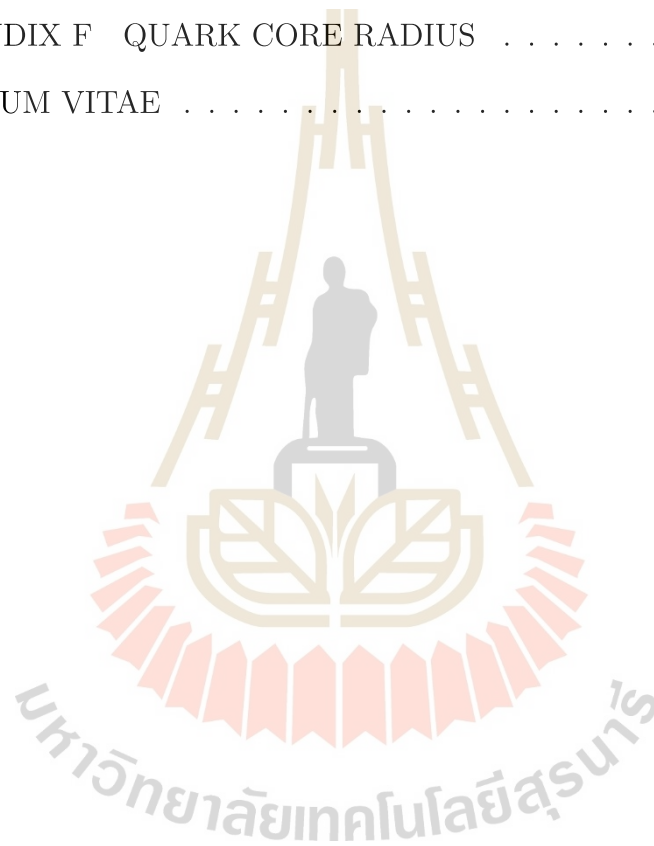
	Page
ABSTRACT IN THAI	I
ABSTRACT IN ENGLISH	II
ACKNOWLEDGEMENTS	III
CONTENTS	IV
LIST OF TABLES	VII
LIST OF FIGURES	IX
CHAPTER	
I INTRODUCTION	1
II WAVE FUNCTIONS FOR MULTI QUARK SYSTEM	5
2.1 q^3 octet baryon states	5
2.2 $q^4\bar{q}$ pentaquark states	6
2.3 Spatial wave functions	7
III ELECTRIC FORM FACTOR	11
3.1 Nucleon electric form factor	11
3.2 Proton electric form factor in non-relativistic approximation	13
3.3 Proton electric form factor from the fitting of low-lying baryon mass spectra	14
3.4 Extraction of proton from the proton electric form factor	16
IV HELICITY AMPLITUDES	18
4.1 Transverse and longitudinal helicity amplitudes	18
4.2 Helicity amplitudes of $N(1440)$	21

CONTENTS (Continued)

	Page
4.2.1 Helicity amplitudes of $N(1440)$ in non-relativistic approximation	21
4.2.2 Helicity amplitudes of $N(1440)$ with the wave function from mass spectrum fitting	23
4.2.3 Extraction of quark distribution of $N(1440)$	24
4.3 Helicity amplitudes of $N(1520)$ and $N(1535)$	28
4.3.1 Helicity amplitudes of $N(1520)$ and $N(1535)$ in non-relativistic approximation	28
4.3.2 Helicity amplitudes of $N(1520)$ and $N(1535)$ with the wave function from the mass spectra fitting	30
4.3.3 Extraction of quark distribution of $N(1520)$ and $N(1535)$	32
V DISCUSSIONS AND CONCLUSIONS	34
5.1 Helicity amplitudes with pentaquark wave function	35
5.1.1 Transverse and longitudinal helicity amplitudes for pentaquark	35
5.2 future work	38
REFERENCES	39
APPENDICES	
APPENDIX A q^3 AND $q^4\bar{q}$ FULL WAVE FUNCTION IN SU(3) FLAVOR SYMMETRY	49
A.1 q^3 full wave function	49
A.2 $q^2\bar{Q}$ full wave function	51
A.3 $q^4\bar{q}$ full wave function	52
APPENDIX B SPATIAL WAVE FUNCTION	55

CONTENTS (Continued)

	Page
APPENDIX C PENTAQUARK WAVE FUNCTION	83
APPENDIX D Coefficient $C_{[X]_x[Y]_y}^{[Z]_z}$	84
APPENDIX E SPIN WAVE FUNCTION OF PENTAQUARK	86
APPENDIX F QUARK CORE RADIUS	88
CURRICULUM VITAE	89



LIST OF TABLES

Table		Page
2.1	J^P pentaquark states corresponding to the q^4q configurations . . .	7
B.1	Normalized 3-quark spatial wave functions $L = 2$ $2N - 2$ 2, 56 multiplet	55
B.1	(Continued) Normalized 3-quark spatial wave functions $L = 2$ $2N$ 2 2.	56
B.2	Normalized 3-quark spatial wave functions for $L=0$ $2N - 0$ 0 70 multiplet	56
B.3	Normalized 3-quark spatial wave functions for $L = 1$ $2N + 1$ 1 1 70 multiplet	58
B.3	(Continued) Normalized 3-quark spatial wave functions for $L = 1$ $2N + 1$ 1 1 70 multiplet.	59
B.3	(Continued) Normalized 3-quark spatial wave functions for $L = 1$ $2N + 1$ 1 1 70 multiplet.	60
B.4	Normalized 3-quark spatial wave functions $L = 2$ $2N - 2$ 2, 56 multiplet	60
B.5	Normalized 3-quark spatial wave functions for $L = 2$ $2N - 2$ 2 70 multiplet	62
B.6	Normalized 3-quark spatial wave functions for $L = 1$ $2N - 1$ 1 20 multiplet	64
B.7	Normalized pentaquark (q^4 symmetry) spatial wave functions quan- tum number: $2N - 0$ 0	66

LIST OF TABLE (Continued)

Table		Page
B.8	Normalized pentaquark (q^4 symmetry) spatial wave functions quantum number: $2N + 1 \ 1 \ 0$	77
B.9	Normalized pentaquark (q^4 symmetry) spatial wave functions quantum number: $2N \ 1 \ 0$	80
D.1	The $C_{[31]_i[211]_j}^{[1111]}$ coefficients	84
D.2	The $C_{[4][31]_j}^{[31]_k}$ coefficients	84
D.3	The $C_{[31]_i[22]_j}^{[31]_k}$ coefficients	84
D.4	The $C_{[31]_i[31]_j}^{[31]_k}$ coefficients	85
D.5	The $C_{[22]_i[31]_j}^{[31]_k}$ coefficients	85
D.6	The $C_{[31]_i[4]}^{[31]_k}$ coefficients	85

LIST OF FIGURES

Figure		Page
3.1	Diagram of $N\gamma^* \rightarrow N^*$ in three-quark picture	12
3.2	Proton electric form factor	15
3.3	Proton spatial wave function	17
4.1	Diagram of $N\gamma^* \rightarrow N^*$ in three-quark picture	19
4.2	The transverse helicity amplitude of $N(1440)$	25
4.3	The longitudinal helicity amplitude of $N(1440)$	26
4.4	The spatial wave functions of $N(1440)$	28
4.5	The transverse helicity amplitude of $N(1520)$	30
4.6	The transverse helicity amplitude of $N(1535)$	31
5.1	Diagram of $N\gamma^* \rightarrow N^*$ in pentaquark picture	35
F.1	Quark core radius	88

CHAPTER I

INTRODUCTION

In recent years, the experiments on electro- and photoproduction of many particles have accumulated a large amount of data of the helicity amplitudes over the virtuality four-momentum transfer Q^2 of the exchanged photon (Zyla et al., 2020; Aznauryan et al., 2009; Mokeev et al., 2012; Mokeev et al., 2016). The most accurate and complete experimental data has been obtained for the three lowest nucleon excited states, which have been measured in a range of Q^2 up to 8 GeV^2 for $N(1535)$ and up to 4.5 GeV^2 for the Roper resonance and $N(1520)$ (see reviews (Tiator et al., 2011; Tiator et al., 2009)).

Plenty of theoretical models analyze of the transverse transition amplitudes $A_{1/2}$ and $A_{3/2}$, and longitudinal transition amplitudes $S_{1/2}$ over Q^2 varied in a large range, reveal the properties and structures of many nucleon resonance states (Aznauryan, 2007; Aznauryan et al., 2008; Capstick et al., 2007; Ramalho and Tsushima, 2010; Golli et al., 2009; Burkert and Roberts, 2019; Li and Riska, 2006; Obukhovskiy et al., 2011; Cano and Gonzalez, 1998; Segovia, 2016; Štajner et al., 2017). However, as the lowest radial excited state of the proton, the Roper resonance's electro- and photoproduction data still can not be well described by the conventional quark models (Aznauryan, 2007; Aznauryan et al., 2008; Capstick et al., 2007; Ramalho and Tsushima, 2010; Golli et al., 2009). And the mass ordering problem of the Roper resonance with the lowest negative-parity baryon resonance states $N(1520)$ and $N(1535)$ (Capstick and Roberts, 2000) and the large decay width (Sarantsev et al., 2008) are quite unclear as well. A good discussion

about the Roper resonance can be found in a good review paper (Burkert and Roberts, 2019).

Among many of the theoretical approaches, the light-front three-quark model as one of the most successful ones can give a good description of experimental data of $N(1440)$ helicity amplitudes in the hard region which is $1.5 \leq Q^2 \leq 4.5$ GeV^2 (Aznauryan, 2007; Aznauryan et al., 2008; Capstick et al., 2007). So do for the covariant spectator quark model (Ramalho and Tsushima, 2010) and chiral quark models (Golli et al., 2009), but the theoretical results are not compatible with the helicity amplitude data of $N(1440)$ in the low Q^2 values. Pentaquark component is included in both the proton and excited nucleon states to reproduce the helicity amplitudes in the soft region $0 \leq Q^2 \leq 1.5$ GeV^2 (Li and Riska, 2006). And the hadron molecule component has been discussed for describing the whole helicity amplitudes data in Ref. (Obukhovskiy et al., 2011). The meson-baryon dressing or meson cloud obscures the three-quark core in the $N(1440)$ resonance have been discussed in Refs. (Cano and Gonzalez, 1998; Segovia et al., 2015; Štajner et al., 2017). In this model the core mass is reduced by the meson cloud contribution and the photoproduction helicity amplitudes for a large region including the photon point were reproduced.

The $\gamma^*N \rightarrow N(1520)$ reaction is therefore characterized by three independent helicity amplitudes: the two transverse amplitudes $A_{1/2}$, $A_{3/2}$, and the longitudinal amplitude $S_{1/2}$. Only recently was the longitudinal amplitude measured for the first time (Aznauryan et al., 2009; Moiseev et al., 2012). The $\gamma^*N \rightarrow N(1520)$ was previously studied by various frameworks and models. The framework of non-relativistic and relativistic quark models (Close and Gilman, 1972; Koniuk and Isgur, 1980; Warns et al., 1990; Aiello et al., 1998; Merten et al., 2002; Santopinto and Giannini, 2012; Capstick and Keister, 1995; Aznauryan and Burk-

ert, 2012; Ronniger and Metsch, 2013; Golli and Širca, 2013), the single quark transition model (SQTM) (Close, 1979; Burkert et al., 2003; Burkert and Lee, 2004) and a collective for baryons (Bijker et al., 1996). The EBAC (Jlab) analysis estimated the electromagnetic structure of $N(1520)$ within a coupled-channel dynamical model for the meson-baryon systems (Julia-Diaz et al., 2008). The study of the empirical charge density distribution of the $N(1520)$ can be found in Refs. (Tiator et al., 2011; Tiator et al., 2009). For the experimental side, there are the MAID (Mainz) analysis (Tiator et al., 2011; Tiator et al., 2009; Drechsel et al., 2007), the old data from DESY, and the recent data from CLAS (at Jlab) (Aznauryan et al., 2009; Mokeev et al., 2012).

The available data for the $\gamma^*N \rightarrow N(1535)$ transition for the amplitudes $A_{1/2}$ and $S_{1/2}$ are mainly from CLAS at Jlab (Aznauryan et al., 2009). Some estimates of helicity amplitudes from MAID (Drechsel et al., 2007; Tiator et al., 2009) base on data from different experiments (including CLAS). Quark model give a partial explanation by suggesting that it is dominated by valence quark degrees of freedom (Juliá-Díaz et al., 2009; Ramalho and Peña, 2011; Ramalho and Tsushima, 2011; Ramalho et al., 2012). The calculations of the baryon states generated by baryon-meson resonances based on chiral quark models suggest that the Pauli form factor at low Q^2 is dominated by meson cloud effects (Ramalho and Tsushima, 2011; Ramalho et al., 2012; Jido et al., 2008). The results of light-front relativistic quark model indicate the meson cloud contribution to the $\gamma^*N \rightarrow N(1535)$ transition form factors have an iso-vector character (Aznauryan and Burkert, 2017).

Based on the previous works (Xu et al., 2019; Xu et al., 2020), where the mass ordering of $N(1440)$, $N(1520)$, and $N(1535)$ is described by including ground state light pentaquark components, we study the photoproduction transi-

tions $\gamma^*p \rightarrow N^*$ where N^* are in both three-quark and $q^4\bar{q}$ pentaquark pictures. However, the $N(1440)$, $N(1520)$, and $N(1535)$ resonances are studied mainly as the three-quark nucleon states in this thesis. The $N(1440)$ is assumed to be the first radial excited state of the proton, and $N(1520)$ and $N(1535)$ are the lowest negative parity state corresponding to the lowest three-quark $L = 1$ states with mixed symmetry.

The thesis is organized as follows. In Chapter II, we briefly present the construction of wave functions for multi-quark system including higher order spatial wave functions in the harmonic oscillator model, and the details are shown in Appendix B. The electric form factor of proton is calculated in Chapter III and the proton spatial wave function in the three-quark picture is extracted by comparing the theoretical results with experimental data. The formalism of the helicity transition amplitudes for the photoproduction of the nucleon resonance, the comparison of the theoretical results with experimental data, as well as the analysis of the spatial wave function of the resonances $N(1440)$, $N(1520)$, and $N(1535)$ are given in Chapter IV. Chapter V is devoted to discussion, conclusions, and outlook for future works.

CHAPTER II

WAVE FUNCTIONS FOR MULTI QUARK SYSTEM

2.1 q^3 octet baryon states

The baryon wave functions of proton, $N(1440)$, $N(1520)$, and $N(1535)$ are constructed in the harmonic oscillator model. The total wave functions, consisting of the spatial, spin, flavor, and color degrees of freedom, are constructed systematically in the form of a Yamanouchi basis,

$$\begin{aligned}\Psi_{L=0}^{(q^3)} &= \frac{1}{\sqrt{2}} \psi_{[3]}^O (\psi_{[21]_\lambda}^F \psi_{[21]_\lambda}^S + \psi_{[21]_\rho}^F \psi_{[21]_\rho}^S) \psi_{[111]}^C, \\ \Psi_{L=1}^{(q^3)} &= \frac{1}{2} [\psi_{[21]_\lambda}^O (\psi_{[21]_\rho}^F \psi_{[21]_\rho}^S - \psi_{[21]_\lambda}^F \psi_{[21]_\lambda}^S) \\ &\quad + \psi_{[21]_\rho}^O (\psi_{[21]_\lambda}^F \psi_{[21]_\lambda}^S + \psi_{[21]_\rho}^F \psi_{[21]_\rho}^S)] \psi_{[111]}^C.\end{aligned}\quad (2.1)$$

With $i = \lambda, \rho$ types, the flavor ($\psi_{[21]_i}^F$) and spin ($\psi_{[21]_i}^S$) wave functions are

$$\begin{aligned}\psi_{[21]_\lambda}^F &= \frac{1}{\sqrt{6}} (2ud - duu - udu), & \psi_{[21]_\rho}^F &= \frac{1}{\sqrt{2}} (udu - duu), \\ \psi_{[21]_\lambda}^S &= \frac{1}{\sqrt{6}} (2 \uparrow\uparrow\downarrow - \downarrow\uparrow\uparrow - \uparrow\downarrow\uparrow), & \psi_{[21]_\rho}^S &= \frac{1}{\sqrt{2}} (\uparrow\downarrow\uparrow - \downarrow\uparrow\uparrow).\end{aligned}\quad (2.2)$$

The total color wave function is

$$\psi_{[111]}^C = \frac{1}{\sqrt{6}} [(RG - GR)B + (GB - BG)R + (BR - RB)G]. \quad (2.3)$$

The details of spatial wave function are in the Section 2.3.

2.2 $q^4\bar{q}$ pentaquark states

The algebraic structure of pentaquark states consists of the spin-flavor and color algebras $SU_{SF}(6) \otimes SU_C(3)$ with $SU_{SF}(6) = SU_S(2) \otimes SU_F(3)$. The construction of the pentaquark wave function follows the rules that a $q^4\bar{q}$ state must be a color singlet and antisymmetric under any permutation between identical quarks. The permutation symmetry of the q^4 configurations of pentaquark states is characterized by S_4 Young tabloids [4], [31], [22], and [1111]. Here we will analyze the symmetry of the pentaquark state in the language of a permutation group.

The pentaquark color singlet is represented by $[222]_C$ but the color part of the \bar{q} in the pentaquark is represented by $[11]_C$, and thus the color part of the q^4 is represented by $[211]_C$. The total wave function of the q^4 must be antisymmetric but the q^4 color part is $[211]_C$ leads to that the spatial-spin-flavor part which is in the conjugated representation of the q^4 [211] configuration as $[31]_{OSF}$.

In general, one may combine different freedoms to form total states of various symmetries. Consider a system with the degrees of freedom M and N described respectively by the wave functions ψ^M and ψ^N , then the total wave function may be constructed by the linear combination of the products ψ^M and ψ^N ,

$$\psi_{[Z]_z}^{MN} = \sum_{x,y=\{S,A,\rho,\lambda,\eta\}} C_{[X]_x[Y]_y}^{[Z]_z} \psi_{[X]_x}^M \psi_{[Y]_y}^N, \quad (2.4)$$

where $[X]$, $[Y]$, and $[Z]$ are irreducible representations, and x , y , and z are permutation symmetries. In the above equation, x, y are summed over S (fully symmetric), A (fully antisymmetric), λ (λ -type), ρ (ρ -type), and η (η -type). $C_{[X]_x[Y]_y}^{[Z]_z}$ are the coefficients determined by permutation operators of S_4 permutation group. The coefficients $C_{[X]_x[Y]_y}^{[Z]_z}$ are shown in Tables D.1-D.6.

Table 2.1 J^P pentaquark states corresponding to the q^4q configurations, where the color part of the q^4 is $[211]_C$ and the spatial part of the q^4 is fully symmetric $[4]_O$.

J^P	$q^4\bar{q}$ configurations
$\frac{1}{2}^-$	$[31]_{FS}[4]_F[31]_S, [31]_{FS}[31]_F[31]_S, [31]_{FS}[31]_F[22]_S, [31]_{FS}[22]_F[31]_S$
$\frac{3}{2}^-$	$[31]_{FS}[4]_F[31]_S, [31]_{FS}[31]_F[4]_S, [31]_{FS}[31]_F[31]_S, [31]_{FS}[22]_F[31]_S$

The total wave function of the q^4 configurations is written in the general form as,

$$\Psi^{q^4}_{\text{total}} = \sum_{i,j,w,x,y,z=\{S,A,\rho,\lambda,\eta\}} C_{[31]_i[211]_j}^{[1111]} C_{[W]_w[X]_x}^{[31]_i} C_{[Y]_y[Z]_z}^{[X]_x} \psi_{[211]_j}^C \psi_{[W]_w}^O \psi_{[Y]_y}^S \psi_{[Z]_z}^F. \quad (2.5)$$

The explicit form of spin ($\psi_{[Y]_y}^S$) and flavor ($\psi_{[Z]_z}^F$) wave functions can be derived by the projection operator in the framework of Yamanochi basis (Yan and Srisuphaphon, 2012). The explicit forms of spin and flavor wave functions are listed in Appendix E. The J^P pentaquark states, corresponding to the q^4q configurations, are shown in Table 2.1 where the color part of the q^4 is $[211]_C$, and the spatial part of the q^4 is fully symmetric $[4]_O$.

2.3 Spatial wave functions

The spatial wave functions of three quarks in Eq. (2.1) and pentaquark in Eq. (2.5) are represented in the harmonic oscillator bases of three-quark and pentaquark systems. The bases of the three-quark and pentaquark harmonic oscillator, are the solutions of Schrödinger equations for the Hamiltonian in the following form, (the two coefficients C in Eq. (2.6) are just coupling constants.)

$$H^{q^3} = \frac{p_\lambda^2}{2m} + \frac{p_\rho^2}{2m} + \frac{1}{2}C(\lambda^2 + \rho^2),$$

$$H^{q^4\bar{q}} = \frac{p_\lambda^2}{2m} + \frac{p_\rho^2}{2m} + \frac{p_\eta^2}{2m} + \frac{p_\xi^2}{2m} + \frac{1}{2}C (\lambda^2 + \rho^2 + \eta^2 + \xi^2), \quad (2.6)$$

with the relative Jacobi coordinates,

$$\begin{aligned} \boldsymbol{\rho} &= \frac{1}{\sqrt{2}}(\mathbf{r}_1 - \mathbf{r}_2), \\ \boldsymbol{\lambda} &= \frac{1}{\sqrt{6}}(\mathbf{r}_1 + \mathbf{r}_2 - 2\mathbf{r}_3), \\ \boldsymbol{\eta} &= \frac{1}{\sqrt{12}}(\mathbf{r}_1 + \mathbf{r}_2 + \mathbf{r}_3 - 3\mathbf{r}_4), \\ \boldsymbol{\xi} &= \frac{1}{\sqrt{20}}(\mathbf{r}_1 + \mathbf{r}_2 + \mathbf{r}_3 + \mathbf{r}_4 - 4\mathbf{r}_5), \\ \mathbf{R}^{q^3} &= \frac{1}{\sqrt{3}}(\mathbf{r}_1 + \mathbf{r}_2 + \mathbf{r}_3), \\ \mathbf{R}^{q^4\bar{q}} &= \frac{1}{\sqrt{5}}(\mathbf{r}_1 + \mathbf{r}_2 + \mathbf{r}_3 + \mathbf{r}_4 + \mathbf{r}_5). \end{aligned} \quad (2.7)$$

The spatial wave functions, being the eigenfunctions of the Hamiltonian, take the general form,

$$\begin{aligned} \Psi_{NLM}^O &= \sum_{n_\lambda, n_\rho, l_\lambda, l_\rho} A(n_\lambda, n_\rho, l_\lambda, l_\rho) \\ &\quad \times \psi_{n_\lambda l_\lambda m_\lambda}(\boldsymbol{\lambda}) \psi_{n_\rho l_\rho m_\rho}(\boldsymbol{\rho}) \\ &\quad \times C(l_\lambda, m_\lambda; l_\rho, m_\rho; l_{\lambda\rho}, m_{\lambda\rho}) \end{aligned} \quad (2.8)$$

with

$$N = 2(n_\lambda + n_\rho) + l_\lambda + l_\rho,$$

$$\psi_{nlm}(\mathbf{r}) = \left[\frac{2\alpha^3 n!}{(\frac{1}{2} + n + l)!} \right]^{\frac{1}{2}} (\alpha r)^l e^{-\frac{1}{2}\alpha^2 r^2} L_n^{l+\frac{1}{2}}(\alpha^2 r^2) Y_{lm}(\hat{\mathbf{r}}),$$

$$\langle \Psi_{NLM}^O | \Psi_{N'L'M'}^O \rangle = \delta_{NN'} \delta_{LL'} \delta_{MM'},$$

$$\langle \psi_{nlm} | \psi_{n'l'm'} \rangle = \delta_{nn'} \delta_{ll'} \delta_{mm'}, \quad (2.9)$$

for q^3 system where A is constants obtained by analyzing the symmetry in permutation group, C here is the Clebsch-Gordan (CG) coefficients, and $Y_{lm}(\hat{\mathbf{r}})$ is the spherical harmonic. $L_n^{l+\frac{1}{2}}$ is the associated Laguerre polynomial which takes the form

$$L_n^{l+\frac{1}{2}}(r^2) = \sum_{k=0}^n \frac{(-1)^k}{k!} \frac{(n+l+1/2)!}{(n-k)!(k+l+1/2)!} r^{2k}. \quad (2.10)$$

And

$$\begin{aligned} \Psi_{NLM}^O = & \sum_{n_\lambda, n_\rho, n_\eta, n_\xi, l_\lambda, l_\rho, l_\eta, l_\xi} A(n_\lambda, n_\rho, n_\eta, n_\xi, l_\lambda, l_\rho, l_\eta, l_\xi) \\ & \times \psi_{n_\lambda l_\lambda m_\lambda}(\boldsymbol{\lambda}) \psi_{n_\rho l_\rho m_\rho}(\boldsymbol{\rho}) \psi_{n_\eta l_\eta m_\eta}(\boldsymbol{\eta}) \psi_{n_\xi l_\xi m_\xi}(\boldsymbol{\xi}) \\ & \times C(l_\lambda, m_\lambda; l_\rho, m_\rho; l_{\lambda\rho}, m_{\lambda\rho}) \\ & \times C(l_{\lambda\rho}, m_{\lambda\rho}; l_\eta, m_\eta, l_{\lambda\rho\eta}, m_{\lambda\rho\eta}) \\ & \times C(l_{\lambda\rho\eta}, m_{\lambda\rho\eta}; l_\xi, m_\xi, LM), \end{aligned} \quad (2.11)$$

with

$$N = 2(n_\lambda + n_\rho + n_\eta + n_\xi) + l_\lambda + l_\rho + l_\eta + l_\xi, \quad (2.12)$$

for $q^4\bar{q}$ system. The bases of spatial wave function with the corresponding irreducible representation and permutation symmetry are shown in Appendix B

In the calculation, the wave functions are transformed to be the momentum space from the position space for convenience. The wave functions in the position space are transformed to in the momentum space by following relation:

$$\Psi_{NLM}^O(\{\mathbf{r}\}) = (-i)^N \Psi_{NLM}^O(\{\mathbf{p}\}). \quad (2.13)$$

The spatial wave function of the three-quark state (Eq. (2.1)) and the pentaquark state (Eq. (2.5)) are represented in the harmonic oscillator basis of a three-quark system (Eq. (2.8)) and a five-quark system (Eq. (2.11)) in the following form:

$$\psi_{[X]}^O = \sum_{N,L,M} A_{NLM}^{[X]} \Psi_{NLM}^O, \quad (2.14)$$

where $A_{NLM}^{[X]}$ is the general normalization factor,

$$\sum_{N,L,M} |A_{NLM}^{[X]}|^2 = 1. \quad (2.15)$$

The spatial wave function of the Roper resonance $N(1440)$ is constructed as the first radial excited state of proton. This lowest positive parity state corresponds to the $L = 0$ state with symmetric type, so $N(1440)$ wave function takes the form of linear combination of $L = 0$ states:

$$\psi_{[3]}^O = \sum_{N=0,2,4,\dots} A_{N00}^{[3]} \Psi_{N00}^O. \quad (2.16)$$

The $N(1520)$ and $N(1535)$ resonances are in the lowest negative parity state corresponding to the $L = 1$ state for a three-quark system and $L = 0$ ground state for pentaquark system. The $N(1520)$ and $N(1535)$ wave functions of three-quark system take the form as

$$\psi_{[21]iM}^O = \sum_{N=1,3,5,\dots} A_{N1M}^{[21]i} \Psi_{N1M}^O, \quad (2.17)$$

where i represents λ and ρ type, and $M = -1, 0, 1$. And the spatial wave function for the pentaquark state is

$$\psi_{[4]}^O = \sum_{N=0,2,4,\dots} A_{N00}^{[4]} \Psi_{N00}^O. \quad (2.18)$$

CHAPTER III

ELECTRIC FORM FACTOR

3.1 Nucleon electric form factor

In this chapter, we study the electromagnetic transition of the process $N\gamma^* \rightarrow N$ within a constituent quark model. We derive the proton electric form factor (G_E) in both non-relativistic and relativistic calculations. The corresponding diagram is displayed in Figure 3.1. In this case, we assume that the nucleon and resonance states are composed of three quarks. By studying this proton electric form factor, we hope that the relevant information regarding its internal structure will be extracted, especially its wave function. The proton electric form factor which is the time component of the electromagnetic current is derived in the Breit frame (also known as infinite-momentum frame or brick-wall frame). In the Breit frame, the momenta of the initial- and final-state nucleon and photon are defined as,

$$P_i = (E_N, 0, 0, -|\mathbf{k}/2|), \quad P_f = (E_N, 0, 0, |\mathbf{k}/2|), \quad k = (0, 0, 0, |\mathbf{k}|), \quad (3.1)$$

where P_i is the four-momentum of the initial-state nucleon, while P_f and k are those for the final-state nucleon and photon, respectively. The nucleon energy is denoted by E_N whereas the magnitude of the three-momentum of the photon is defined by $|\mathbf{k}|$. Therefore, the square of the four-momentum transfer is expressed by $Q^2 = -k^2 = |\mathbf{k}|^2$. In this case, the Breit frame is defined as the frame where $\mathbf{P}_i + \mathbf{P}_f = 0$. Hence, the photon energy $\omega = 0$ and $|\mathbf{k}|/Q = 1$.

The electric form factor can be expressed by the transition amplitudes of all

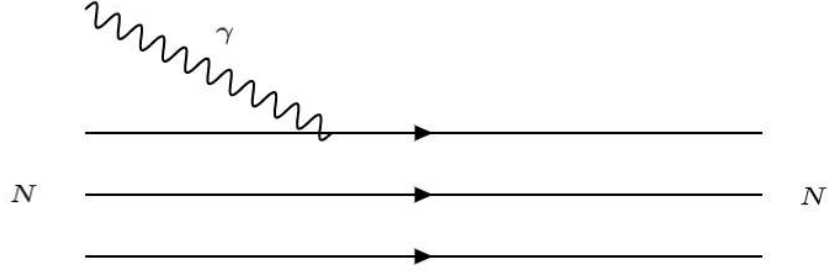


Figure 3.1 The diagram for the electromagnetic transition process $N\gamma^* \rightarrow N^*$ where the initial state nucleon and final state resonance are composed of three quarks. One of the incoming quarks interacts with the incoming photon while the remaining ones are spectators throughout the process.

possible quantum states of quarks from the initial-state nucleon to the final-state resonance in q^3 picture as,

$$G_E = \left\langle N, S'_z = \frac{1}{2} \left| q'_1 q'_2 q'_3 \right\rangle T_B(q_1 q_2 q_3 \rightarrow q'_1 q'_2 q'_3) \left\langle q_1 q_2 q_3 \left| N, S_z = \frac{1}{2} \right\rangle \right|_{\text{Breit frame}}, \quad (3.2)$$

where the nucleon wave function $\langle q_1 q_2 q_3 | N, S_z \rangle$, which is composed by three quarks $q_1 q_2 q_3$ with the spin projection S_z , has been already introduced in Chapter II. In Eq. (3.2), one need to perform a summation over all possible quantum numbers of the intermediate three quarks and integrates over the momenta of all quarks.

The transition amplitude of the process $\gamma q \rightarrow q'$ as displayed in Figure 3.1 is described by the transition amplitude $T_B(q_1 q_2 q_3 \rightarrow q'_1 q'_2 q'_3)$ in Eq. (3.2). This amplitude is calculated from the matrix element of the quark current operator coupled to the photon field. The spin-state of the interacting quark is fixed as the one with $s_z = \uparrow$:

$$T_B(q_1 q_2 q_3 \rightarrow q'_1 q'_2 q'_3) = e_3 \bar{u}_\uparrow(p') \gamma^\mu u_\uparrow(p) \epsilon_\mu(k) \langle q'_1 q'_2 | q_1 q_2 \rangle$$

$$\begin{aligned}
&= e_3 \left[\frac{(E' + m)(E + m)}{4E'E} \right]^{\frac{1}{2}} \left(1 + \frac{p'_z p_z + 2p'_- p_+}{(E' + m)(E + m)} \right) \\
&\quad \times \langle q'_1 q'_2 | q_1 q_2 \rangle, \tag{3.3}
\end{aligned}$$

where E and E' are respectively the energy of the interacting initial-quark and final-quark with the dynamical quark mass of u and d quarks as m . The momentum p_{\pm} is defined by $p_{\pm} = \frac{1}{\sqrt{2}}(p_x \pm ip_y)$. The quark electric charge of the third quark is defined by e_3 and the polarization vector of the photon which enters Eq. 3.3 is defined as $\epsilon = (1, 0, 0, 0)$.

3.2 Proton electric form factor in non-relativistic approximation

We consider the simplest case when the proton electric form factor is derived from Eq. (3.2) in the non-relativistic calculation. The proton and $N(1440)$ wave functions in this case respectively are the three-quark baryon state in the ground state and first radial excited state of a harmonic oscillator. The length parameter (a) is evaluated from the fit with the proton electric form factor. By employing the corresponding length parameter which obtained from the fit, the helicity amplitudes $A_{1/2}$, $A_{3/2}$, and $S_{1/2}$ in the non-relativistic case will be calculated by using the proton and $N(1440)$ wave functions.

The electromagnetic transition amplitude in this case can be simplified by using Eq. (3.3). By performing the non-relativistic approximation, it is written as

$$T_B(q_1 q_2 q_3 \rightarrow q'_1 q'_2 q'_3) \approx e_3 \langle q'_1 q'_2 | q_1 q_2 \rangle. \tag{3.4}$$

Then, we substitute the electromagnetic transition amplitude in Eq. (3.4) into

Eq. (3.2), the expression of the proton electric form factor in the non-relativistic case is

$$G_E^{NR}(Q^2) = e^{-\frac{Q^2}{6a^2}}, \quad (3.5)$$

where a is the length parameter and the constituent quark mass in this case is $m = 340$ MeV.

The length parameter is fitted by using the proton charge radius $r_p = 0.841$ fm from Particle Data Group (Zyla et al., 2020). The mean-square charge radius of a charged baryon is related to the baryon electric form factor as

$$\langle r_E^2 \rangle = - \frac{6}{G_E(0)} \frac{d}{dQ^2} G_E(Q^2) \Big|_{Q^2=0}. \quad (3.6)$$

By substituting the electric form factor from Eq. (3.5) into Eq. (3.6), the following results $a = 234.3$ MeV and $\langle r_E^2 \rangle^{1/2} = 0.841$ fm are obtained.

The proton electric form factor, obtained from the non-relativistic approximation, is shown in Figure 3.2 as the green dashed line. From the comparison of the proton electric form factor between the theoretical result and the experimental data, the curve is in good agreement only in the small Q^2 region.

3.3 Proton electric form factor from the fitting of low-lying baryon mass spectra

In the previous section, we employ the proton wave function as the ground-state harmonic oscillator in the non-relativistic case, where the results of the proton form factor can reproduce the data only in the small Q^2 region. Now, we will improve our result of the electric form factor by performing the relativistic calculation. The spatial wave functions of the proton are derived within the framework

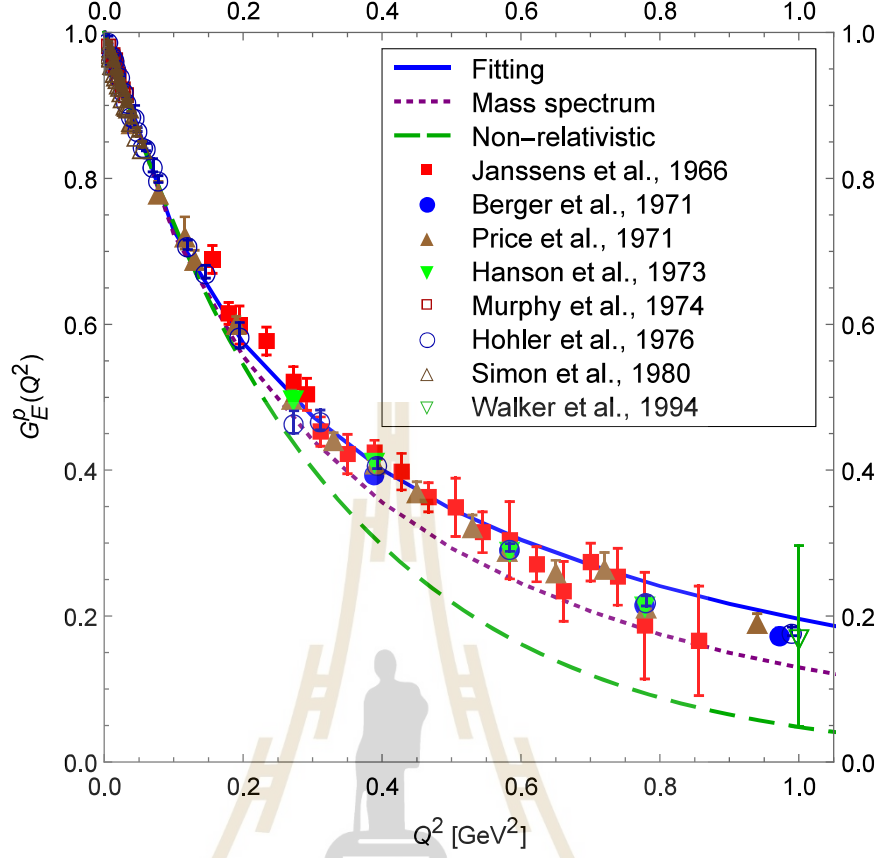


Figure 3.2 Proton electric form factor G_E from the process $p\gamma \rightarrow N(1440)$. The solid, dotted, and dashed curves are the results obtained by using the extracted proton spatial wave functions, the proton spatial wave function from low-lying baryon mass spectra, and the proton spatial wave function from the ground state harmonic oscillator in the non-relativistic helicity amplitude calculation, respectively. The data points are taken from (Janssens et al., 1966; Berger et al., 1971; Price et al., 1971; Hanson et al., 1973; Murphy et al., 1974; Höhler et al., 1976; Simon et al., 1980; Walker et al., 1994).

of the low-lying baryon mass spectra as mentioned in Ref. (Xu et al., 2020). In this approach, the wave functions of the particles such as the proton, $N(1440)$, $N(1520)$, and $N(1535)$, are obtained by solving the eigenvalue problem and they are assumed to be a pure three-quark state.

The Hamiltonian in this approach includes one-gluon exchange contribution and Cornell-like potential. By adjusting the model parameters and solving the eigenvalue problem, the eigenvalues and eigenvectors are then obtained. The spatial wave functions for the proton, $N(1440)$, $N(1520)$, and $N(1535)$ which are the eigenvectors of the mass spectrum are applied to evaluate the proton electric form factor and the helicity amplitudes.

By using the wave function extracted from the low-lying baryon mass spectra, the result for the proton electric form factor is shown in Figure 3.2 as the red dotted line. In this case, the quark mass $m = 327$ MeV is used. The result is obviously improved in a comparison to the one from the non-relativistic case.

3.4 Extraction of proton from the proton electric form factor

We now extract the proton spatial wave function in three-quark picture by fitting the theoretical result of the proton electric form factor to the experimental data. This modified proton spatial wave function will be used to study other states such as the $N(1440)$, $N(1520)$, and $N(1535)$ by fitting to the helicity amplitudes in the next chapter.

The method for fitting the theoretical results to the experimental data in this study is the least square method. The theoretical result is evaluated by Eq. (3.2) where the model parameters used in this fitting are the quark mass $m = 5$ MeV and length parameter $a = 400$ MeV. The number of basis is six: $N = 0, 2, 4, \dots, 10$. The quark core radius evaluated by Eq. (F.1) is $\langle r^2 \rangle^{1/2} = 0.54$ fm. The result of the extracted proton is shown as the blue solid line in Figure 3.2. The spatial wave function of the extracted proton comparing to the proton spatial wave function from the approach of low-lying baryon mass spectra is shown

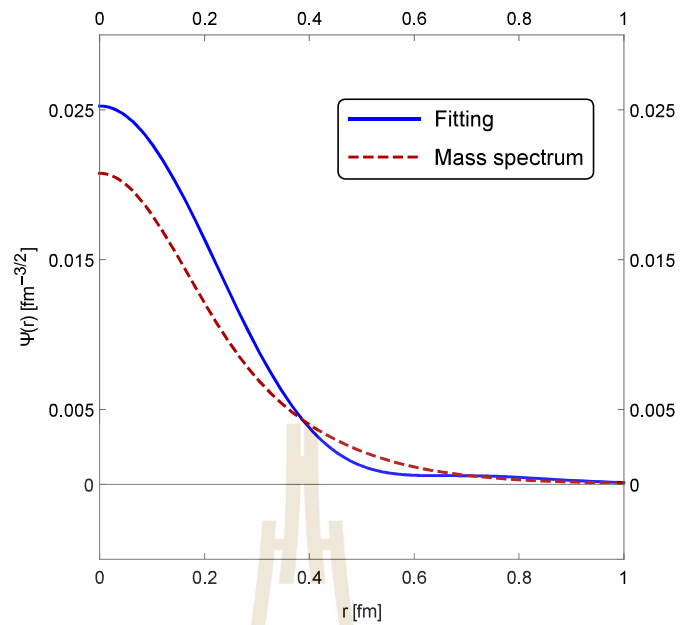


Figure 3.3 The spatial wave function of the extracted proton comparing to the proton spatial wave function from the approach of low-lying baryon mass spectra.

in Figure 3.3.



CHAPTER IV

HELICITY AMPLITUDES

4.1 Transverse and longitudinal helicity amplitudes

In this chapter, we study the helicity amplitudes in the process $N\gamma^* \rightarrow N^*$, where the nucleon and resonance states are in the three-quark picture. The corresponding diagram is displayed in Figure 4.1. The transverse helicity amplitudes ($A_{1/2}$, $A_{3/2}$) and a longitudinal helicity amplitude ($S_{1/2}$) are commonly defined in a N^* rest frame where the initial momentum of the nucleon (P_i), final momentum of the resonance (P_f), and the photon momentum $k = P_f - P_i$, along the z-axis, are represented as,

$$P_i = (E_N, 0, 0, -|\mathbf{k}|), \quad P_f = (M_{N^*}, 0, 0, 0), \quad k = (\omega, 0, 0, |\mathbf{k}|), \quad (4.1)$$

with

$$E_N = \frac{M_{N^*}^2 + M_N^2 + Q^2}{2M_{N^*}},$$

$$\omega = \frac{M_{N^*}^2 - M_N^2 - Q^2}{2M_{N^*}},$$

$$|\mathbf{k}| = \left[Q^2 + \left(\frac{M_{N^*}^2 - M_N^2 - Q^2}{2M_{N^*}} \right)^2 \right]^{\frac{1}{2}}, \quad (4.2)$$

where E_N and ω respectively are the nucleon and photon energies, $|\mathbf{k}|$ is the magnitude of the photon three-momentum, and the square of the four-momentum transfer is expressed by $Q^2 = -k^2$.

The transverse helicity amplitudes ($A_{1/2}$, $A_{3/2}$) and the longitudinal helicity

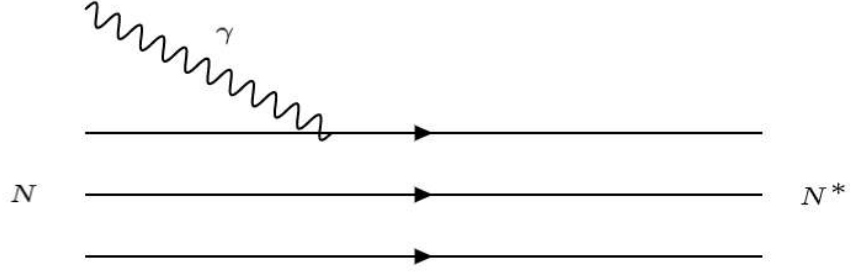


Figure 4.1 The diagram for the electromagnetic transition process $N\gamma^* \rightarrow N^*$ where the initial nucleon and final resonance are composed of three quarks. One of the incoming quarks interacts with the incoming photon while the remaining ones are spectators throughout the process.

amplitude ($S_{1/2}$) for photoproduction are defined by the transition amplitudes between the initial state N and the final state N^* for helicity $\lambda = +1$ and 0 respectively,

$$\begin{aligned}
 A_{1/2} &= \frac{1}{\sqrt{2K}} \left\langle N^*, S'_z = \frac{1}{2} \left| q'_1 q'_2 q'_3 \right. \right\rangle T_{s's}^+(q_1 q_2 q_3 \rightarrow q'_1 q'_2 q'_3) \left\langle q_1 q_2 q_3 \left| N, S_z = -\frac{1}{2} \right. \right\rangle, \\
 A_{3/2} &= \frac{1}{\sqrt{2K}} \left\langle N^*, S'_z = \frac{3}{2} \left| q'_1 q'_2 q'_3 \right. \right\rangle T_{s's}^+(q_1 q_2 q_3 \rightarrow q'_1 q'_2 q'_3) \left\langle q_1 q_2 q_3 \left| N, S_z = \frac{1}{2} \right. \right\rangle, \\
 S_{1/2} &= \frac{1}{\sqrt{2K}} \left\langle N^*, S'_z = \frac{1}{2} \left| q'_1 q'_2 q'_3 \right. \right\rangle T_{s's}^0(q_1 q_2 q_3 \rightarrow q'_1 q'_2 q'_3) \left\langle q_1 q_2 q_3 \left| N, S_z = \frac{1}{2} \right. \right\rangle \frac{|\mathbf{k}|}{Q},
 \end{aligned} \tag{4.3}$$

with

$$K = \frac{M_{N^*}^2 - M_N^2}{2M_{N^*}}, \tag{4.4}$$

where K is the real-photon momentum in the N^* rest frame, M_{N^*} and M_N denote the mass of N^* and N respectively. The N and N^* wave functions which have been described in Chapter II in the Harmonic oscillation model, are projected to three-quark picture as $\langle q_1 q_2 q_3 | N, S_z \rangle$ and $\langle q'_1 q'_2 q'_3 | N^*, S'_z \rangle$. In Eq. (4.3), one need to

perform the summation over all the possible quantum numbers of the intermediate three-quark states, including the initial-state of quarks $q_1 q_2 q_3$ in the nucleon with the spin projection S_Z and the final-state of quarks $q'_1 q'_2 q'_3$ in the resonance with the spin projection S'_z , and integrates over the momenta of all quarks.

And the transition amplitude $T_{s's}^\lambda(q_1 q_2 q_3 \rightarrow q'_1 q'_2 q'_3)$ in Eq. (4.3) is simply the transition amplitude of the process $\gamma q \rightarrow q'$, with s' , s corresponding to single quark spin projections (spin up \uparrow and spin down \downarrow) and λ for helicity, is simplified as

$$\begin{aligned} T_{s's}^\lambda(q_1 q_2 q_3 \rightarrow q'_1 q'_2 q'_3) &= e_3 \bar{u}_{s'}(p') \gamma^\mu u_s(p) \epsilon_\mu^\lambda(k) \langle q'_1 q'_2 | q_1 q_2 \rangle \\ &= e_3 T_{s's}^\lambda \langle q'_1 q'_2 | q_1 q_2 \rangle, \end{aligned} \quad (4.5)$$

where e_3 is the quark electric charge of the third quark, and the photon polarization vectors $\epsilon_\mu^\lambda(k)$ of the longitudinal ($\lambda = 0$) and transverse ($\lambda = 1$) helicity amplitudes in the Lorentz gauge are defined as,

$$\epsilon_\mu^0 = \frac{1}{Q} (|\mathbf{k}|, 0, 0, \omega), \quad \epsilon_\mu^\pm = -\frac{1}{\sqrt{2}} (0, 1, i, 0). \quad (4.6)$$

Then the matrix elements of the electromagnetic transition for helicity $\lambda = 0, 1$ are derived in detail,

$$\begin{aligned} T_{\uparrow\uparrow}^0 &= \left[\frac{(E' + m)(E + m)}{4E'E} \right]^{\frac{1}{2}} \left[\frac{|\mathbf{k}|}{Q} \left(1 + \frac{p'_z p_z + 2p'_- p_+}{(E' + m)(E + m)} \right) \right. \\ &\quad \left. - \frac{\omega}{Q} \left(\frac{p_z}{E + m} + \frac{p'_z}{E' + m} \right) \right], \\ T_{\uparrow\downarrow}^0 &= \left[\frac{(E' + m)(E + m)}{4E'E} \right]^{\frac{1}{2}} \left[\frac{|\mathbf{k}|}{Q} \left(\frac{\sqrt{2}(p'_z p_- - p'_- p_z)}{(E' + m)(E + m)} \right) \right. \\ &\quad \left. - \frac{\omega}{Q} \left(\frac{\sqrt{2}p_-}{E + m} - \frac{\sqrt{2}p'_-}{E' + m} \right) \right], \end{aligned}$$

$$\begin{aligned}
T_{\downarrow\uparrow}^0 &= \left[\frac{(E' + m)(E + m)}{4E'E} \right]^{\frac{1}{2}} \left[\frac{|\mathbf{k}|}{Q} \left(\frac{\sqrt{2}(-p'_z p_+ + p'_+ p_z)}{(E' + m)(E + m)} \right) \right. \\
&\quad \left. - \frac{\omega}{Q} \left(\frac{-\sqrt{2}p_+}{E + m} + \frac{\sqrt{2}p'_+}{E' + m} \right) \right], \\
T_{\downarrow\downarrow}^0 &= \left[\frac{(E' + m)(E + m)}{4E'E} \right]^{\frac{1}{2}} \left[\frac{|\mathbf{k}|}{Q} \left(1 + \frac{p'_z p_z + 2p'_+ p_-}{(E' + m)(E + m)} \right) \right. \\
&\quad \left. - \frac{\omega}{Q} \left(\frac{p_z}{E + m} + \frac{p'_z}{E' + m} \right) \right], \\
T_{\uparrow\uparrow}^+ &= \left[\frac{(E' + m)(E + m)}{4E'E} \right]^{\frac{1}{2}} \left[\frac{2p_+}{E + m} \right], \\
T_{\uparrow\downarrow}^+ &= \left[\frac{(E' + m)(E + m)}{4E'E} \right]^{\frac{1}{2}} \left[-\frac{\sqrt{2}p_z}{E + m} + \frac{\sqrt{2}p'_z}{E' + m} \right], \\
T_{\downarrow\uparrow}^+ &= 0, \\
T_{\downarrow\downarrow}^+ &= \left[\frac{(E' + m)(E + m)}{4E'E} \right]^{\frac{1}{2}} \left[\frac{2p'_+}{E' + m} \right], \tag{4.7}
\end{aligned}$$

where E and E' are respectively the energies of the initial state and the final state of the interacting quark with the dynamical quark mass of u and d quarks as m , and $p_{\pm} = \frac{1}{\sqrt{2}}(p_x \pm ip_y)$.

4.2 Helicity amplitudes of $N(1440)$

4.2.1 Helicity amplitudes of $N(1440)$ in non-relativistic approximation

The helicity amplitudes for photoproduction of the Roper resonance on the proton which are defined by $A_{1/2}$ and $S_{1/2}$ are derived with Eq. (4.3) in the non-relativistic approximation. The proton and the $N(1440)$ states are in the

ground state and first radial excited state harmonic oscillator wave functions of three-quark picture since it is the simplest approximation for nucleon resonance states. The length parameter takes 234.3 MeV which is the value for fitting to the data of the proton electric form factor in the non-relativistic approximation in the previous chapter.

The helicity amplitudes $S_{1/2}$ and $A_{1/2}$ of the Roper resonance in the non-relativistic approximation are,

$$S_{1/2}^{NR} = \frac{ek^2 e^{-\frac{k^2}{6a^2}}}{36\sqrt{6K}ma^2Q^2} \left(6k^2m + (12a^2 - k^2)\sqrt{k^2 - Q^2} \right),$$

$$A_{1/2}^{NR} = \frac{ek^3 e^{-\frac{k^2}{6a^2}}}{12\sqrt{3K}ma^2}. \quad (4.8)$$

The matrix elements of the electromagnetic transition in the calculation of $S_{1/2}$ and $A_{1/2}$ from Eq. (4.7) are simplified as,

$$T_{\uparrow\downarrow}^+ \approx \frac{k}{\sqrt{2}m}, \quad T_{\uparrow\uparrow}^0 \approx 1, \quad (4.9)$$

where $T_{\uparrow\downarrow}^+$ is used in $A_{1/2}$, and $T_{\uparrow\uparrow}^0$ is used in $S_{1/2}$, and the constitute quark mass is $m = 340$ MeV.

The theoretical results of the transverse and the longitudinal helicity amplitudes over Q^2 of the Roper resonance are shown with the green dashed line in Figures 4.2 and 4.3. The result is consistent with the non-relativistic quark model prediction from Refs. (Li et al., 1992; Parsaei and Akbar Rajabi, 2017; Li and Riska, 2006). However, the comparison to the experimental data demonstrates that the non-relativistic calculation for helicity amplitudes of the Roper resonance is not acceptable since the theoretical results can not give the changing sign from

negative to positive value.

4.2.2 Helicity amplitudes of $N(1440)$ with the wave function from mass spectrum fitting

In this section, the helicity transition amplitudes of the Roper resonance are calculated from the matrix elements in Eq. (4.7) relativistically. The proton and the Roper spatial wave functions are the eigenvectors of the lowest state and first radial excited state of nucleon resonances of $L = 0$ symmetric type from the Ref. (Xu et al., 2020), where the theoretical results of baryon resonance mass spectra are fitted to the experimental data in three-quark picture. The spatial wave functions of the proton and the Roper resonance are expanded in the harmonic oscillator basis in (Xu et al., 2020),

$$\begin{aligned}\psi_p^O &= \sum_{N=0,2,4,\dots} a_{N00}^{EV} \Psi_{N00}^O, \\ \psi_{N(1440)}^O &= \sum_{N=0,2,4,\dots} b_{N00}^{EV} \Psi_{N00}^O,\end{aligned}\tag{4.10}$$

where a_{N00}^{EV} and b_{N00}^{EV} are determined by fitting the baryon mass spectrum.

The theoretical results of transverse and longitudinal helicity amplitudes of the Roper resonance with the spatial wave functions from Eq. 4.10 are shown with the dotted line in Figures 4.2 and 4.3 respectively. For both $A_{1/2}$ and $S_{1/2}$, the theoretical results can describe the experimental data at large Q^2 region ($1.5 \leq Q^2 \leq 4.5 \text{ GeV}^2$), where the three-quark core plays the main role in the photoproduction of the Roper resonance. And this is consistent with the theoretical results obtained from the light-front three-quark model (Aznauryan, 2007) and covariant spectator quark model (Ramalho and Tsushima, 2010). However, for the small values of $Q^2 \leq 1.5 \text{ GeV}^2$, both the helicity amplitudes $A_{1/2}$ and $S_{1/2}$

of the Roper resonance as a pure three-quark state has been overestimated by the theoretical calculations. The theoretical result of $S_{1/2}$ at the real photon point is even an infinite large value. At the low Q^2 region, the behavior of the helicity amplitudes may be more sensitive to the other degree of freedom than those of the three-dressed quark, i.e., the meson cloud contributions (Segovia et al., 2015), hadronic molecular component (Obukhovskiy et al., 2011). The predictions of the helicity amplitudes of the Roper resonance when the proton and the Roper resonance are treated as the pure three-quark states in the relativistic calculation confirmed that the Roper is mainly a three-quark state, but there may be some considerable components of others than the three-quark core in the Roper resonance.

4.2.3 Extraction of quark distribution of $N(1440)$

The proton spatial wave function has been fixed in Sec. 3.4 by fitting the theoretical result of the proton electric form factor to the experimental data. Then we assign the Roper spatial wave function as the linear combination of the Harmonic oscillator bases for $L = 0$ symmetric type, which is in the form,

$$\psi_{N(1440)}^O = \sum_{N=0,2,4,\dots} b'_{N00} \Psi_{N00}^O. \quad (4.11)$$

The $N(1440)$ spatial wave function are still in three-quark picture, but may contain any higher radial excited contribution of nucleon resonances for $L = 0$ symmetric type. The coefficient b'_{N00} are fixed by fitting the theoretical result of the helicity amplitudes of the Roper resonance to the experimental data in two cases:

Fitting I: the proton and the $N(1440)$ spatial wave functions are orthogonal each other, $\langle \psi_p^O | \psi_{N(1440)}^O \rangle = 0$ which constrains the $N(1440)$ spatial wave function to be the radial excitation of the nucleon;

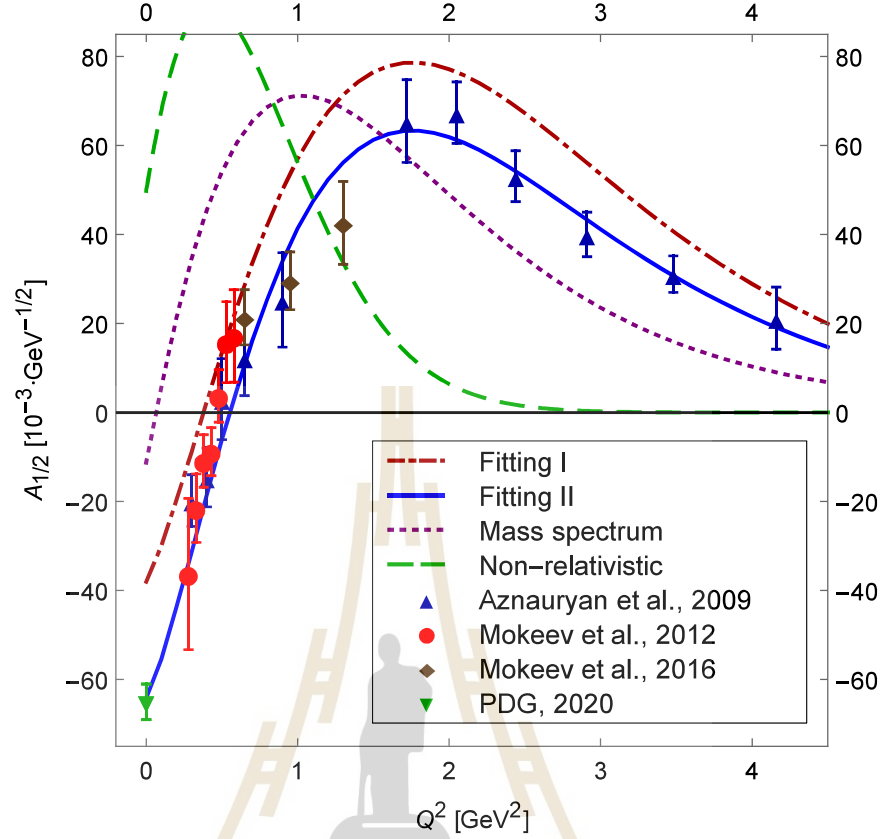


Figure 4.2 The transverse helicity amplitude $A_{1/2}$ for the $p\gamma^* \rightarrow N(1440)$ transition in comparison to the data points from (Aznauryan et al., 2009; Mokeev et al., 2012; Mokeev et al., 2016; Zyla et al., 2020). The dash-dotted, solid, dotted, and dashed curve are the results obtained, respectively, from the relativistic calculations for fitting I, fitting II, baryon mass spectrum, and non-relativistic calculation.

Fitting II: the proton and the $N(1440)$ spatial wave functions may not be orthogonal each other, which allows the $N(1440)$ spatial wave function compose of the radial excitation of the nucleon as well as others.

The theoretical results of the helicity amplitudes of the Roper resonance with both the spatial wave functions of the proton and the Roper resonance from Fitting I are shown in Figures 4.2 and 4.3 with the red dash-dotted line and the

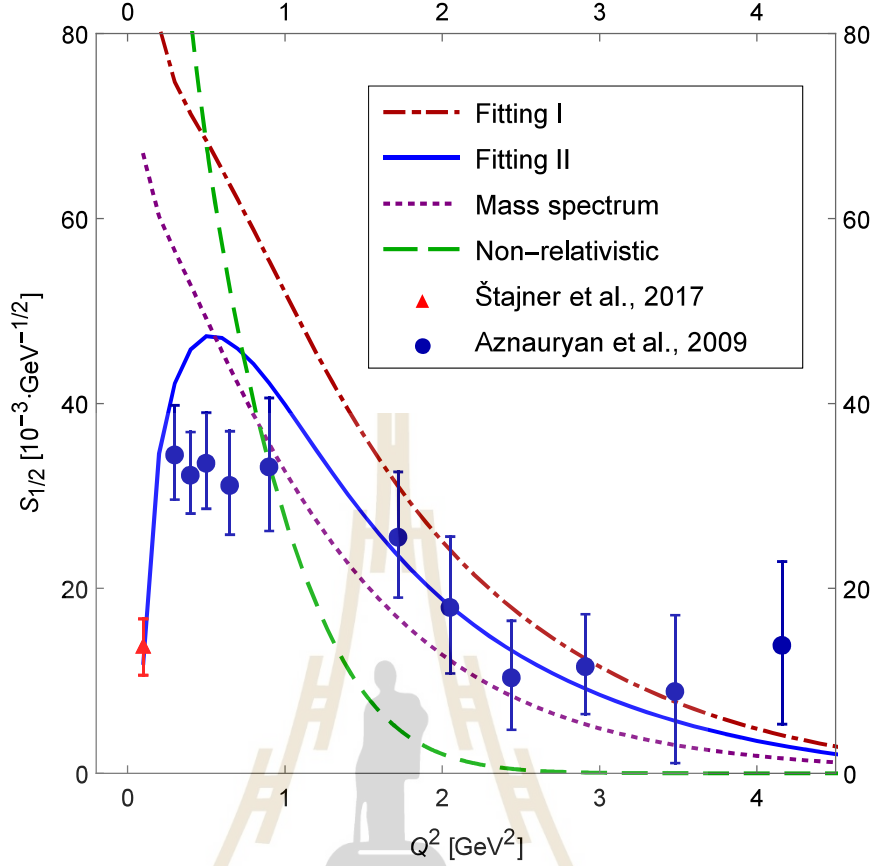


Figure 4.3 The longitudinal helicity amplitude $S_{1/2}$ of $p\gamma^* \rightarrow N(1440)$ in comparison to the data points from (Štajner et al., 2017; Aznauryan et al., 2009). The notation of the curves is the same as the one in Figure 4.2.

results with the wave functions from the Fitting II are in the blue solid line.

The theoretical results of $A_{1/2}$ of the Roper resonance in Fitting I (orthogonal case) gives a proper description of the $A_{1/2}$ data only in the small Q^2 region, but overestimate both $A_{1/2}$ and $S_{1/2}$ in the higher Q^2 region. It is noted that the theoretical results for $S_{1/2}$ at the small Q^2 region are much larger than the experimental data. These results are actually a slightly improved version of the predictions in the mass spectra fitting case. The fact that the experimental data can not be well described when we constrain the Roper as the first radial excited state of the proton indicates that the Roper may have a component of others

than three-quark core in the Roper resonance. And the similar results of fitting I case and mass spectra fitting case also convince us that the three-quark core may mainly determine the $A_{1/2}$ and $S_{1/2}$ helicity amplitudes of the Roper resonance at the higher Q^2 region.

The theoretical results of $A_{1/2}$ of the Roper resonance in Fitting II (non-orthogonal case) give a good description for the whole Q^2 region, while fairly describe the data of $S_{1/2}$. The results of Fitting I and II together indicates that it is necessary to include components other than radial excited three quarks in the Roper resonance, like meson cloud, hadronic molecular or pentaquark.

To reveal the structure of $N(1440)$, the difference between the $N(1440)$ spatial wave function by the Fitting I and II are compared in Figure 4.4 as the function of the relative distance of the quark to the center of the mass. The spatial wave functions from Fitting I and II cases are respectively in the solid line and dashed line. A condition that $r_\lambda = r_\rho$ is taken to simply the three-dimensional spatial wave functions to a 2D plot, due to the full permutation symmetry of the three quark states. The difference of the first peak in Figure 4.4 indicates that the quark density of the Fitting I around the center of three-quark core is smaller than the Fitting II, and this structure other than the three-quark core which may be resulted from some non-3-quark composite like meson cloud, hadronic molecular or pentaquark weaken the orthogonality of the $N(1440)$ resonance wave function in Fitting I at the same time. The spatial wave function of the Fitting I is consistent with the $N(1440)$ quark spatial wave function in Lattice QCD (Roberts et al., 2013) calculations.

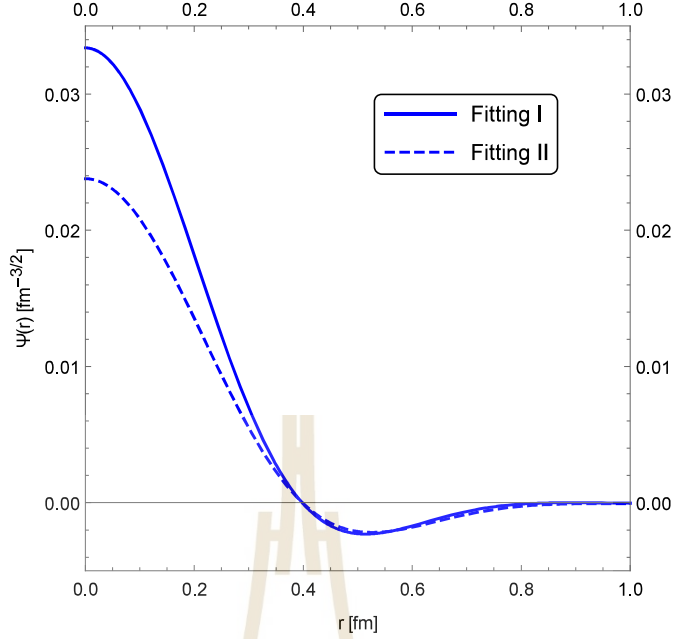


Figure 4.4 The $N(1440)$ spatial wave functions in the Fitting I and II are shown in terms of the relative distance of the quark to the center of the three-quark core.

4.3 Helicity amplitudes of $N(1520)$ and $N(1535)$

4.3.1 Helicity amplitudes of $N(1520)$ and $N(1535)$ in non-relativistic approximation

In this section, we calculate the helicity amplitudes $A_{1/2}$, $A_{3/2}$, and $S_{1/2}$ for photoproduction of the lowest negative parity states in the non-relativistic approximation with Eq. (4.3). The nucleon and resonance states are still in the three-quark picture, while the proton is in the ground state harmonic oscillator wave function of $L = 0$ with symmetric type; $N(1520)$, and $N(1535)$ are both in the lowest state harmonic oscillator wave functions of $L = 1$ state with mixed symmetric type. The length parameter is 234.3 MeV with which we get a proper fit to the experimental data of the proton electric form factor and also the helicity

amplitudes of the Roper resonance.

The transition matrix elements in the calculation of $A_{1/2}$, $A_{3/2}$, and $S_{1/2}$ from Eq. (4.7) are simplified in non-relativistic approximation as

$$T_{\uparrow\uparrow}^+ \approx \frac{p_+}{m}, \quad T_{\uparrow\downarrow}^+ \approx \frac{k}{\sqrt{2}m}, \quad T_{\downarrow\downarrow}^+ \approx \frac{p'_+}{m}, \quad T_{\uparrow\uparrow}^0 \approx 1. \quad (4.12)$$

The results of helicity amplitudes in the non-relativistic approximation for the $N(1520)3/2^-$ are

$$\begin{aligned} S_{1/2}^{NR} &= -\frac{eke^{-\frac{k^2}{6a^2}}}{3a\sqrt{2K}}, \\ A_{1/2}^{NR} &= \frac{e(a^2 - k^2)e^{-\frac{k^2}{6a^2}}}{6ma\sqrt{K}}, \\ A_{3/2}^{NR} &= \frac{eae^{-\frac{k^2}{6a^2}}}{2m\sqrt{3K}}, \end{aligned} \quad (4.13)$$

and for the $N(1535)1/2^-$,

$$\begin{aligned} S_{1/2}^{NR} &= \frac{eke^{-\frac{k^2}{6a^2}}}{6a\sqrt{K}}, \\ A_{1/2}^{NR} &= \frac{e(2a^2 + k^2)e^{-\frac{k^2}{6a^2}}}{6ma\sqrt{2K}}, \end{aligned} \quad (4.14)$$

where the constituent quark mass is $m = 340$ MeV.

The theoretical result of the $A_{1/2}$ of $N(1520)$ and $N(1535)$ respectively are with the green dashed line in Figures 4.5 and 4.6. The non-relativistic calculation are not able to describe the experimental data of $A_{1/2}$ helicity amplitudes for both $N(1520)$ and $N(1535)$ states, but a simple trend was provided by the non-relativistic approximation which helps us to check our relativistic calculations.

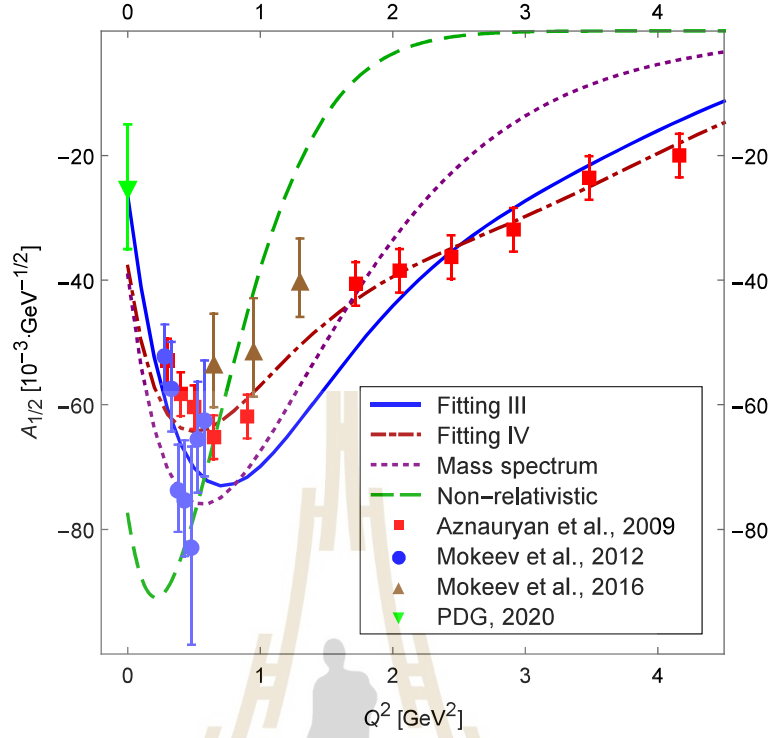


Figure 4.5 The transverse helicity amplitude $A_{1/2}$ of $N(1520)$ for $p\gamma^* \rightarrow N(1520)$ process with data points from (Aznauryan et al., 2009; Mokeev et al., 2012; Mokeev et al., 2016; Zyla et al., 2020). The notation of the curves is the same as the one in Figure 4.2.

4.3.2 Helicity amplitudes of $N(1520)$ and $N(1535)$ with the wave function from the mass spectra fitting

In this section, we carry out the same relativistic calculation of the $N(1520)$ and $N(1535)$ as the Roper resonance where their spatial wave functions are the eigenvectors derived from the mass spectra fitting. Both the $N(1520)$ and $N(1535)$ spatial wave functions correspond to the lowest $L = 1$ mixed symmetric states. The proton spatial wave function is still the same eigenvector as the one in Sec. 4.2.2.

The theoretical result of $A_{1/2}$ of the $N(1520)$ and $N(1535)$ are shown with

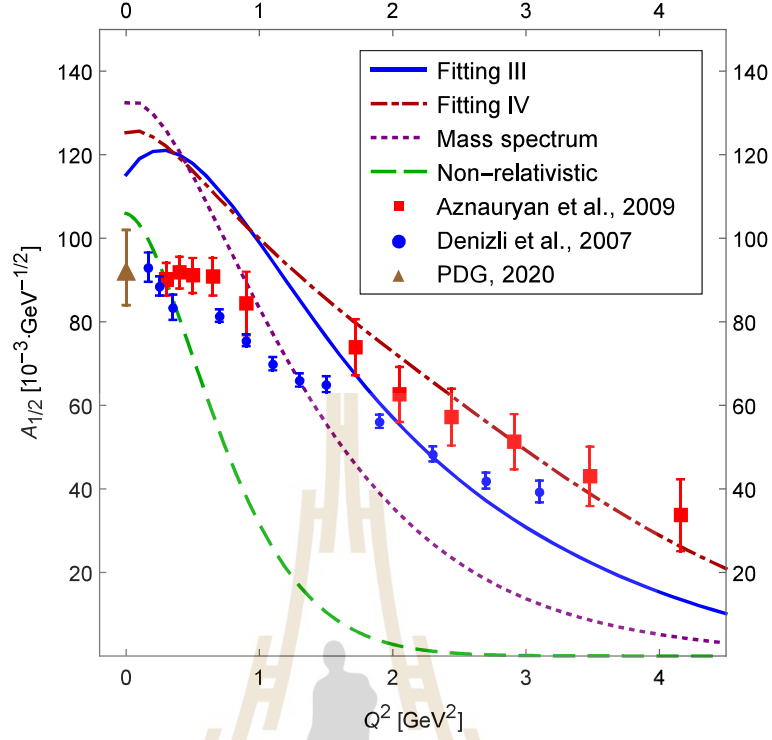


Figure 4.6 The transverse helicity amplitude $A_{1/2}$ of $N(1535)$ for $p\gamma \rightarrow N(1535)$ process with data points from (Aznauryan et al., 2009; Denizli et al., 2007; Zyla et al., 2020). The notation of the curves is the same as the one in Figure 4.2.

the red dotted line in Figures 4.5 and 4.6. It is found that the helicity amplitudes for the $N(1520)$ and $N(1535)$ resonances can not be well described in the model, that is, the theoretical results largely overestimates the amplitudes at small Q^2 but underestimate the amplitudes for higher Q^2 region. However, the trend of both the helicity amplitudes are consistent with the line shape of the experimental data, which may indicates that the $N(1520)$ and $N(1535)$ are mainly three-quark states.

4.3.3 Extraction of quark distribution of $N(1520)$ and $N(1535)$

The method applied to extract the spatial wave function of the $N(1520)$ and $N(1535)$ is the same as the one used to extract the $N(1440)$ spatial wave function. The proton spatial wave function is the one derived by fitting the theoretical result of the proton electric form factor to the experimental data in Sec. 3.4. The spatial wave function of the $N(1520)$ and $N(1535)$ are extracted by fitting to the experimental data of the $A_{1/2}$ helicity amplitudes with two different conditions on their spatial wave functions. And we discuss them in two different cases as Fitting III and Fitting IV.

Fitting III: the spatial wave functions of the $N(1520)$ and $N(1535)$ are both in the lowest $L = 1$ nucleon state with mixed symmetry and their spatial wave functions are the same.

Fitting IV: the spatial wave functions of the $N(1520)$ and $N(1535)$ are both in the lowest $L = 1$ nucleon state with mixed symmetry but their spatial wave functions are independent to each other.

The theoretical results of the $A_{1/2}$ helicity amplitude of the $N(1520)$ and $N(1535)$ in the Fitting III and the Fitting IV are shown with the blue solid line and the red dash-dotted line in Figures 4.5 and 4.6, respectively. Both the theoretical results in the Fitting III and IV are closer to the experimental data of the $A_{1/2}$ helicity amplitude than the results where the $N(1520)$ and $N(1535)$ wave functions are imported from the mass spectra fitting. The fact that both Fitting III and IV are unable to describe the experimental data, where the $N(1520)$ and $N(1535)$ are in the three-quark picture as the lowest $L = 1$ nucleon state with mixed symmetry may indicate that the $N(1520)$ and $N(1535)$ may contain other components. This argument is consistent with the one that we got from the studies of the mass

spectra of negative-parity baryons. To investigate further the inner structure of these nucleon states, one may study the helicity amplitudes of the the $N(1520)$ and $N(1535)$ by including pentaquark components as well as higher $L = 1$ three-quark states.



CHAPTER V

DISCUSSIONS AND CONCLUSIONS

In this work, we study the helicity amplitudes for photoproduction of the nucleon resonance states, $N(1440)$, $N(1520)$, and $N(1535)$ via the process of $p\gamma^* \rightarrow N^*$. The theoretical results of the transverse helicity amplitude $A_{1/2}$ and longitudinal helicity amplitude $S_{1/2}$ of the all three nucleon states in the three-quark pictures are compared to the experimental data. The spatial wave functions of the proton, $N(1440)$, $N(1520)$, and $N(1535)$ had been extracted by fitting the theoretical results to the experimental data of the proton electric form factor and helicity amplitudes.

The theoretical results of the proton electric form factor in the three-quark picture give the proper description of the experimental result which has convinced us that, the three-quark core of the proton makes the dominating role in the proton structure. The fair fits to the experimental data of the Roper resonance helicity amplitudes in the whole Q^2 region in three relativistic calculations reveal that the Roper is mainly the first radial excited state but may also include a small component of others like pentaquark components and $L = 2$ three-quark states.

The theoretical results in the three relativistic calculations of the helicity amplitudes for photoproduction of the $N(1520)$ and $N(1535)$ in the three-quark picture are not compatible with the experimental data, but have the same tendency as the line shape of the experimental data may indicate that higher $L = 1$ three quark states or non three-quark composite components like meson cloud, hadronic molecule, pentaquark may play a role. The success of a newly reproduced negative-

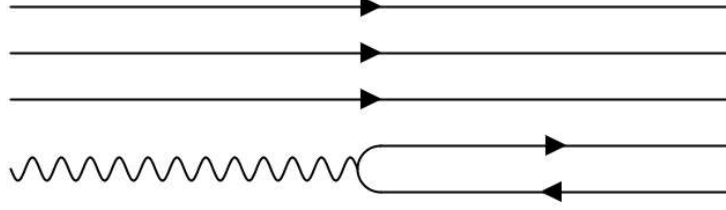


Figure 5.1 $N\gamma^* \rightarrow N^*$ in electromagnetic transition where the initial-state nucleon is three-quark system and final-state resonance is pentaquark system

parity nucleon mass spectrum in the Ref. (Xu et al., 2020) by including light pentaquark components has inspired us that the ground state pentaquark may likely be the missing components in the $N(1520)$ and $N(1535)$ states. The helicity amplitudes of the pentaquark resonance state in the process $\gamma^*p \rightarrow N^*$ where N^* is the ground state light pentaquark are derived in the next section. We expect to give a proper description of the experimental data of the helicity amplitudes by mixing the three-quark and pentaquark components in the future.

5.1 Helicity amplitudes with pentaquark wave function

5.1.1 Transverse and longitudinal helicity amplitudes for pentaquark

The transverse helicity amplitudes ($A_{1/2}$, $A_{3/2}$), and the longitudinal helicity amplitude ($S_{1/2}$) for the pentaquark state are defined at the pentaquark N^* rest frame. The initial (P_i) and final (P_f) momenta at the N^* rest frame are defined equally as the ones in Eqs. (4.1) and (4.2). The helicity amplitudes for the pentaquark states are defined by the transition amplitudes between the initial state of the nucleon and final state of the pentaquark for helicity $\lambda = +1$ and 0

respectively, similar to the Eq. (4.3):

$$\begin{aligned}
A_{1/2} &= \frac{1}{\sqrt{2K}} \left\langle N^*, S'_z = \frac{1}{2} \left| q'_1 q'_2 q'_3 q'_4 \bar{q}'_5 \right\rangle T'_{s's}{}^{+\lambda}(q_1 q_2 q_3 \rightarrow q'_1 q'_2 q'_3 q'_4 \bar{q}'_5) \right. \\
&\quad \times \left\langle q_1 q_2 q_3 \left| N, S_z = -\frac{1}{2} \right\rangle, \\
A_{3/2} &= \frac{1}{\sqrt{2K}} \left\langle N^*, S'_z = \frac{3}{2} \left| q'_1 q'_2 q'_3 q'_4 \bar{q}'_5 \right\rangle T'_{s's}{}^{+\lambda}(q_1 q_2 q_3 \rightarrow q'_1 q'_2 q'_3 q'_4 \bar{q}'_5) \right. \\
&\quad \times \left\langle q_1 q_2 q_3 \left| N, S_z = \frac{1}{2} \right\rangle, \\
S_{1/2} &= \frac{1}{\sqrt{2K}} \left\langle N^*, S'_z = \frac{1}{2} \left| q'_1 q'_2 q'_3 q'_4 \bar{q}'_5 \right\rangle T'_{s's}{}^{0\lambda}(q_1 q_2 q_3 \rightarrow q'_1 q'_2 q'_3 q'_4 \bar{q}'_5) \right. \\
&\quad \times \left\langle q_1 q_2 q_3 \left| N, S_z = \frac{1}{2} \right\rangle \frac{|\mathbf{k}|}{Q}, \tag{5.1}
\end{aligned}$$

where $\langle N^*, S'_z = \frac{1}{2} | q'_1 q'_2 q'_3 q'_4 \bar{q}'_5 \rangle$ is the wave function of pentaquark state shown in Section 2.2. Again, in Eq. (5.1), one need to perform the summation over all the possible quantum numbers of the intermediate three and five quarks, and integrates over the momenta of all quarks. The transition amplitude $T'_{s's}{}^{\lambda}(q_1 q_2 q_3 \rightarrow q'_1 q'_2 q'_3 q'_4 \bar{q}'_5)$ in Eq. (5.1) is simply the transition amplitude of the quark-pair creation of electroproduction process $\gamma \rightarrow q\bar{q}$ with spin up \uparrow and spin down \downarrow for single quark or antiquark spin projections with the helicity λ . It is simplified as

$$\begin{aligned}
T'_{s's}{}^{\lambda}(q_1 q_2 q_3 \rightarrow q'_1 q'_2 q'_3 q'_4 \bar{q}'_5) &= e_4 \bar{u}_{s'}(p') \gamma^\mu v_s(p) \epsilon_\mu^\lambda(k) \langle q'_1 q'_2 q'_3 | q_1 q_2 q_3 \rangle \\
&= e_4 T'_{s's}{}^{\lambda} \langle q'_1 q'_2 q'_3 | q_1 q_2 q_3 \rangle, \tag{5.2}
\end{aligned}$$

with the detail form as,

$$T'_{\uparrow\uparrow}{}^{0\lambda} = \sqrt{\frac{(E' + m)(E + m)}{4E'E}} \left[\frac{|\mathbf{k}|}{Q} \left(\frac{\sqrt{2}p_-}{E + m} + \frac{\sqrt{2}p'_-}{E' + m} \right) \right]$$

$$\begin{aligned}
& -\frac{\omega}{Q} \left(\frac{\sqrt{2}p'_z p_- + \sqrt{2}p'_- p_z}{(E' + m)(E + m)} \right) \Big], \\
T'_{\uparrow\downarrow}{}^0 &= \sqrt{\frac{(E' + m)(E + m)}{4E'E}} \left[\frac{|\mathbf{k}|}{Q} \left(\frac{p_z}{E + m} + \frac{p'_z}{E' + m} \right) \right. \\
& \quad \left. - \frac{\omega}{Q} \left(1 + \frac{p'_z p_z - 2p'_- p_+}{(E' + m)(E + m)} \right) \right], \\
T'_{\downarrow\uparrow}{}^0 &= -\sqrt{\frac{(E' + m)(E + m)}{4E'E}} \left[\frac{|\mathbf{k}|}{Q} \left(\frac{p_z}{E + m} + \frac{p'_z}{E' + m} \right) \right. \\
& \quad \left. - \frac{\omega}{Q} \left(1 + \frac{p'_z p_z - 2p'_- p_+}{(E' + m)(E + m)} \right) \right], \\
T'_{\downarrow\downarrow}{}^0 &= \sqrt{\frac{(E' + m)(E + m)}{4E'E}} \left[\frac{|\mathbf{k}|}{Q} \left(\frac{\sqrt{2}p_+}{E + m} + \frac{\sqrt{2}p'_+}{E' + m} \right) \right. \\
& \quad \left. - \frac{\omega}{Q} \left(\frac{\sqrt{2}p'_z p_+ + \sqrt{2}p'_+ p_z}{(E' + m)(E + m)} \right) \right], \\
T'_{\uparrow\uparrow}{}^+ &= \sqrt{\frac{(E' + m)(E + m)}{4E'E}} \left[1 - \frac{p'_z p_z}{(E' + m)(E + m)} \right], \\
T'_{\uparrow\downarrow}{}^+ &= \sqrt{\frac{(E' + m)(E + m)}{4E'E}} \left[\frac{\sqrt{2}p'_z p_+}{(E' + m)(E + m)} \right], \\
T'_{\downarrow\uparrow}{}^+ &= \sqrt{\frac{(E' + m)(E + m)}{4E'E}} \left[\frac{-\sqrt{2}p'_+ p_z}{(E' + m)(E + m)} \right], \\
T'_{\downarrow\downarrow}{}^+ &= \sqrt{\frac{(E' + m)(E + m)}{4E'E}} \left[\frac{2p'_+ p_+}{(E' + m)(E + m)} \right], \tag{5.3}
\end{aligned}$$

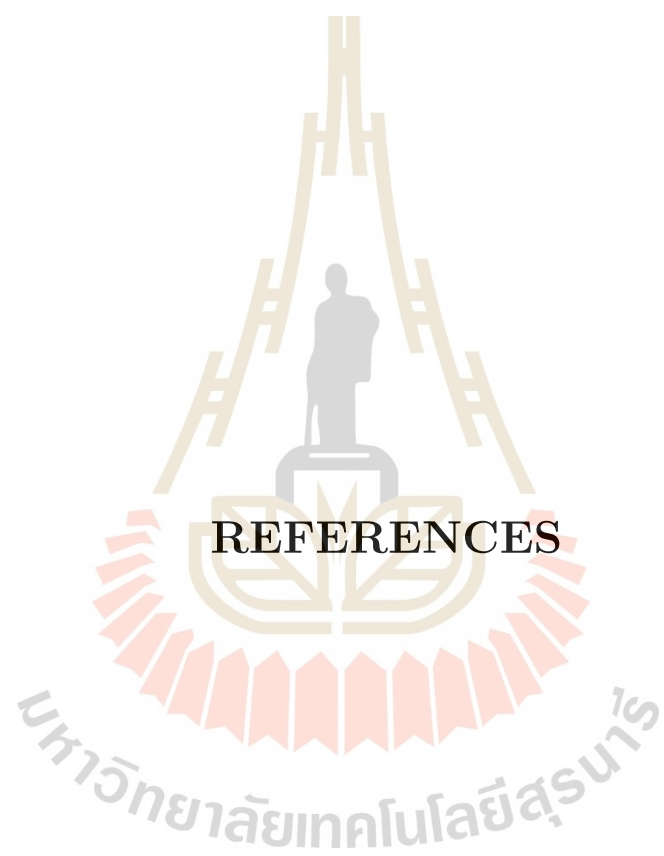
where E and E' respectively are the energy of antiquark and quark with the dynamical quark mass m , $p_{\pm} = \frac{1}{\sqrt{2}}(p_x \pm ip_y)$, $e_{A'}$ is the electric charge of the quark in the quark-antiquark pair production, s and s' respectively are the spin projection of the antiquark and quark, and the helicity $\lambda = 0$ (longitudinal helicity amplitude) and $\lambda = 1$ (transverse helicity amplitude).

5.2 future work

The comparison between the theoretical results and experimental data on the helicity amplitudes $A_{1/2}$ and $S_{1/2}$ and the analysis of the spatial wave function of the $N(1440)$, $N(1520)$ and $N(1535)$ resonances reveal that the $N(1440)$ resonance is mainly the q^3 first radial excitation but may have a small component of others while the $N(1520)$ and $N(1535)$ resonances may have a considerable pentaquark component or others. Therefore, we may carry out our future research in the following directions:

1. Study the helicity amplitudes $A_{1/2}$ and $S_{1/2}$ of the process $\gamma^*p \rightarrow N(1440)$ by including in the $N(1440)$ resonance $q^4\bar{q}$ components in both the compact pentaquark picture and molecular picture.
2. Study the helicity amplitudes $A_{1/2}$ and $S_{1/2}$ of the process $\gamma^*p \rightarrow N(1440)$ by including in the $N(1440)$ resonance higher positive parity states like the 70-plet $L = 2$ states.
3. Study the helicity amplitudes $A_{1/2}$ and $S_{1/2}$ of the processes $\gamma^*p \rightarrow N(1535)$ and $\gamma^*p \rightarrow N(1520)$ by including in the $N(1535)$ and $N(1520)$ resonances $q^4\bar{q}$ components.
4. Study the helicity amplitudes $A_{1/2}$ and $S_{1/2}$ of the processes $\gamma^*p \rightarrow N(1535)$ and $\gamma^*p \rightarrow N(1520)$ by including in the $N(1535)$ and $N(1520)$ resonances higher negative parity states like the 70-plet $L = 1$ spin-triplet states.

We expect that the researches mentioned above will lead us to a better understanding of the internal structure of the $N(1440)$, $N(1535)$ and $N(1520)$ resonances.



REFERENCES

REFERENCES

- Aiello, M., Giannini, M. M., and Santopinto, E. (1998). Electromagnetic transition form-factors of negative parity nucleon resonances. **J. Phys. G** 24: 753–762.
- Aznauryan, I. G. (2007). Electroexcitation of the roper resonance in relativistic quark models. **Phys. Rev. C** 76: 025212.
- Aznauryan, I. G. and Burkert, V. D. (2012). Nucleon electromagnetic form factors and electroexcitation of low-lying nucleon resonances in a light-front relativistic quark model. **Phys. Rev. C** 85: 055202.
- Aznauryan, I. G. and Burkert, V. D. (2017). Electroexcitation of nucleon resonances of the $[70, 1^-]$ multiplet in a light-front relativistic quark model. **Phys. Rev. C** 95: 065207.
- Aznauryan, I. G., Burkert, V. D., Biselli, A. S., Egiyan, H., Joo, K., Kim, W., Park, K., Smith, L. C., Ungaro, M., Adhikari, K. P., Anghinolfi, M., Avakian, H., Ball, J., Battaglieri, M., Batourine, V., et al. (2009). Electroexcitation of nucleon resonances from clas data on single pion electroproduction. **Phys. Rev. C** 80: 055203.
- Aznauryan, I. G., Burkert, V. D., Kim, W., Park, K., Adams, G., Amaryan, M. J., Ambrozewicz, P., Anghinolfi, M., Asryan, G., Avakian, H., Bagdasaryan, H., Baillie, N., Ball, J. P., Baltzell, N. A., Barrow, S., et al. (2008). Electroexcitation of the roper resonance for $1.7 < Q^2 < 4.5 \text{ GeV}^2$ in $ep \rightarrow en\pi^+$. **Phys. Rev. C** 78: 045209.

- Berger, C., Burkert, V., Knop, G., Langenbeck, B., and Rith, K. (1971). Electromagnetic form-factors of the proton at squared four momentum transfers between 10-fm^{*-2} and 50 fm^{*-2} . **Phys. Lett. B** 35: 87–89.
- Bijker, R., Iachello, F., and Leviatan, A. (1996). Electromagnetic form-factors in a collective model of the nucleon. **Phys. Rev. C** 54: 1935–1953.
- Burkert, V. D., De Vita, R., Battaglieri, M., Ripani, M., and Mokeev, V. (2003). Single quark transition model analysis of electromagnetic nucleon resonance transitions in the $[70,1^-]$ supermultiplet. **Phys. Rev. C** 67: 035204.
- Burkert, V. D. and Lee, T. S. H. (2004). Electromagnetic meson production in the nucleon resonance region. **Int. J. Mod. Phys. E** 13: 1035–1112.
- Burkert, V. D. and Roberts, C. D. (2019). Colloquium: Roper resonance: Toward a solution to the fifty year puzzle. **Rev. Mod. Phys.** 91: 011003.
- Cano, F. and Gonzalez, P. (1998). A Consistent explanation of the Roper phenomenology. **Phys. Lett. B** 431: 270–276.
- Capstick, S. and Keister, B. D. (1995). Baryon current matrix elements in a light front framework. **Phys. Rev. D** 51: 3598–3612.
- Capstick, S., Keister, B. D., and Morel, D. (2007). Nucleon to resonance form factor calculations. **Journal of Physics: Conference Series** 69: 012016.
- Capstick, S. and Roberts, W. (2000). Quark models of baryon masses and decays. **Prog. Part. Nucl. Phys.** 45: S241–S331.
- Close, F. E. (1979). **An Introduction to Quarks and Partons**. London: Academic Press.

- Close, F. E. and Gilman, F. J. (1972). Helicity structure of nucleon resonance electroproduction and the symmetric quark model. **Phys. Lett. B** 38: 541–543.
- Denizli, H., Mueller, J., Dytman, S., Leber, M. L., Levine, R. D., Miles, J., Kim, K. Y., Adams, G., Amarian, M. J., Ambrozewicz, P., Anghinolfi, M., Asavapibhop, B., Asryan, G., Avakian, H., Bagdasaryan, H., et al. (2007). Q^2 dependence of the $S_{11}(1535)$ photocoupling and evidence for a p -wave resonance in η electroproduction. **Phys. Rev. C** 76: 015204.
- Drechsel, D., Kamalov, S. S., and Tiator, L. (2007). Unitary Isobar Model - MAID2007. **Eur. Phys. J. A** 34: 69–97.
- Golli, B., Sirca, S., and Fiolhais, M. (2009). Pion electro-production in the Roper region in chiral quark models. **Eur. Phys. J. A** 42: 185–193.
- Golli, B. and Širca, S. (2013). A chiral quark model for meson electroproduction in the region of D-wave resonances. **Eur. Phys. J. A** 49: 111.
- Hanson, K. M., Dunning, J. R., Goitein, M., Kirk, T., Price, L. E., and Wilson, R. (1973). Large-angle quasielastic electron-deuteron scattering. **Phys. Rev. D** 8: 753–778.
- Höhler, G., Pietarinen, E., Sabba-Stefanescu, I., Borkowski, F., Simon, G., Walther, V., and Wendling, R. (1976). Analysis of electromagnetic nucleon form factors. **Nucl. Phys. B** 114(3): 505–534.
- Štajner, S., Achenbach, P., Beranek, T., Beričić, J., Bernauer, J. C., Bosnar, D., Böhm, R., Correa, L., Denig, A., Distler, M. O., Esser, A., Fonvieille, H., Friedrich, J. M., Friščić, I., Kegel, S., et al. (2017). Beam-recoil

- polarization measurement of π^0 electroproduction on the proton in the region of the roper resonance. **Phys. Rev. Lett.** 119: 022001.
- Janssens, T., Hofstadter, R., Hughes, E. B., and Yearian, M. R. (1966). Proton form factors from elastic electron-proton scattering. **Phys. Rev.** 142: 922–931.
- Jido, D., Döring, M., and Oset, E. (2008). Transition form factors of the $N^*(1535)$ as a dynamically generated resonance. **Phys. Rev. C** 77: 065207.
- Juliá-Díaz, B., Kamano, H., Lee, T.-S. H., Matsuyama, A., Sato, T., and Suzuki, N. (2009). Dynamical coupled-channels analysis of ${}^1\text{H}(e, e' \pi)n$ reactions. **Phys. Rev. C** 80: 025207.
- Julia-Diaz, B., Lee, T. S. H., Matsuyama, A., Sato, T., and Smith, L. C. (2008). Dynamical coupled-channels effects on pion photoproduction. **Phys. Rev. C** 77: 045205.
- Koniuk, R. and Isgur, N. (1980). Baryon decays in a quark model with chromodynamics. **Phys. Rev. D** 21: 1868–1886.
- Li, Q. B. and Riska, D. O. (2006). Role of $q\bar{q}$ components in the $n(1440)$ resonance. **Phys. Rev. C** 74: 015202.
- Li, Z., Burkert, V., and Li, Z. (1992). Electroproduction of the roper resonance as a hybrid state. **Phys. Rev. D** 46: 70–74.
- Merten, D., Loring, U., Kretzschmar, K., Metsch, B., and Petry, H. R. (2002). Electroweak form-factors of nonstrange baryons. **Eur. Phys. J. A** 14: 477–489.

- Moiseev, V. I., Burkert, V. D., Carman, D. S., Elouadrhiri, L., Fedotov, G. V., Golovatch, E. N., Gothe, R. W., Hicks, K., Ishkhanov, B. S., Isupov, E. L., and Skorodumina, I. (2016). New results from the studies of the $n(1440)1/2^+$, $n(1520)3/2^-$, and $\Delta(1620)1/2^-$ resonances in exclusive $ep \rightarrow e'p'\pi^+\pi^-$ electroproduction with the clas detector. **Phys. Rev. C** 93: 025206.
- Moiseev, V. I., Burkert, V. D., Elouadrhiri, L., Fedotov, G. V., Golovatch, E. N., Gothe, R. W., Ishkhanov, B. S., Isupov, E. L., Adhikari, K. P., Aghasyan, M., Anghinolfi, M., Avakian, H., Baghdasaryan, H., Ball, J., Baltzell, N. A., et al. (2012). Experimental study of the $P_{11}(1440)$ and $D_{13}(1520)$ resonances from the clas data on $ep \rightarrow e'\pi^+\pi^-p'$. **Phys. Rev. C** 86: 035203.
- Murphy, J. J., Shin, Y. M., and Skopik, D. M. (1974). Proton form factor from 0.15 to 0.79 fm^{-2} . **Phys. Rev. C** 9: 2125–2129.
- Obukhovskiy, I. T., Faessler, A., Fedorov, D. K., Gutsche, T., and Lyubovitskiy, V. E. (2011). Electroproduction of the roper resonance on the proton: The role of the three-quark core and the molecular $n\sigma$ component. **Phys. Rev. D** 84: 014004.
- Parsaei, S. and Akbar Rajabi, A. (2017). Electromagnetic transitions of the Roper resonance $\gamma^*p \rightarrow p_{11}(1440)$ within the nonrelativistic quark model. **Eur. Phys. J. Plus** 132(10): 413.
- Price, L. E., Dunning, J. R., Goitein, M., Hanson, K., Kirk, T., and Wilson, R. (1971). Backward-angle electron-proton elastic scattering and proton electromagnetic form-factors. **Phys. Rev. D** 4: 45–53.

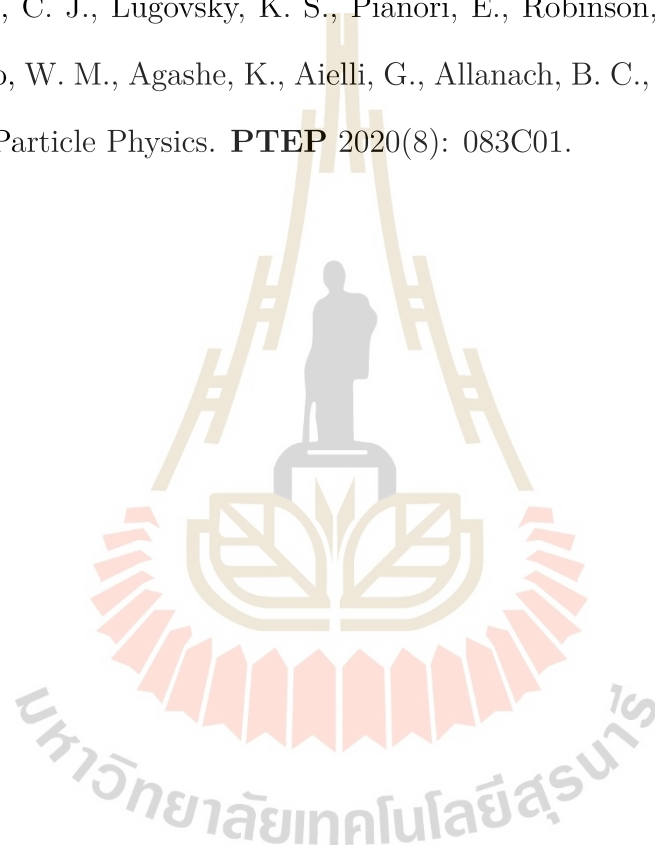
- Ramalho, G., Jido, D., and Tsushima, K. (2012). Valence quark and meson cloud contributions for the $\gamma^*\Lambda \rightarrow \Lambda^*$ and $\gamma^*\Sigma^0 \rightarrow \Lambda^*$ reactions. **Phys. Rev. D** 85: 093014.
- Ramalho, G. and Peña, M. T. (2011). Covariant model for the $\gamma n \rightarrow n(1535)$ transition at high momentum transfer. **Phys. Rev. D** 84: 033007.
- Ramalho, G. and Tsushima, K. (2010). Valence quark contributions for the $\gamma n \rightarrow P_{11}(1440)$ form factors. **Phys. Rev. D** 81: 074020.
- Ramalho, G. and Tsushima, K. (2011). Simple relation between the $\gamma n \rightarrow n(1535)$ helicity amplitudes. **Phys. Rev. D** 84: 051301.
- Roberts, D. S., Kamleh, W., and Leinweber, D. B. (2013). Wave function of the roper from lattice qcd. **Phys. Lett. B** 725: 164–169.
- Ronniger, M. and Metsch, B. C. (2013). Effects of a spin-flavour dependent interaction on light-flavoured baryon helicity amplitudes. **Eur. Phys. J. A** 49: 8.
- Santopinto, E. and Giannini, M. M. (2012). Systematic study of longitudinal and transverse helicity amplitudes in the hypercentral constituent quark model. **Phys. Rev. C** 86: 065202.
- Sarantsev, A., Fuchs, M., Kotulla, M., Thoma, U., Ahrens, J., Annand, J., Anisovich, A., Anton, G., Bantes, R., Bartholomy, O., Beck, R., Beloglazov, Y., Castelijns, R., Crede, V., Ehmanns, A., et al. (2008). New results on the Roper resonance and the P(11) partial wave. **Phys. Lett. B** 659: 94–100.
- Segovia, J. (2016). Strong diquark correlations inside the proton. **EPJ Web Conf.** 113: 05025.

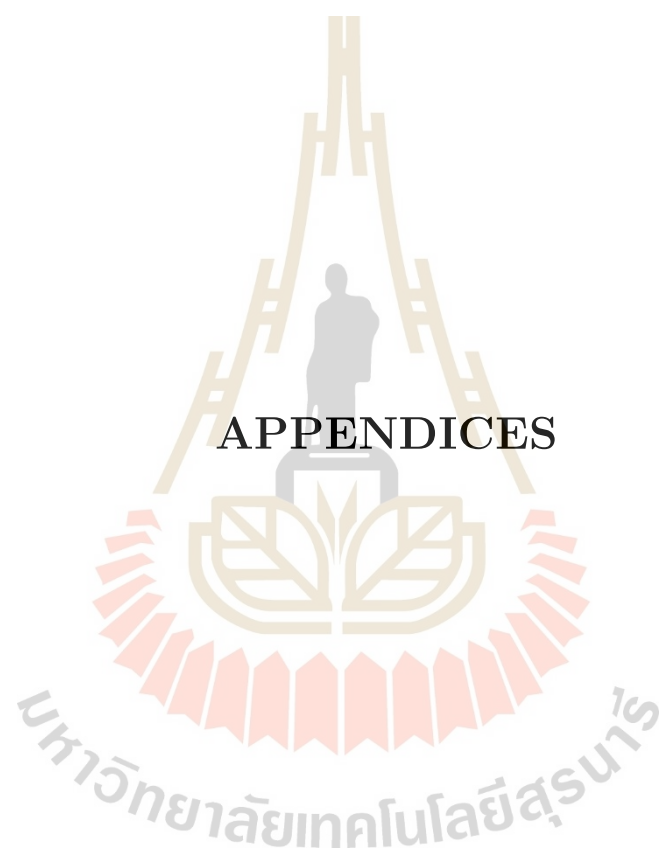
- Segovia, J., El-Bennich, B., Rojas, E., Cloët, I. C., Roberts, C. D., Xu, S.-S., and Zong, H.-S. (2015). Completing the picture of the roper resonance. **Phys. Rev. Lett.** 115: 171801.
- Simon, G. G., Schmitt, C., Borkowski, F., and Walther, V. H. (1980). Absolute electron Proton Cross-Sections at Low Momentum Transfer Measured with a High Pressure Gas Target System. **Nucl. Phys. A** 333: 381–391.
- Tiator, L., Drechsel, D., Kamalov, S. S., and Vanderhaeghen, M. (2009). Baryon Resonance Analysis from MAID. **Chin. Phys. C** 33: 1069–1076.
- Tiator, L., Drechsel, D., Kamalov, S. S., and Vanderhaeghen, M. (2011). Electromagnetic Excitation of Nucleon Resonances. **Eur. Phys. J. ST** 198: 141–170.
- Walker, R. C., Filippone, B. W., Jourdan, J., Milner, R., McKeown, R., Potterveld, D., Andivahis, L., Arnold, R., Benton, D., Bosted, P., deChambrier, G., Lung, A., Rock, S. E., Szalata, Z. M., Para, A., et al. (1994). Measurements of the proton elastic form factors for $1 \leq Q^2 \leq 3$ (GeV/c)² at slac. **Phys. Rev. D** 49: 5671–5689.
- Warns, M., Pfeil, W., and Rollnik, H. (1990). Helicity and isospin asymmetries in the electroproduction of nucleon resonances. **Phys. Rev. D** 42: 2215–2225.
- Xu, K., Kaewsnod, A., Liu, X. Y., Srisuphaphon, S., Limphirat, A., and Yan, Y. (2019). Complete basis for the pentaquark wave function in a group theory approach. **Phys. Rev. C** 100: 065207.
- Xu, K., Kaewsnod, A., Zhao, Z., Liu, X. Y., Srisuphaphon, S., Limphirat, A., and

Yan, Y. (2020). Pentaquark components in low-lying baryon resonances. **Phys. Rev. D** 101: 076025.

Yan, Y. and Srisuphaphon, S. (2012). Construction of multiquark states in group theory. **Prog. Part. Nucl. Phys.** 67: 496–501.

Zyla, P. A., Barnett, R. M., Beringer, J., Dahl, O., Dwyer, D. A., Groom, D. E., Lin, C. J., Lugovsky, K. S., Pianori, E., Robinson, D. J., Wohl, C. G., Yao, W. M., Agashe, K., Aielli, G., Allanach, B. C., et al. (2020). Review of Particle Physics. **PTEP** 2020(8): 083C01.





APPENDICES

APPENDIX A

q^3 AND $q^4\bar{q}$ FULL WAVE FUNCTION IN SU(3)

FLAVOR SYMMETRY

A.1 q^3 full wave function

q^3 baryons wave function and possible J^P , (not including LS coupling for all the cases yet)

(1) $N, L = (0, 0), [56, 0^+]$

$$\begin{aligned}\Psi(q^3)_{Octet} &= \frac{1}{2}\psi_{[111]}^c[\phi_{00s}^2(\Phi_\lambda\chi_\rho + \Phi_\rho\chi_\lambda), J^P = \frac{1}{2}^+ \\ \Psi(q^3)_{Decuplet} &= \frac{1}{\sqrt{2}}\psi_{[111]}^c\Phi_S(\phi_{00\lambda}^2\chi_\lambda + \phi_{00\rho}^2\chi_\rho), J^P = \frac{3}{2}^+\end{aligned}\quad (A.1)$$

(2) $N, L = (1, 1), [70, 1^-]$ (for non-strange nucleon state singlet state doesn't exist)

$$\begin{aligned}\Psi_{Singlet}^{(q^3)} &= \frac{1}{\sqrt{2}}\psi_{[111]}^c\Phi_\Lambda(\phi_{1m\lambda}^1\chi_\rho - \phi_{1m\rho}^1\chi_\lambda), J^P = \frac{1}{2}^-, \frac{3}{2}^- \\ \Psi_{Octet1}^{(q^3)} &= \frac{1}{2}\psi_{[111]}^c[\phi_{1m\rho}^1(\Phi_\lambda\chi_\rho + \Phi_\rho\chi_\lambda), J^P = \frac{1}{2}^-, \frac{3}{2}^- \\ &\quad + \phi_{1m\lambda}^1(\Phi_\rho\chi_\rho - \Phi_\lambda\chi_\lambda)], \\ \Psi_{Octet2}^{(q^3)} &= \frac{1}{\sqrt{2}}\psi_{[111]}^c\chi_S(\phi_{1m\lambda}^1\Phi_\lambda + \phi_{1m\rho}^1\Phi_\rho), J^P = \frac{1}{2}^-, \frac{3}{2}^-, \frac{5}{2}^- \\ \Psi_{Decuplet}^{(q^3)} &= \frac{1}{\sqrt{2}}\psi_{[111]}^c\Phi_S(\phi_{1m\lambda}^1\chi_\lambda + \phi_{1m\rho}^1\chi_\rho), J^P = \frac{1}{2}^-, \frac{3}{2}^-\end{aligned}\quad (A.2)$$

(3) $N, L = (2, 0)$, $[56, 0^+]$ spatial part symmetric

$$\begin{aligned}\Psi_{Octet}^{(q^3)} &= \frac{1}{\sqrt{2}}\psi_{[111]}^c\phi_{00S}^2(\Phi_\rho\chi_\rho + \Phi_\lambda\chi_\lambda), \quad J^P = \frac{1}{2}^+ \\ \Psi_{Decuplet}^{(q^3)} &= \psi_{[111]}^c\phi_{00S}^2\Phi_S\chi_S, \quad J^P = \frac{3}{2}^+\end{aligned}\quad (\text{A.3})$$

$N, L = (2, 0)$, $[70, 0^+]$ spatial part mixed symmetric

$$\begin{aligned}\Psi_{Singlet}^{(q^3)} &= \frac{1}{\sqrt{2}}\psi_{[111]}^c\Phi_A(\phi_{00\lambda}^2\chi_\rho - \phi_{00\rho}^2\chi_\lambda), \quad J^P = \frac{1}{2}^+ \\ \Psi_{Octet1}^{(q^3)} &= \frac{1}{2}\psi_{[111]}^c[\phi_{00\rho}^2(\Phi_\lambda\chi_\rho + \Phi_\rho\chi_\lambda), \quad J^P = \frac{1}{2}^+ \\ &\quad + \phi_{00\lambda}^2(\Phi_\rho\chi_\rho - \Phi_\lambda\chi_\lambda)], \\ \Psi_{Octet2}^{(q^3)} &= \frac{1}{\sqrt{2}}\psi_{[111]}^c\chi_S(\phi_{00\lambda}^2\Phi_\lambda + \phi_{00\rho}^2\Phi_\rho), \quad J^P = \frac{3}{2}^+ \\ \Psi_{Decuplet}^{(q^3)} &= \frac{1}{\sqrt{2}}\psi_{[111]}^c\Phi_S(\phi_{00\lambda}^2\chi_\lambda + \phi_{00\rho}^2\chi_\rho), \quad J^P = \frac{1}{2}^+\end{aligned}\quad (\text{A.4})$$

(4) $N, L = (2, 2)$, $[56, 2^+]$ spatial part symmetric

$$\begin{aligned}\Psi_{Octet}^{(q^3)} &= \frac{1}{\sqrt{2}}\psi_{[111]}^c\phi_{2mS}^2(\Phi_\rho\chi_\rho + \Phi_\lambda\chi_\lambda), \quad J^P = \frac{3}{2}^+, \frac{5}{2}^+ \\ \Psi_{Decuplet}^{(q^3)} &= \psi_{[111]}^c\phi_{2mS}^2\Phi_S\chi_S, \quad J^P = \frac{1}{2}^+, \frac{3}{2}^+, \frac{5}{2}^+, \frac{7}{2}^+\end{aligned}\quad (\text{A.5})$$

$N, L = (2, 2)$, $[70, 2^+]$ spatial part mixed symmetric (for non-strange nucleon state singlet state doesn't exist)

$$\begin{aligned}\Psi_{Singlet}^{(q^3)} &= \frac{1}{\sqrt{2}}\psi_{[111]}^c\Phi_A(\phi_{2m\lambda}^2\chi_\rho - \phi_{2m\rho}^2\chi_\lambda), \quad J^P = \frac{3}{2}^+, \frac{5}{2}^+ \\ \Psi_{Octet1}^{(q^3)} &= \frac{1}{2}\psi_{[111]}^c[\phi_{2m\rho}^2(\Phi_\lambda\chi_\rho + \Phi_\rho\chi_\lambda), \quad J^P = \frac{3}{2}^+, \frac{5}{2}^+ \\ &\quad + \phi_{2m\lambda}^2(\Phi_\rho\chi_\rho - \Phi_\lambda\chi_\lambda)],\end{aligned}$$

$$\begin{aligned}
\Psi_{Octet2}^{(q^3)} &= \frac{1}{\sqrt{2}} \psi_{[111]}^c \chi_S (\phi_{2m\lambda}^2 \Phi_\lambda + \phi_{2m\rho}^2 \Phi_\rho), \quad J^P = \frac{1^+}{2}, \frac{3^+}{2}, \frac{5^+}{2}, \frac{7^+}{2} \\
\Psi_{Decuplet}^{(q^3)} &= \frac{1}{\sqrt{2}} \psi_{[111]}^c \Phi_S (\phi_{2m\lambda}^2 \chi_\lambda + \phi_{2m\rho}^2 \chi_\rho), \quad J^P = \frac{3^+}{2}, \frac{5^+}{2}
\end{aligned} \tag{A.6}$$

A.2 $q^2\bar{Q}$ full wave function

In q^2Q charm baryons and bottom baryons,

$$\begin{aligned}
\Psi^{(q^2)} &= \Psi_{[11]}^c \Psi_{[x]_s}^{sf}, \\
\Psi_{[x]_s}^{sf} &= \sum_{i,j} a_{ij} \Psi_{[X]_i}^s \Psi_{[Y]_j}^f
\end{aligned} \tag{A.7}$$

In which,

$$\begin{aligned}
\Psi_{[X]_i}^s &= \{ \Psi_{[2]_S}^s, \Psi_{[11]_A}^s \} \\
\Psi_{[Y]_j}^f &= \{ \Psi_{[2]_S}^f, \Psi_{[11]_A}^f \}
\end{aligned} \tag{A.8}$$

The possible $\Psi_{sf}^{(q^2)}$ wave function are,

$$\Psi_{[x]_s}^{sf} = \Psi_{[2]_S}^s \Psi_{[2]_S}^f, \Psi_{[11]_A}^s \Psi_{[11]_A}^f \tag{A.9}$$

The total color wave function is the same as low lying baryon

$$\begin{aligned}
\Psi_{[111]}^c &= (RGB - GRB + GBR - BGR \\
&\quad + BRG - RBG)
\end{aligned} \tag{A.10}$$

So the total q^2Q wave function is the coupling of $\Psi_{[x]_s}^{sf}$ with the single heavy quark, which is,

$$\Psi(q^2Q) = \Psi_{[111]}^c \Psi_{[3]}^o (\Psi_{[x]_s}^{(q^2)sf} \otimes \Psi(Q)^{sf}) \tag{A.11}$$

A.3 $q^4\bar{q}$ full wave function

$q^4\bar{q}$ configuration young tabloid construction

$$\begin{array}{|c|c|} \hline \square & \square \\ \hline \square & \square \\ \hline \square & \square \\ \hline \end{array} (q^4\bar{q}) = \begin{array}{|c|c|} \hline \square & \square \\ \hline \square & \\ \hline \square & \\ \hline \end{array} (q^4) \otimes \begin{array}{|c|} \hline \square \\ \hline \square \\ \hline \end{array} (\bar{q})$$

For flavor configuration [211], there is no possible states for non-strange baryons.

For q^4 systems, the projection operators according to Young tableaux of ρ , λ and η types,

The projection operator of $\begin{array}{|c|c|} \hline \square & \square \\ \hline \square & \\ \hline \square & \\ \hline \end{array}$

$$\begin{aligned} P_{[211]_\rho} &= 6 - 6(12) + 3(13) - 5(14) + 3(23) - 5(24) - 2(34) \\ &\quad + 2(12)(34) - 4(14)(23) - 4(13)(24) \\ &\quad - 3(123) + 5(124) - 3(132) - (134) + 5(142) - (143) - (234) - (243) \\ &\quad (1234) + (1243) + 4(1324) + (1342) + 4(1423) + (1432), \end{aligned}$$

$$\begin{aligned} P_{[211]_\lambda} &= 2 + 2(12) - (13) - (14) - (23) - (24) - 2(34) \\ &\quad - 2(12)(34) \\ &\quad - (123) - (124) - (132) + (134) - (142) + (143) + (234) + (243) \\ &\quad + (1234) + (1243) + (1342) + (1432), \end{aligned}$$

$$\begin{aligned} P_{[211]_\eta} &= 3 - 3(12) - 3(13) + (14) - 3(23) + (24) + (34) \\ &\quad - (12)(34) - (14)(23) - (13)(24) \\ &\quad + 3(123) - (124) + 3(132) - (134) - (142) - (143) - (234) - (243) \end{aligned}$$

$$+(1234) + (1243) + (1324) + (1342) + (1423) + (1432). \quad (\text{A.12})$$

q^4 color wave functions can be derived by applying the λ -, ρ - and η -type projection operators of the S_4 $IR[211]$ in Yamanouchi basis,

$$\left\langle \begin{array}{|c|c|} \hline 1 & 2 \\ \hline 3 & \\ \hline 4 & \\ \hline \end{array}, \begin{array}{|c|c|} \hline R & R \\ \hline G & \\ \hline B & \\ \hline \end{array} \right\rangle = P_{[211]_\lambda}(RRGB) \implies \psi_{[211]_\lambda}^c(R) :$$

$$\frac{1}{\sqrt{16}}(2|RRGB\rangle - 2|RRBG\rangle - |GRRB\rangle - |RGRB\rangle - |BRGR\rangle \\ - |RBGR\rangle + |BRRG\rangle + |GRBR\rangle + |RBRG\rangle + |RGBR\rangle)$$

$$\left\langle \begin{array}{|c|c|} \hline 1 & 3 \\ \hline 2 & \\ \hline 4 & \\ \hline \end{array}, \begin{array}{|c|c|} \hline R & R \\ \hline G & \\ \hline B & \\ \hline \end{array} \right\rangle = P_{[211]_\rho}(RGRB) \implies \psi_{[211]_\rho}^c(R) :$$

$$\frac{1}{\sqrt{48}}(3|RGRB\rangle - 3|GRRB\rangle + 3|BRRG\rangle - 3|RBRG\rangle + 2|GBRR\rangle \\ - 2|BGRR\rangle - |BRGR\rangle + |RBGR\rangle + |GRBR\rangle - |RGBR\rangle)$$

$$\left\langle \begin{array}{|c|c|} \hline 1 & 4 \\ \hline 2 & \\ \hline 3 & \\ \hline \end{array}, \begin{array}{|c|c|} \hline R & R \\ \hline G & \\ \hline B & \\ \hline \end{array} \right\rangle = P_{[211]_\eta}(RGBR) \implies \psi_{[211]_\eta}^c(R) :$$

$$\frac{1}{\sqrt{6}}(|RGBR\rangle + |GBRR\rangle + |BRGR\rangle - |RBGR\rangle - |GRBR\rangle - |BGRR\rangle)$$

The singlet color wave function $\Psi_{[211]_j}^c$ ($j = \lambda, \rho, \eta$) of pentaquarks is given by

$$\Psi_{[211]_j}^c = \frac{1}{\sqrt{3}} \left(\psi_{[211]_j}^c(R) \bar{R} + \psi_{[211]_j}^c(G) \bar{G} + \psi_{[211]_j}^c(B) \bar{B} \right).$$

q^3 and $Q\bar{Q}$ in color singlet state:

$$\begin{aligned}\Psi(q^3)_{Octet} &= \frac{1}{\sqrt{2}}\Psi_{[111]}^c\Psi_{[3]}^o(\Psi_{[21]_\lambda}^f\Psi_{[21]_\lambda}^s + \Psi_{[21]_\rho}^f\Psi_{[21]_\rho}^s), \\ \Psi(q^3)_{Decuplet} &= \Psi_{[111]}^c\Psi_{[3]}^o\Psi_{[3]_{sym}}^f\Psi_{[3]_{sym}}^s\end{aligned}\quad (A.13)$$

Hidden color states, q^3 and $Q\bar{Q}$ ($c\bar{c}$, $b\bar{b}$) in color [21] states:

$$\begin{aligned}\Psi(q^3) &= \frac{1}{\sqrt{2}}(\Psi_{[21]_\lambda}^c\Psi_{[21]_\rho}^{sf} - \Psi_{[21]_\rho}^c\Psi_{[21]_\lambda}^{sf}), \\ \Psi^{sf} &= \sum_{i,j} a_{ij}\Psi_{[X]_i}^s\Psi_{[Y]_j}^f\end{aligned}\quad (A.14)$$

with

$$\Psi_{[X]_i}^s = \{\Psi_{[3]_S}^s, \Psi_{[21]_{\lambda,\rho}}^s\}, \quad \Psi_{[Y]_j}^f = \{\Psi_{[3]_S}^f, \Psi_{[21]_{\lambda,\rho}}^f\}\quad (A.15)$$

With color wave function:

$$\Psi_{[222]}^c = \frac{1}{\sqrt{8}}\sum_i \Psi_{[21]_i}^c(q^3)\Psi_{[21]_i}^c(Q\bar{Q})\quad (A.16)$$

And $q^3Q\bar{Q}$ ($q^3c\bar{c}, q^3b\bar{b}$) color singlet young tabloid construction

$$\begin{array}{|c|c|} \hline & \\ \hline & \\ \hline & \\ \hline \end{array} (q^4\bar{q}) = \begin{array}{|c|} \hline \\ \hline \\ \hline \\ \hline \end{array} (q^3) \otimes \begin{array}{|c|} \hline \\ \hline \\ \hline \\ \hline \end{array} (Q\bar{Q})$$

$q^3Q\bar{Q}$ ($q^3c\bar{c}, q^3b\bar{b}$) hidden color octet young tabloid construction

$$\begin{array}{|c|c|} \hline & \\ \hline & \\ \hline & \\ \hline \end{array} (q^4\bar{q}) = \begin{array}{|c|c|} \hline & \\ \hline & \\ \hline & \\ \hline \end{array} (q^3) \otimes \begin{array}{|c|c|} \hline & \\ \hline & \\ \hline & \\ \hline \end{array} (Q\bar{Q})$$

may be discussed in the future.

APPENDIX B

SPATIAL WAVE FUNCTION

Here the spatial wave function of q^3 and $q^4\bar{q}$ in the harmonic oscillator basis are displayed, all the principle quantum number N stands for the real harmonic oscillation band which means the physical state since all functions fulfill the permutation symmetry of corresponding configuration. For $L = 0$, 56 multiplets till $N = 40$ states are showed below, while 70 multiplets is till $N = 20$. And $L = 1$, 70 multiplets is for $N = 19$ and $L = 2$, 56 multiplets show $N = 20$.

For q^3 permutation symmetry, ρ and λ type spatial wave function is listed below. The total principle quantum number is N is written as:

$$N = 2n_\rho + l_\rho + 2n_\lambda + l_\lambda \quad (\text{B.1})$$

C is the normalization factor.

Table B.1 Normalized 3-quark spatial wave functions $L = 2 \ 2N \ 2 \ 2$.

NLM	$C(n_\rho, l_\rho, n_\lambda, l_\lambda)$
$000_{[3]_S}$	$(0, 0, 0, 0)$
$200_{[3]_S}$	$\frac{1}{\sqrt{2}}(1, 0, 0, 0), \frac{1}{\sqrt{2}}(0, 0, 1, 0)$
$400_{[3]_S}$	$\frac{\sqrt{5}}{4}(2, 0, 0, 0), \sqrt{\frac{3}{8}}(1, 0, 1, 0), \frac{\sqrt{5}}{4}(0, 0, 2, 0)$
$600_{[3]_S}$	$\frac{\sqrt{14}}{8}(3, 0, 0, 0), \frac{\sqrt{18}}{8}(2, 0, 1, 0), \frac{\sqrt{18}}{8}(1, 0, 2, 0), \frac{\sqrt{14}}{8}(0, 0, 3, 0)$
$800_{[3]_S}$	$\frac{\sqrt{42}}{16}(4, 0, 0, 0), \frac{\sqrt{14}}{8}(3, 0, 1, 0), \frac{\sqrt{15}}{8}(2, 0, 2, 0), \frac{\sqrt{14}}{8}(1, 0, 3, 0),$ $\frac{\sqrt{42}}{16}(0, 0, 4, 0)$
$1000_{[3]_S}$	$\frac{\sqrt{33}}{16}(5, 0, 0, 0), \frac{\sqrt{45}}{16}(4, 0, 1, 0), \frac{\sqrt{50}}{16}(3, 0, 2, 0), \frac{\sqrt{50}}{16}(2, 0, 3, 0),$

Table B.1 (Continued) Normalized 3-quark spatial wave functions $L = 2 \ 2N \ 2$

NLM	$C(n_\rho, l_\rho, n_\lambda, l_\lambda)$
	$\frac{\sqrt{45}}{16}(1, 0, 4, 0), \frac{\sqrt{33}}{16}(0, 0, 5, 0)$
$1200_{[3]_S}$	$\frac{\sqrt{429}}{64}(6, 0, 0, 0), \frac{\sqrt{594}}{64}(5, 0, 1, 0), \frac{\sqrt{675}}{64}(4, 0, 2, 0), \frac{\sqrt{175}}{32}(3, 0, 3, 0),$ $\frac{\sqrt{675}}{64}(2, 0, 4, 0), \frac{\sqrt{594}}{64}(1, 0, 5, 0), \frac{\sqrt{429}}{64}(0, 0, 6, 0)$
$1400_{[3]_S}$	$\frac{\sqrt{1430}}{128}(7, 0, 0, 0), \frac{\sqrt{2002}}{128}(6, 0, 1, 0), \frac{\sqrt{2310}}{128}(5, 0, 2, 0), \frac{\sqrt{2450}}{128}(4, 0, 3, 0),$ $\frac{\sqrt{2450}}{128}(3, 0, 4, 0), \frac{\sqrt{2310}}{128}(2, 0, 5, 0), \frac{\sqrt{2002}}{128}(1, 0, 6, 0), \frac{\sqrt{1430}}{128}(0, 0, 7, 0)$
$1600_{[3]_S}$	$\frac{\sqrt{4862}}{256}(8, 0, 0, 0), \frac{\sqrt{429}}{64}(7, 0, 1, 0), \frac{\sqrt{2002}}{128}(6, 0, 2, 0), \frac{\sqrt{539}}{64}(5, 0, 3, 0),$ $\frac{\sqrt{2205}}{128}(4, 0, 4, 0), \frac{\sqrt{539}}{64}(3, 0, 5, 0), \frac{\sqrt{2002}}{128}(2, 0, 6, 0), \frac{\sqrt{429}}{64}(1, 0, 7, 0),$ $\frac{\sqrt{4862}}{256}(0, 0, 8, 0)$
$1800_{[3]_S}$	$\frac{\sqrt{4199}}{256}(9, 0, 0, 0), \frac{\sqrt{5967}}{256}(8, 0, 1, 0), \frac{\sqrt{1755}}{128}(7, 0, 2, 0), \frac{\sqrt{1911}}{128}(6, 0, 3, 0),$ $\frac{\sqrt{7938}}{256}(5, 0, 4, 0), \frac{\sqrt{7938}}{256}(4, 0, 5, 0), \frac{\sqrt{1911}}{128}(3, 0, 6, 0), \frac{\sqrt{1755}}{128}(2, 0, 7, 0),$ $\frac{\sqrt{5967}}{256}(1, 0, 8, 0), \frac{\sqrt{4199}}{256}(0, 0, 9, 0)$
$2000_{[3]_S}$	$\frac{\sqrt{58786}}{1024}(10, 0, 0, 0), \frac{\sqrt{20995}}{512}(9, 0, 1, 0), \frac{\sqrt{99450}}{1024}(8, 0, 2, 0), \frac{\sqrt{6825}}{256}(7, 0, 3, 0),$ $\frac{\sqrt{28665}}{512}(6, 0, 4, 0), \frac{\sqrt{29106}}{512}(5, 0, 5, 0), \frac{\sqrt{28665}}{512}(4, 0, 6, 0), \frac{\sqrt{6825}}{256}(3, 0, 7, 0),$ $\frac{\sqrt{99450}}{1024}(2, 0, 8, 0), \frac{\sqrt{20995}}{512}(1, 0, 9, 0), \frac{\sqrt{58786}}{1024}(0, 0, 10, 0)$
$2200_{[3]_S}$	$\frac{\sqrt{52003}}{1024}(11, 0, 0, 0), \frac{\sqrt{74613}}{1024}(10, 0, 1, 0), \frac{\sqrt{88825}}{1024}(9, 0, 2, 0), \frac{\sqrt{98175}}{1024}(8, 0, 3, 0),$ $\frac{\sqrt{103950}}{1024}(7, 0, 4, 0), \frac{\sqrt{106722}}{1024}(6, 0, 5, 0), \frac{\sqrt{106722}}{1024}(5, 0, 6, 0), \frac{\sqrt{103950}}{1024}(4, 0, 7, 0),$ $\frac{\sqrt{98175}}{1024}(3, 0, 8, 0), \frac{\sqrt{88825}}{1024}(2, 0, 9, 0), \frac{\sqrt{74613}}{1024}(1, 0, 10, 0), \frac{\sqrt{52003}}{1024}(0, 0, 11, 0)$

Table B.2 Normalized 3-quark spatial wave functions for $L = 0 \ 2N \ 0 \ 0 \ 70$ multiplet.

NLM	$C(n_\rho, l_\rho, n_\lambda, l_\lambda)$
$200_{[21]_\rho}$	$(0, 1, 0, 1)$

Table B.2 (Continued) Normalized 3-quark spatial wave functions for $L = 0$ $2N$ $0\ 0\ 70$ multiplet.

NLM	$C(n_\rho, l_\rho, n_\lambda, l_\lambda)$
$200_{[21]_\lambda}$	$\frac{1}{\sqrt{2}}(1, 0, 0, 0), -\frac{1}{\sqrt{2}}(0, 0, 1, 0)$
$400_{[21]_\rho}$	$\frac{1}{\sqrt{2}}(1, 1, 0, 1), \frac{1}{\sqrt{2}}(0, 1, 1, 1)$
$400_{[21]_\lambda}$	$\frac{1}{\sqrt{2}}(2, 0, 0, 0), -\frac{1}{\sqrt{2}}(0, 0, 2, 0)$
$600_{[21]_\rho}$	$\frac{\sqrt{42}}{12}(2, 1, 0, 1), \frac{\sqrt{15}}{6}(1, 1, 1, 1), \frac{\sqrt{42}}{12}(0, 1, 2, 1)$
$600_{[21]_\lambda}$	$\frac{\sqrt{7}}{4}(3, 0, 0, 0), \frac{1}{4}(2, 0, 1, 0), -\frac{1}{4}(1, 0, 2, 0), -\frac{\sqrt{7}}{4}(0, 0, 3, 0)$
$800_{[21]_\rho}$	$\frac{\sqrt{3}}{4}(3, 1, 0, 1), \frac{\sqrt{5}}{4}(2, 1, 1, 1), \frac{\sqrt{5}}{4}(1, 1, 2, 1), \frac{\sqrt{3}}{4}(0, 1, 3, 1)$
$800_{[21]_\lambda}$	$\frac{\sqrt{6}}{4}(4, 0, 0, 0), \frac{\sqrt{2}}{4}(3, 0, 1, 0), -\frac{\sqrt{2}}{4}(1, 0, 2, 0), -\frac{\sqrt{6}}{4}(1, 0, 3, 0)$
$1000_{[21]_\rho}$	$\frac{\sqrt{33}}{16}(4, 1, 0, 1), \frac{\sqrt{15}}{8}(3, 1, 1, 1), \frac{\sqrt{70}}{16}(2, 1, 2, 1), \frac{\sqrt{15}}{8}(1, 1, 3, 1),$ $\frac{\sqrt{33}}{16}(0, 1, 4, 1)$
$1000_{[21]_\lambda}$	$\frac{\sqrt{330}}{32}(5, 0, 0, 0), \frac{9\sqrt{2}}{32}(4, 0, 1, 0), \frac{\sqrt{5}}{16}(3, 0, 2, 0), -\frac{\sqrt{5}}{16}(2, 0, 3, 0),$ $-\frac{9\sqrt{2}}{32}(1, 0, 4, 0), -\frac{\sqrt{330}}{32}(0, 0, 5, 0)$
$1200_{[21]_\rho}$	$\frac{\sqrt{858}}{96}(5, 1, 0, 1), \frac{5\sqrt{66}}{96}(4, 1, 1, 1), \frac{5\sqrt{21}}{48}(3, 1, 2, 1), \frac{5\sqrt{21}}{48}(2, 1, 3, 1),$ $\frac{5\sqrt{66}}{96}(1, 1, 4, 1), \frac{\sqrt{858}}{96}(0, 1, 5, 1)$
$1200_{[21]_\lambda}$	$\frac{\sqrt{286}}{32}(6, 0, 0, 0), \frac{\sqrt{11}}{8}(5, 0, 1, 0), \frac{5\sqrt{2}}{32}(4, 0, 2, 0), -\frac{5\sqrt{2}}{32}(2, 0, 4, 0),$ $-\frac{\sqrt{11}}{8}(1, 0, 5, 0), -\frac{\sqrt{286}}{32}(0, 0, 6, 0)$
$1400_{[21]_\rho}$	$\frac{\sqrt{286}}{64}(6, 1, 0, 1), \frac{\sqrt{143}}{32}(5, 1, 1, 1), \frac{\sqrt{770}}{64}(4, 1, 2, 1), \frac{\sqrt{210}}{32}(3, 1, 3, 1),$ $\frac{\sqrt{770}}{64}(2, 1, 4, 1), \frac{\sqrt{143}}{32}(1, 1, 5, 1), \frac{\sqrt{286}}{64}(0, 1, 6, 1)$
$1400_{[21]_\lambda}$	$\frac{\sqrt{1001}}{64}(7, 0, 0, 0), \frac{\sqrt{715}}{64}(6, 0, 1, 0), \frac{3\sqrt{33}}{64}(5, 0, 2, 0), \frac{\sqrt{35}}{64}(4, 0, 3, 0),$ $-\frac{\sqrt{35}}{64}(3, 0, 4, 0), -\frac{3\sqrt{33}}{64}(2, 0, 5, 0), -\frac{\sqrt{715}}{64}(1, 0, 6, 0), -\frac{\sqrt{1001}}{64}(0, 0, 7, 0)$
$1600_{[21]_\rho}$	$\frac{\sqrt{221}}{64}(7, 1, 0, 1), \frac{\sqrt{455}}{64}(6, 1, 1, 1), \frac{7\sqrt{13}}{64}(5, 1, 2, 1), \frac{\sqrt{2450}}{128}(4, 1, 3, 1),$ $\frac{\sqrt{2450}}{128}(3, 1, 4, 1), \frac{7\sqrt{13}}{64}(2, 1, 5, 1), \frac{\sqrt{455}}{64}(1, 1, 6, 1), \frac{\sqrt{221}}{64}(0, 1, 7, 1)$
$1600_{[21]_\lambda}$	$\frac{\sqrt{221}}{32}(8, 0, 0, 0), \frac{3\sqrt{78}}{64}(7, 0, 1, 0), \frac{\sqrt{91}}{32}(6, 0, 2, 0), \frac{7\sqrt{2}}{64}(5, 0, 3, 0),$

Table B.2 (Continued) Normalized 3-quark spatial wave functions for $L = 0$ $2N$ $0\ 0\ 70$ multiplet.

NLM	$C(n_\rho, l_\rho, n_\lambda, l_\lambda)$
	$-\frac{7\sqrt{2}}{64}(3, 0, 5, 0), -\frac{\sqrt{91}}{32}(2, 0, 6, 0), -\frac{3\sqrt{78}}{64}(1, 0, 7, 0), -\frac{\sqrt{221}}{32}(0, 0, 8, 0)$
$1800_{[21]_\rho}$	$\frac{\sqrt{25194}}{768}(8, 1, 0, 1), \frac{\sqrt{3315}}{192}(7, 1, 1, 1), \frac{7\sqrt{390}}{384}(6, 1, 2, 1), \frac{7\sqrt{13}}{64}(5, 1, 3, 1),$ $\frac{7\sqrt{55}}{128}(4, 1, 4, 1), \frac{7\sqrt{13}}{64}(3, 1, 5, 1), \frac{7\sqrt{390}}{384}(2, 1, 6, 1), \frac{\sqrt{3315}}{192}(1, 1, 7, 1),$ $\frac{\sqrt{25194}}{768}(0, 1, 8, 1)$
$1800_{[21]_\lambda}$	$\frac{\sqrt{12597}}{256}(9, 0, 0, 0), \frac{7\sqrt{221}}{256}(8, 0, 1, 0), \frac{5\sqrt{65}}{128}(7, 0, 2, 0), \frac{7\sqrt{13}}{128}(6, 0, 3, 0),$ $\frac{7\sqrt{6}}{256}(5, 0, 4, 0), -\frac{7\sqrt{6}}{256}(4, 0, 5, 0), -\frac{7\sqrt{13}}{128}(3, 0, 6, 0), -\frac{5\sqrt{65}}{128}(2, 0, 7, 0),$ $-\frac{7\sqrt{221}}{256}(1, 0, 8, 0), -\frac{\sqrt{12597}}{256}(0, 0, 9, 0)$
$2000_{[21]_\rho}$	$\frac{\sqrt{2261}}{256}(9, 1, 0, 1), \frac{\sqrt{4845}}{256}(8, 1, 1, 1), \frac{\sqrt{1785}}{128}(7, 1, 2, 1), \frac{21\sqrt{5}}{128}(6, 1, 3, 1),$ $\frac{21\sqrt{22}}{256}(5, 1, 4, 1), \frac{21\sqrt{22}}{256}(4, 1, 5, 1), \frac{21\sqrt{5}}{128}(3, 1, 6, 1), \frac{\sqrt{1785}}{128}(2, 1, 7, 1),$ $\frac{\sqrt{4845}}{256}(1, 1, 8, 1), \frac{\sqrt{2261}}{256}(0, 1, 9, 1)$
$2000_{[21]_\lambda}$	$\frac{\sqrt{11305}}{256}(10, 0, 0, 0), \frac{\sqrt{646}}{64}(9, 0, 1, 0), \frac{9\sqrt{85}}{256}(8, 0, 2, 0), \frac{\sqrt{210}}{64}(7, 0, 3, 0),$ $\frac{21\sqrt{2}}{256}(6, 0, 4, 0), -\frac{21\sqrt{2}}{256}(4, 0, 6, 0), -\frac{\sqrt{210}}{64}(3, 0, 7, 0), -\frac{9\sqrt{85}}{256}(2, 0, 8, 0),$ $-\frac{\sqrt{646}}{64}(1, 0, 9, 0), -\frac{\sqrt{11305}}{256}(0, 0, 10, 0)$

Table B.3 Normalized 3-quark spatial wave functions for $L = 1$ $2N + 1$ $1\ 1\ 70$ multiplet.

NLM	$C(n_\rho, l_\rho, n_\lambda, l_\lambda)$
$111_{[21]_\rho}$	$(0, 1, 0, 0)$
$111_{[21]_\lambda}$	$(0, 0, 0, 1)$
$311_{[21]_\rho}$	$\frac{\sqrt{10}}{4}(1, 1, 0, 0), \frac{\sqrt{6}}{4}(0, 1, 1, 0)$
$311_{[21]_\lambda}$	$\frac{\sqrt{10}}{4}(0, 0, 1, 1), \frac{\sqrt{6}}{4}(1, 0, 0, 1)$
$511_{[21]_\rho}$	$\frac{\sqrt{7}}{4}(2, 1, 0, 0), \frac{\sqrt{6}}{4}(1, 1, 1, 0), \frac{\sqrt{3}}{4}(0, 1, 2, 0)$

Table B.3 (Continued) Normalized 3-quark spatial wave functions for $L = 1$
 $2N + 1 \quad 1 \quad 1 \quad 70$ multiplet.

NLM	$C(n_\rho, l_\rho, n_\lambda, l_\lambda)$
$511_{[21]_\lambda}$	$\frac{\sqrt{7}}{4}(0, 0, 2, 1), \frac{\sqrt{6}}{4}(1, 0, 1, 1), \frac{\sqrt{3}}{4}(2, 0, 0, 1)$
$711_{[21]_\rho}$	$\frac{\sqrt{21}}{8}(3, 1, 0, 0), \frac{\sqrt{21}}{8}(2, 1, 1, 0), \frac{\sqrt{15}}{8}(1, 1, 2, 0), \frac{\sqrt{7}}{8}(0, 1, 3, 0)$
$711_{[21]_\lambda}$	$\frac{\sqrt{21}}{8}(0, 0, 3, 1), \frac{\sqrt{21}}{8}(1, 0, 2, 1), \frac{\sqrt{15}}{8}(2, 0, 1, 1), \frac{\sqrt{7}}{8}(3, 0, 0, 1)$
$911_{[21]_\rho}$	$\frac{\sqrt{66}}{16}(4, 1, 0, 0), \frac{\sqrt{18}}{8}(3, 1, 1, 0), \frac{\sqrt{15}}{8}(2, 1, 2, 0), \frac{\sqrt{10}}{8}(1, 1, 3, 0),$ $\frac{\sqrt{18}}{16}(0, 1, 4, 0)$
$911_{[21]_\lambda}$	$\frac{\sqrt{66}}{16}(0, 0, 4, 1), \frac{\sqrt{18}}{8}(1, 0, 3, 1), \frac{\sqrt{15}}{8}(2, 0, 2, 1), \frac{\sqrt{10}}{8}(3, 0, 1, 1),$ $\frac{\sqrt{18}}{16}(4, 0, 0, 1)$
$1111_{[21]_\rho}$	$\frac{\sqrt{858}}{64}(5, 1, 0, 0), \frac{3\sqrt{110}}{64}(4, 1, 1, 0), \frac{15}{32}(3, 1, 2, 0), \frac{5\sqrt{7}}{32}(2, 1, 3, 0),$ $\frac{15\sqrt{2}}{64}(1, 1, 4, 0), \frac{3\sqrt{22}}{64}(0, 1, 5, 0)$
$1111_{[21]_\lambda}$	$\frac{\sqrt{858}}{64}(0, 0, 5, 1), \frac{3\sqrt{110}}{64}(1, 0, 4, 1), \frac{15}{32}(2, 0, 3, 1), \frac{5\sqrt{7}}{32}(3, 0, 2, 1),$ $\frac{15\sqrt{2}}{64}(4, 0, 1, 1), \frac{3\sqrt{22}}{64}(5, 0, 0, 1)$
$1311_{[21]_\rho}$	$\frac{\sqrt{715}}{64}(6, 1, 0, 0), \frac{\sqrt{858}}{64}(5, 1, 1, 0), \frac{5\sqrt{33}}{64}(4, 1, 2, 0), \frac{5\sqrt{7}}{32}(3, 1, 3, 0),$ $\frac{5\sqrt{21}}{64}(2, 1, 4, 0), \frac{\sqrt{330}}{64}(1, 1, 5, 0), \frac{\sqrt{143}}{64}(0, 1, 6, 0)$
$1311_{[21]_\lambda}$	$\frac{\sqrt{715}}{64}(0, 0, 6, 1), \frac{\sqrt{858}}{64}(1, 0, 5, 1), \frac{5\sqrt{33}}{64}(2, 0, 4, 1), \frac{5\sqrt{7}}{32}(3, 0, 3, 1),$ $\frac{5\sqrt{21}}{64}(4, 0, 2, 1), \frac{\sqrt{330}}{64}(5, 0, 1, 1), \frac{\sqrt{143}}{64}(6, 0, 0, 1)$
$1511_{[21]_\rho}$	$\frac{\sqrt{2431}}{128}(7, 1, 0, 0), \frac{\sqrt{3003}}{128}(6, 1, 1, 0), \frac{\sqrt{3003}}{128}(5, 1, 2, 0), \frac{7\sqrt{55}}{128}(4, 1, 3, 0),$ $\frac{21\sqrt{5}}{128}(3, 1, 4, 0), \frac{7\sqrt{33}}{128}(2, 1, 5, 0), \frac{\sqrt{1001}}{128}(1, 1, 6, 0), \frac{\sqrt{429}}{128}(0, 1, 7, 0)$
$1511_{[21]_\lambda}$	$\frac{\sqrt{2431}}{128}(0, 0, 7, 1), \frac{\sqrt{3003}}{128}(1, 0, 6, 1), \frac{\sqrt{3003}}{128}(2, 0, 5, 1), \frac{7\sqrt{55}}{128}(3, 0, 4, 1),$ $\frac{21\sqrt{5}}{128}(4, 0, 3, 1), \frac{7\sqrt{33}}{128}(5, 0, 2, 1), \frac{\sqrt{1001}}{128}(6, 0, 1, 1), \frac{\sqrt{429}}{128}(7, 0, 0, 1)$
$1711_{[21]_\rho}$	$\frac{\sqrt{8398}}{256}(8, 1, 0, 0), \frac{\sqrt{663}}{64}(7, 1, 1, 0), \frac{\sqrt{2730}}{128}(6, 1, 2, 0), \frac{7\sqrt{13}}{64}(5, 1, 3, 0),$ $\frac{21\sqrt{5}}{128}(4, 1, 4, 0), \frac{21}{64}(3, 1, 5, 0), \frac{7\sqrt{26}}{128}(2, 1, 6, 0), \frac{\sqrt{195}}{64}(1, 1, 7, 0),$ $\frac{\sqrt{1326}}{256}(0, 1, 8, 0)$

Table B.3 (Continued) Normalized 3-quark spatial wave functions for $L = 1$
 $2N + 1 \quad 1 \quad 1 \quad 70$ multiplet.

NLM	$C(n_\rho, l_\rho, n_\lambda, l_\lambda)$
1711 _{[21]λ}	$\frac{\sqrt{8398}}{256}(0, 0, 8, 1), \frac{\sqrt{663}}{64}(1, 0, 7, 1), \frac{\sqrt{2730}}{128}(2, 0, 6, 1), \frac{7\sqrt{13}}{64}(3, 0, 5, 1),$ $\frac{21\sqrt{5}}{128}(4, 0, 4, 1), \frac{21}{64}(5, 0, 3, 1), \frac{7\sqrt{26}}{128}(6, 0, 2, 1), \frac{\sqrt{195}}{64}(7, 0, 1, 1),$ $\frac{\sqrt{1326}}{256}(8, 0, 0, 1)$
1911 _{[21]ρ}	$\frac{\sqrt{29393}}{512}(9, 1, 0, 0), \frac{3\sqrt{4199}}{512}(8, 1, 1, 0), \frac{3\sqrt{1105}}{256}(7, 1, 2, 0), \frac{7\sqrt{195}}{256}(6, 1, 3, 0),$ $\frac{21\sqrt{78}}{512}(5, 1, 4, 0), \frac{21\sqrt{66}}{512}(4, 1, 5, 0), \frac{21\sqrt{13}}{256}(3, 1, 6, 0), \frac{3\sqrt{455}}{256}(2, 1, 7, 0),$ $\frac{3\sqrt{1105}}{512}(1, 1, 8, 0), \frac{\sqrt{4199}}{512}(0, 1, 9, 0)$
1911 _{[21]λ}	$\frac{\sqrt{29393}}{512}(0, 0, 9, 1), \frac{3\sqrt{4199}}{512}(1, 0, 8, 1), \frac{3\sqrt{1105}}{256}(2, 0, 7, 1), \frac{7\sqrt{195}}{256}(3, 0, 6, 1),$ $\frac{21\sqrt{78}}{512}(4, 0, 5, 1), \frac{21\sqrt{66}}{512}(5, 0, 4, 1), \frac{21\sqrt{13}}{256}(6, 0, 3, 1), \frac{3\sqrt{455}}{256}(7, 0, 2, 1),$ $\frac{3\sqrt{1105}}{512}(8, 0, 1, 1), \frac{\sqrt{4199}}{512}(9, 0, 0, 1)$

Table B.4 Normalized 3-quark spatial wave functions $L = 2 \quad 2N \quad 2 \quad 2$.

NLM	$C(n_\rho, l_\rho, n_\lambda, l_\lambda)$
222[3] _S	$\frac{1}{\sqrt{2}}(0, 2, 0, 0), \frac{1}{\sqrt{2}}(0, 0, 0, 2)$
422[3] _S	$\frac{\sqrt{35}}{10}(1, 2, 0, 0), \frac{\sqrt{15}}{10}(0, 2, 1, 0), \frac{\sqrt{15}}{10}(1, 0, 0, 2), \frac{\sqrt{35}}{10}(0, 0, 1, 2)$
622[3] _S	$\frac{\sqrt{105}}{20}(2, 2, 0, 0), \frac{\sqrt{18}}{8}(1, 2, 1, 0), \frac{\sqrt{18}}{8}(0, 2, 2, 0), \frac{\sqrt{14}}{8}(2, 0, 0, 2)$ $\frac{\sqrt{675}}{64}(1, 0, 1, 2), \frac{\sqrt{594}}{64}(0, 0, 2, 2)$
822[3] _S	$\frac{\sqrt{330}}{40}(3, 2, 0, 0), \frac{\sqrt{270}}{40}(2, 2, 1, 0), \frac{\sqrt{6}}{8}(1, 2, 2, 0), \frac{\sqrt{2}}{8}(0, 2, 3, 0),$ $\frac{\sqrt{2}}{8}(3, 0, 0, 2), \frac{\sqrt{6}}{8}(2, 0, 1, 2), \frac{\sqrt{270}}{40}(1, 0, 2, 2), \frac{\sqrt{330}}{40}(0, 0, 3, 2)$
1022[3] _S	$\frac{\sqrt{4290}}{160}(4, 2, 0, 0), \frac{\sqrt{990}}{80}(3, 2, 1, 0), \frac{\sqrt{27}}{16}(2, 2, 2, 0), \frac{\sqrt{14}}{16}(1, 2, 3, 0),$ $\frac{\sqrt{18}}{32}(0, 2, 4, 0), \frac{\sqrt{18}}{32}(4, 0, 0, 2), \frac{\sqrt{14}}{16}(3, 0, 1, 2), \frac{\sqrt{27}}{16}(2, 0, 2, 2),$ $\frac{\sqrt{990}}{80}(1, 0, 3, 2), \frac{\sqrt{4290}}{160}(0, 0, 4, 2)$
1222[3] _S	$\frac{\sqrt{143}}{32}(5, 2, 0, 0), \frac{\sqrt{143}}{32}(4, 2, 1, 0), \frac{\sqrt{110}}{32}(3, 2, 2, 0), \frac{\sqrt{70}}{32}(2, 2, 3, 0),$

Table B.4 (Continued) Normalized 3-quark spatial wave functions $L = 2 \ 2N = 2$

NLM	$C(n_\rho, l_\rho, n_\lambda, l_\lambda)$
	$\frac{\sqrt{35}}{32}(1, 2, 4, 0), \frac{\sqrt{11}}{32}(0, 2, 5, 0), \frac{\sqrt{11}}{32}(5, 0, 0, 2), \frac{\sqrt{35}}{32}(4, 0, 1, 2),$ $\frac{\sqrt{70}}{32}(3, 0, 2, 2), \frac{\sqrt{110}}{32}(2, 0, 3, 2), \frac{\sqrt{143}}{32}(1, 0, 4, 2), \frac{\sqrt{143}}{32}(0, 0, 5, 2)$
1422[3] _S	$\frac{\sqrt{12155}}{320}(6, 2, 0, 0), \frac{\sqrt{12870}}{320}(5, 2, 1, 0), \frac{\sqrt{429}}{64}(4, 2, 2, 0), \frac{\sqrt{77}}{32}(3, 2, 3, 0),$ $\frac{\sqrt{189}}{64}(2, 2, 4, 0), \frac{\sqrt{2310}}{320}(1, 2, 5, 0), \frac{\sqrt{715}}{320}(0, 2, 6, 0), \frac{\sqrt{715}}{320}(6, 0, 0, 2),$ $\frac{\sqrt{2310}}{320}(5, 0, 1, 2), \frac{\sqrt{189}}{64}(4, 0, 2, 2), \frac{\sqrt{77}}{32}(3, 0, 3, 2), \frac{\sqrt{429}}{64}(2, 0, 4, 2),$ $\frac{\sqrt{12870}}{320}(1, 0, 5, 2), \frac{\sqrt{12155}}{320}(0, 0, 6, 2)$
1622[3] _S	$\frac{\sqrt{41990}}{640}(7, 2, 0, 0), \frac{\sqrt{46410}}{640}(6, 2, 1, 0), \frac{\sqrt{1638}}{128}(5, 2, 2, 0), \frac{\sqrt{1274}}{128}(4, 2, 3, 0),$ $\frac{\sqrt{882}}{128}(3, 2, 4, 0), \frac{\sqrt{13230}}{640}(2, 2, 5, 0), \frac{\sqrt{6370}}{640}(1, 2, 6, 0), \frac{\sqrt{78}}{128}(0, 2, 7, 0),$ $\frac{\sqrt{78}}{128}(7, 0, 0, 2), \frac{\sqrt{6370}}{640}(6, 0, 1, 2), \frac{\sqrt{13230}}{640}(5, 0, 2, 2), \frac{\sqrt{882}}{128}(4, 0, 3, 2),$ $\frac{\sqrt{1274}}{128}(3, 0, 4, 2), \frac{\sqrt{1638}}{128}(2, 0, 5, 2), \frac{\sqrt{46410}}{640}(1, 0, 6, 2), \frac{\sqrt{41990}}{640}(0, 0, 7, 2)$
1822[3] _S	$\frac{\sqrt{146965}}{1280}(8, 2, 0, 0), \frac{\sqrt{41990}}{640}(7, 2, 1, 0), \frac{\sqrt{1547}}{128}(6, 2, 2, 0), \frac{\sqrt{1274}}{128}(5, 2, 3, 0),$ $\frac{\sqrt{3822}}{256}(4, 2, 4, 0), \frac{\sqrt{16170}}{640}(3, 2, 5, 0), \frac{\sqrt{9555}}{640}(2, 2, 6, 0), \frac{\sqrt{182}}{128}(1, 2, 7, 0),$ $\frac{\sqrt{221}}{256}(0, 2, 8, 0), \frac{\sqrt{221}}{256}(8, 0, 0, 2), \frac{\sqrt{182}}{128}(7, 0, 1, 2), \frac{\sqrt{9555}}{640}(6, 0, 2, 2),$ $\frac{\sqrt{16170}}{640}(5, 0, 3, 2), \frac{\sqrt{3822}}{256}(4, 0, 4, 2), \frac{\sqrt{1274}}{128}(3, 0, 5, 2), \frac{\sqrt{1547}}{128}(2, 0, 6, 2),$ $\frac{\sqrt{41990}}{640}(1, 0, 7, 2), \frac{\sqrt{146965}}{1280}(0, 0, 8, 2)$
2022[3] _S	$\frac{\sqrt{520030}}{2560}(9, 2, 0, 0), \frac{\sqrt{610470}}{2560}(8, 2, 1, 0), \frac{\sqrt{5814}}{256}(7, 2, 2, 0), \frac{\sqrt{4998}}{256}(6, 2, 3, 0),$ $\frac{63}{256}(5, 2, 4, 0), \frac{\sqrt{72765}}{1280}(4, 2, 5, 0), \frac{\sqrt{48510}}{1280}(3, 2, 6, 0), \frac{\sqrt{1134}}{256}(2, 2, 7, 0),$ $\frac{\sqrt{2142}}{512}(1, 2, 8, 0), \frac{\sqrt{646}}{512}(0, 2, 9, 0), \frac{\sqrt{646}}{512}(9, 0, 0, 2), \frac{\sqrt{2142}}{512}(8, 0, 1, 2),$ $\frac{\sqrt{1134}}{256}(7, 0, 2, 2), \frac{\sqrt{48510}}{1280}(6, 0, 3, 2), \frac{\sqrt{72765}}{1280}(5, 0, 4, 2), \frac{63}{256}(4, 0, 5, 2),$ $\frac{\sqrt{4998}}{256}(3, 0, 6, 2), \frac{\sqrt{5814}}{256}(2, 0, 7, 2), \frac{\sqrt{610470}}{2560}(1, 0, 8, 2), \frac{\sqrt{520030}}{2560}(0, 0, 9, 2)$

Table B.5 Normalized 3-quark spatial wave functions for $L = 2$ $2N = 2, 2, 70$ multiplet.

NLM	$C(n_\rho, l_\rho, n_\lambda, l_\lambda)$
$222_{[21]\rho}$	$(0, 1, 0, 1)$
$222_{[21]\lambda}$	$\frac{1}{\sqrt{2}}(0, 2, 0, 0), -\frac{1}{\sqrt{2}}(0, 2, 0, 0)$
$422_{[21]\rho}$	$\frac{1}{\sqrt{2}}(1, 1, 0, 1), \frac{1}{\sqrt{2}}(0, 1, 1, 1)$
$422_{[21]\lambda}$	$\frac{\sqrt{35}}{10}(1, 2, 0, 0), \frac{\sqrt{15}}{10}(0, 2, 1, 0), -\frac{\sqrt{15}}{10}(1, 0, 0, 2), -\frac{\sqrt{35}}{10}(0, 0, 1, 2)$
$622_{[21]\rho}$	$\frac{\sqrt{42}}{12}(2, 1, 0, 1), \frac{\sqrt{15}}{6}(1, 1, 1, 1), \frac{\sqrt{42}}{12}(0, 1, 2, 1)$
$622_{[21]\lambda}$	$\frac{\sqrt{105}}{20}(2, 2, 0, 0), \frac{\sqrt{70}}{20}(1, 2, 1, 0), \frac{1}{4}(0, 2, 2, 0), -\frac{1}{4}(2, 0, 0, 2),$ $-\frac{\sqrt{70}}{20}(1, 0, 1, 2), -\frac{\sqrt{105}}{20}(0, 0, 2, 2)$
$822_{[21]\rho}$	$\frac{\sqrt{3}}{4}(3, 1, 0, 1), \frac{\sqrt{5}}{4}(2, 1, 1, 1), \frac{\sqrt{5}}{4}(1, 1, 2, 1), \frac{\sqrt{3}}{4}(0, 1, 3, 1)$
$822_{[21]\lambda}$	$\frac{\sqrt{330}}{40}(3, 2, 0, 0), \frac{\sqrt{21}}{8}(2, 2, 1, 0), \frac{\sqrt{15}}{8}(1, 2, 2, 0), \frac{\sqrt{7}}{8}(0, 2, 3, 0),$ $\frac{\sqrt{330}}{40}(3, 0, 0, 2), \frac{7\sqrt{33}}{128}(2, 0, 1, 2), \frac{\sqrt{1001}}{128}(1, 0, 2, 2), -\frac{\sqrt{330}}{40}(0, 0, 3, 2)$
$1022_{[21]\rho}$	$\frac{\sqrt{33}}{16}(4, 1, 0, 1), \frac{\sqrt{15}}{8}(3, 1, 1, 1), \frac{\sqrt{70}}{16}(2, 1, 2, 1), \frac{\sqrt{15}}{8}(1, 1, 3, 1),$ $\frac{\sqrt{33}}{16}(0, 1, 4, 1)$
$1022_{[21]\lambda}$	$\frac{\sqrt{4290}}{160}(4, 2, 0, 0), \frac{\sqrt{990}}{80}(3, 2, 1, 0), \frac{\sqrt{27}}{16}(2, 2, 2, 0), \frac{\sqrt{14}}{16}(1, 2, 3, 0),$ $\frac{\sqrt{18}}{32}(0, 2, 4, 0), -\frac{\sqrt{18}}{32}(4, 0, 0, 2), -\frac{\sqrt{14}}{16}(3, 0, 1, 2), -\frac{\sqrt{27}}{16}(2, 0, 2, 2),$ $-\frac{\sqrt{990}}{80}(1, 0, 3, 2), -\frac{\sqrt{4290}}{160}(0, 0, 4, 2)$
$1222_{[21]\rho}$	$\frac{\sqrt{858}}{96}(5, 1, 0, 1), \frac{\sqrt{1650}}{96}(4, 1, 1, 1), \frac{\sqrt{525}}{48}(3, 1, 2, 1), \frac{\sqrt{525}}{48}(2, 1, 3, 1),$ $\frac{\sqrt{1650}}{96}(1, 1, 4, 1), \frac{\sqrt{858}}{96}(0, 1, 5, 1)$
$1222_{[21]\lambda}$	$\frac{\sqrt{143}}{32}(5, 2, 0, 0), \frac{\sqrt{143}}{32}(4, 2, 1, 0), \frac{\sqrt{110}}{32}(3, 2, 2, 0), \frac{\sqrt{70}}{32}(2, 2, 3, 0),$ $\frac{\sqrt{35}}{32}(1, 2, 4, 0), \frac{\sqrt{11}}{32}(0, 2, 5, 0), -\frac{\sqrt{11}}{32}(5, 0, 0, 2), -\frac{\sqrt{35}}{32}(4, 0, 1, 2),$ $-\frac{\sqrt{70}}{32}(3, 0, 2, 2), -\frac{\sqrt{110}}{32}(2, 0, 3, 2), -\frac{\sqrt{143}}{32}(1, 0, 4, 2), -\frac{\sqrt{143}}{32}(0, 0, 5, 2)$
$1422_{[21]\rho}$	$\frac{\sqrt{286}}{64}(6, 1, 0, 1), \frac{\sqrt{143}}{32}(5, 1, 1, 1), \frac{\sqrt{770}}{64}(4, 1, 2, 1), \frac{\sqrt{210}}{32}(3, 1, 3, 1),$ $\frac{\sqrt{770}}{64}(2, 1, 4, 1), \frac{\sqrt{143}}{32}(1, 1, 5, 1), \frac{\sqrt{286}}{64}(0, 1, 6, 1)$

Table B.5 (Continued) Normalized 3-quark spatial wave functions for $L = 2$ $2N$ 2 2 70 multiplet.

NLM	$C(n_\rho, l_\rho, n_\lambda, l_\lambda)$
1422 _{[21]λ}	$\frac{\sqrt{12155}}{320}(6, 2, 0, 0), \frac{\sqrt{12870}}{320}(5, 2, 1, 0), \frac{\sqrt{429}}{64}(4, 2, 2, 0), \frac{\sqrt{77}}{32}(3, 2, 3, 0),$ $\frac{\sqrt{189}}{64}(2, 2, 4, 0), \frac{\sqrt{2310}}{320}(1, 2, 5, 0), \frac{\sqrt{715}}{320}(0, 2, 6, 0), -\frac{\sqrt{715}}{320}(6, 0, 0, 2),$ $-\frac{\sqrt{2310}}{320}(5, 0, 1, 2), -\frac{\sqrt{189}}{64}(4, 0, 2, 2), -\frac{\sqrt{77}}{32}(3, 0, 3, 2), -\frac{\sqrt{429}}{64}(2, 0, 4, 2),$ $-\frac{\sqrt{12870}}{320}(1, 0, 5, 2), -\frac{\sqrt{12155}}{320}(0, 0, 6, 2)$
1622 _{[21]ρ}	$\frac{\sqrt{221}}{64}(7, 1, 0, 1), \frac{\sqrt{637}}{64}(6, 1, 1, 1), \frac{\sqrt{735}}{64}(5, 1, 2, 1), \frac{\sqrt{455}}{64}(4, 1, 3, 1),$ $\frac{\sqrt{455}}{64}(3, 1, 4, 1), \frac{\sqrt{735}}{64}(2, 1, 5, 1), \frac{\sqrt{637}}{64}(1, 1, 6, 1), \frac{\sqrt{221}}{64}(0, 1, 7, 1)$
1622 _{[21]λ}	$\frac{\sqrt{41990}}{640}(7, 2, 0, 0), \frac{\sqrt{46410}}{640}(6, 2, 1, 0), \frac{\sqrt{1638}}{128}(5, 2, 2, 0), \frac{\sqrt{1274}}{128}(4, 2, 3, 0),$ $\frac{\sqrt{882}}{128}(3, 2, 4, 0), \frac{\sqrt{13230}}{640}(2, 2, 5, 0), \frac{\sqrt{6370}}{640}(1, 2, 6, 0), \frac{\sqrt{78}}{128}(0, 2, 7, 0),$ $-\frac{\sqrt{78}}{128}(7, 0, 0, 2), -\frac{\sqrt{6370}}{640}(6, 0, 1, 2), -\frac{\sqrt{13230}}{640}(5, 0, 2, 2),$ $-\frac{\sqrt{882}}{128}(4, 0, 3, 2), -\frac{\sqrt{1274}}{128}(3, 0, 4, 2), -\frac{\sqrt{1638}}{128}(2, 0, 5, 2),$ $-\frac{\sqrt{46410}}{640}(1, 0, 6, 2), -\frac{\sqrt{41990}}{640}(0, 0, 7, 2)$
1822 _{[21]ρ}	$\frac{\sqrt{25194}}{768}(8, 1, 0, 1), \frac{\sqrt{3315}}{192}(7, 1, 1, 1), \frac{\sqrt{19110}}{384}(6, 1, 2, 1), \frac{\sqrt{637}}{64}(5, 1, 3, 1),$ $\frac{\sqrt{2695}}{128}(4, 1, 4, 1), \frac{\sqrt{637}}{64}(3, 1, 5, 1), \frac{\sqrt{19110}}{384}(2, 1, 6, 1), \frac{\sqrt{3315}}{192}(1, 1, 7, 1),$ $\frac{\sqrt{25194}}{768}(0, 1, 8, 1)$
1822 _{[21]λ}	$\frac{\sqrt{146965}}{1280}(8, 2, 0, 0), \frac{\sqrt{41990}}{640}(7, 2, 1, 0), \frac{\sqrt{1547}}{128}(6, 2, 2, 0), \frac{\sqrt{1274}}{128}(5, 2, 3, 0),$ $\frac{\sqrt{3822}}{256}(4, 2, 4, 0), \frac{\sqrt{16170}}{640}(3, 2, 5, 0), \frac{\sqrt{9555}}{640}(2, 2, 6, 0), \frac{\sqrt{182}}{128}(1, 2, 7, 0),$ $\frac{\sqrt{221}}{256}(0, 2, 8, 0), -\frac{\sqrt{221}}{256}(8, 0, 0, 2), -\frac{\sqrt{182}}{128}(7, 0, 1, 2), -\frac{\sqrt{9555}}{640}(6, 0, 2, 2),$ $-\frac{\sqrt{16170}}{640}(5, 0, 3, 2), -\frac{\sqrt{3822}}{256}(4, 0, 4, 2), -\frac{\sqrt{1274}}{128}(3, 0, 5, 2),$ $-\frac{\sqrt{1547}}{128}(2, 0, 6, 2), -\frac{\sqrt{41990}}{640}(1, 0, 7, 2), -\frac{\sqrt{146965}}{1280}(0, 0, 8, 2)$
2022 _{[21]ρ}	$\frac{\sqrt{2261}}{256}(9, 1, 0, 1), \frac{\sqrt{4845}}{256}(8, 1, 1, 1), \frac{\sqrt{1785}}{128}(7, 1, 2, 1), \frac{\sqrt{2205}}{128}(6, 1, 3, 1),$ $\frac{\sqrt{9702}}{256}(5, 1, 4, 1), \frac{\sqrt{9702}}{256}(4, 1, 5, 1), \frac{\sqrt{2205}}{128}(3, 1, 6, 1), \frac{\sqrt{1785}}{128}(2, 1, 7, 1),$ $\frac{\sqrt{4845}}{256}(1, 1, 8, 1), \frac{\sqrt{2261}}{256}(0, 1, 9, 1)$

Table B.5 (Continued) Normalized 3-quark spatial wave functions for $L = 2$ $2N$ 2 2 70 multiplet.

NLM	$C(n_\rho, l_\rho, n_\lambda, l_\lambda)$
2022 _{[21]λ}	$\frac{\sqrt{520030}}{2560}(9, 2, 0, 0), \frac{\sqrt{610470}}{2560}(8, 2, 1, 0), \frac{\sqrt{5814}}{256}(7, 2, 2, 0), \frac{\sqrt{4998}}{256}(6, 2, 3, 0),$ $\frac{63}{256}(5, 2, 4, 0), \frac{\sqrt{72765}}{1280}(4, 2, 5, 0), \frac{\sqrt{48510}}{1280}(3, 2, 6, 0), \frac{\sqrt{1134}}{256}(2, 2, 7, 0),$ $\frac{\sqrt{2142}}{512}(1, 2, 8, 0), \frac{\sqrt{646}}{512}(0, 2, 9, 0), -\frac{\sqrt{646}}{512}(9, 0, 0, 2), -\frac{\sqrt{2142}}{512}(8, 0, 1, 2),$ $-\frac{\sqrt{1134}}{256}(7, 0, 2, 2), -\frac{\sqrt{48510}}{1280}(6, 0, 3, 2), -\frac{\sqrt{72765}}{1280}(5, 0, 4, 2),$ $-\frac{63}{256}(4, 0, 5, 2), -\frac{\sqrt{4998}}{256}(3, 0, 6, 2), -\frac{\sqrt{5814}}{256}(2, 0, 7, 2),$ $-\frac{\sqrt{610470}}{2560}(1, 0, 8, 2), -\frac{\sqrt{520030}}{2560}(0, 0, 9, 2)$

Table B.6 Normalized 3-quark spatial wave functions for $L = 1$ $2N$ 1 1 20 multiplet.

NLM	$C(n_\rho, l_\rho, n_\lambda, l_\lambda)$
211 _{[111]A}	$(0, 1, 0, 1)$
411 _{[111]A}	$\frac{1}{\sqrt{2}}(1, 1, 0, 1), \frac{1}{\sqrt{2}}(0, 1, 1, 1)$
611 _{[111]A}	$\frac{\sqrt{42}}{12}(2, 1, 0, 1), \frac{\sqrt{15}}{6}(1, 1, 1, 1), \frac{\sqrt{42}}{12}(0, 1, 2, 1)$
811 _{[111]A}	$\frac{\sqrt{3}}{4}(3, 1, 0, 1), \frac{\sqrt{5}}{4}(2, 1, 1, 1), \frac{\sqrt{5}}{4}(1, 1, 2, 1), \frac{\sqrt{3}}{4}(0, 1, 3, 1)$
1011 _{[111]A}	$\frac{\sqrt{33}}{16}(4, 1, 0, 1), \frac{\sqrt{15}}{8}(3, 1, 1, 1), \frac{\sqrt{70}}{16}(2, 1, 2, 1), \frac{\sqrt{15}}{8}(1, 1, 3, 1),$ $\frac{\sqrt{33}}{16}(0, 1, 4, 1)$
1211 _{[111]A}	$\frac{\sqrt{858}}{96}(5, 1, 0, 1), \frac{5\sqrt{66}}{96}(4, 1, 1, 1), \frac{5\sqrt{21}}{48}(3, 1, 2, 1), \frac{5\sqrt{21}}{48}(2, 1, 3, 1),$ $\frac{5\sqrt{66}}{96}(1, 1, 4, 1), \frac{\sqrt{858}}{96}(0, 1, 5, 1)$
1411 _{[111]A}	$\frac{\sqrt{286}}{64}(6, 1, 0, 1), \frac{\sqrt{143}}{32}(5, 1, 1, 1), \frac{\sqrt{770}}{64}(4, 1, 2, 1), \frac{\sqrt{210}}{32}(3, 1, 3, 1),$ $\frac{\sqrt{770}}{64}(2, 1, 4, 1), \frac{\sqrt{143}}{32}(1, 1, 5, 1), \frac{\sqrt{286}}{64}(0, 1, 6, 1)$
1611 _{[111]A}	$\frac{\sqrt{221}}{64}(7, 1, 0, 1), \frac{\sqrt{455}}{64}(6, 1, 1, 1), \frac{7\sqrt{13}}{64}(5, 1, 2, 1), \frac{\sqrt{2450}}{128}(4, 1, 3, 1),$

Table B.6 (Continued) Normalized 3-quark spatial wave functions for $L = 1$ $2N$ 1 1 20 multiplet.

NLM	$C(n_\rho, l_\rho, n_\lambda, l_\lambda)$
	$\frac{\sqrt{2450}}{128}(3, 1, 4, 1), \frac{7\sqrt{13}}{64}(2, 1, 5, 1), \frac{\sqrt{455}}{64}(1, 1, 6, 1), \frac{\sqrt{221}}{64}(0, 1, 7, 1)$
$1811_{[111]A}$	$\frac{\sqrt{25194}}{768}(8, 1, 0, 1), \frac{\sqrt{3315}}{192}(7, 1, 1, 1), \frac{7\sqrt{390}}{384}(6, 1, 2, 1), \frac{7\sqrt{13}}{64}(5, 1, 3, 1),$ $\frac{7\sqrt{55}}{128}(4, 1, 4, 1), \frac{7\sqrt{13}}{64}(3, 1, 5, 1), \frac{7\sqrt{390}}{384}(2, 1, 6, 1), \frac{\sqrt{3315}}{192}(1, 1, 7, 1),$ $\frac{\sqrt{25194}}{768}(0, 1, 8, 1)$
$2011_{[111]A}$	$\frac{\sqrt{2261}}{256}(9, 1, 0, 1), \frac{\sqrt{4845}}{256}(8, 1, 1, 1), \frac{\sqrt{1785}}{128}(7, 1, 2, 1), \frac{21\sqrt{5}}{128}(6, 1, 3, 1),$ $\frac{21\sqrt{22}}{256}(5, 1, 4, 1), \frac{21\sqrt{22}}{256}(4, 1, 5, 1), \frac{21\sqrt{5}}{128}(3, 1, 6, 1), \frac{\sqrt{1785}}{128}(2, 1, 7, 1),$ $\frac{\sqrt{4845}}{256}(1, 1, 8, 1), \frac{\sqrt{2261}}{256}(0, 1, 9, 1)$

The total principle quantum number N is written as:

$$\begin{aligned}
 N_{q^4\bar{q}} &= N_\rho + N_\lambda + N_\eta + N_\xi \\
 &= (2n_\rho + l_\rho) + (2n_\lambda + l_\lambda) + (2n_\eta + l_\eta) + (2n_\xi + l_\xi)
 \end{aligned} \tag{B.2}$$

The total orbital angular momentum of any state is obtained by coupling $l_\rho, l_\lambda, l_\eta$ and l_ξ , $\mathbf{L} = \mathbf{l}_\rho + \mathbf{l}_\lambda + \mathbf{l}_\eta + \mathbf{l}_\xi$ and parity of pentaquark is $P = (-1)^{L+1}$.

Only s-wave and p-wave spatial wave function of pentaquark states are derived in possible permutation symmetry of q^4 , the total $L = 0$ or $L = 1$, each harmonic oscillator $l = 0$ or $l = 1$.

The q^4 permutation symmetry can represent the pentaquark symmetry, for q^4 and $q^4\bar{q}$ states, N_ξ is simply added to N_{q^4} to get total principle quantum number N .

$$N_{q^4} = 2n_\rho + l_\rho + 2n_\lambda + l_\lambda + 2n_\eta + l_\eta$$

$$N_{q^4\bar{q}} = N_{q^4} + 2n_\xi + l_\xi$$

$$\mathbf{L} = \mathbf{l}_{q^4} + \mathbf{l}_\xi \quad (\text{B.3})$$

For $L = 0$ and $L = 1, 2N$ or $2N + 1$ oscillation band forms different complete basis with a certain permutation symmetry. $NLM = 2N00, 2N10$ and $(2N + 1)00$ with possible permutation symmetries are listed in three table below. C is the normalization factor.

Table B.7 Normalized pentaquark (q^4 symmetry) spatial wave functions quantum number: $2N \ 0 \ 0$.

NLM	$C(n_\rho, l_\rho, n_\lambda, l_\lambda, n_\eta, l_\eta)$
$000_{[4]S}$	$(0, 0, 0, 0, 0, 0)$
$200_{[4]S}$	$\frac{1}{\sqrt{3}}(1, 0, 0, 0, 0, 0), \frac{1}{\sqrt{3}}(0, 0, 1, 0, 0, 0), \frac{1}{\sqrt{3}}(0, 0, 0, 0, 1, 0)$
$200_{[31]\rho}$	$\frac{1}{\sqrt{3}}(0, 1, 0, 0, 0, 1), \sqrt{\frac{2}{3}}(0, 1, 0, 1, 0, 0)$
$200_{[31]\lambda}$	$\frac{1}{\sqrt{3}}(0, 0, 0, 1, 0, 1), -\frac{1}{\sqrt{3}}(0, 0, 1, 0, 0, 0), \frac{1}{\sqrt{3}}(1, 0, 0, 0, 0, 0)$
$200_{[31]\eta}$	$-\sqrt{\frac{2}{3}}(0, 0, 0, 0, 1, 0), \frac{1}{\sqrt{6}}(0, 0, 1, 0, 0, 0), \frac{1}{\sqrt{6}}(1, 0, 0, 0, 0, 0)$
$200_{[22]\rho}$	$-\frac{1}{\sqrt{3}}(0, 1, 0, 1, 0, 0), \sqrt{\frac{2}{3}}(0, 1, 0, 0, 0, 1)$
$200_{[22]\lambda}$	$\sqrt{\frac{2}{3}}(0, 0, 0, 1, 0, 1), \frac{1}{\sqrt{6}}(0, 0, 1, 0, 0, 0), -\frac{1}{\sqrt{6}}(1, 0, 0, 0, 0, 0)$
$400_{[4]S}$	$\sqrt{\frac{5}{33}}(2, 0, 0, 0, 0, 0), \sqrt{\frac{5}{33}}(0, 0, 2, 0, 0, 0), \sqrt{\frac{5}{33}}(0, 0, 0, 0, 2, 0),$ $\sqrt{\frac{2}{11}}(1, 0, 1, 0, 0, 0), \sqrt{\frac{2}{11}}(1, 0, 0, 0, 1, 0), \sqrt{\frac{2}{11}}(0, 0, 1, 0, 1, 0)$
$400_{[31]\rho}$	$\sqrt{\frac{5}{39}}(0, 1, 0, 0, 1, 1), \sqrt{\frac{2}{13}}(0, 1, 0, 1, 1, 0), \frac{1}{\sqrt{13}}(0, 1, 1, 0, 0, 1),$ $\sqrt{\frac{10}{39}}(0, 1, 1, 1, 0, 0), \sqrt{\frac{5}{39}}(1, 1, 0, 0, 0, 1), \sqrt{\frac{10}{39}}(1, 1, 0, 1, 0, 0)$
$400_{[31]\lambda}$	$\sqrt{\frac{5}{39}}(0, 0, 0, 1, 1, 1), -\frac{1}{\sqrt{13}}(0, 0, 1, 0, 1, 0), \sqrt{\frac{5}{39}}(0, 0, 1, 1, 0, 1),$ $-\sqrt{\frac{10}{39}}(0, 0, 2, 0, 0, 0), \frac{1}{\sqrt{13}}(1, 0, 0, 0, 1, 0), \frac{1}{\sqrt{13}}(1, 0, 0, 1, 0, 1)$ $\sqrt{\frac{10}{39}}(2, 0, 0, 0, 0, 0)$
$400_{[31]\eta}$	$-\sqrt{\frac{20}{39}}(0, 0, 0, 0, 2, 0), -\frac{1}{\sqrt{26}}(0, 0, 1, 0, 1, 0), \sqrt{\frac{5}{39}}(0, 0, 2, 0, 0, 0)$

Table B.7 (Continued) Normalized pentaquark (q^4 symmetry) spatial wave functions quantum number: $2N \ 0 \ 0$.

NLM	$C(n_\rho, l_\rho, n_\lambda, l_\lambda, n_\eta, l_\eta)$
	$-\frac{1}{\sqrt{26}}(1, 0, 0, 0, 1, 0), \sqrt{\frac{2}{13}}(1, 0, 1, 0, 0, 0), \sqrt{\frac{5}{39}}(2, 0, 0, 0, 0, 0)$
$400_{[22]\rho}$	$\sqrt{\frac{10}{39}}(0, 1, 0, 0, 1, 1), -\frac{1}{\sqrt{13}}(0, 1, 0, 1, 1, 0), \sqrt{\frac{2}{13}}(0, 1, 1, 0, 0, 1),$ $-\sqrt{\frac{5}{39}}(0, 1, 1, 1, 0, 0), \sqrt{\frac{10}{39}}(1, 1, 0, 0, 0, 1), -\sqrt{\frac{5}{39}}(1, 1, 0, 1, 0, 0)$
$400_{[22]\lambda}$	$\sqrt{\frac{10}{39}}(0, 0, 0, 1, 1, 1), \frac{1}{\sqrt{26}}(0, 0, 1, 0, 1, 0), \sqrt{\frac{10}{39}}(0, 0, 1, 1, 0, 1),$ $\sqrt{\frac{5}{39}}(0, 0, 2, 0, 0, 0), -\frac{1}{\sqrt{26}}(1, 0, 0, 0, 1, 0), \sqrt{\frac{2}{13}}(1, 0, 0, 1, 0, 1)$ $\sqrt{\frac{5}{39}}(2, 0, 0, 0, 0, 0)$
$600_{[4]S}$	$\sqrt{\frac{35}{429}}(3, 0, 0, 0, 0, 0), \sqrt{\frac{35}{429}}(0, 0, 3, 0, 0, 0), \sqrt{\frac{35}{429}}(0, 0, 0, 0, 3, 0),$ $\sqrt{\frac{15}{143}}(2, 0, 1, 0, 0, 0), \sqrt{\frac{15}{143}}(2, 0, 0, 0, 1, 0), \sqrt{\frac{15}{143}}(1, 0, 2, 0, 0, 0),$ $\sqrt{\frac{15}{143}}(0, 0, 2, 0, 1, 0), \sqrt{\frac{15}{143}}(1, 0, 0, 0, 2, 0), \sqrt{\frac{15}{143}}(0, 0, 1, 0, 2, 0),$ $\sqrt{\frac{18}{143}}(1, 0, 1, 0, 1, 0)$
$600_{[31]\rho}$	$\sqrt{\frac{7}{117}}(0, 1, 0, 0, 2, 1), \sqrt{\frac{2}{39}}(0, 1, 0, 1, 2, 0), \sqrt{\frac{2}{39}}(0, 1, 1, 0, 1, 1),$ $\frac{2}{\sqrt{39}}(0, 1, 1, 1, 1, 0), \frac{1}{\sqrt{39}}(0, 1, 2, 0, 0, 1), \sqrt{\frac{14}{117}}(0, 1, 2, 1, 0, 0),$ $\sqrt{\frac{10}{117}}(1, 1, 0, 0, 1, 1), \frac{2}{\sqrt{39}}(1, 1, 0, 1, 1, 0), \sqrt{\frac{2}{39}}(1, 1, 1, 0, 0, 1),$ $\sqrt{\frac{20}{117}}(1, 1, 1, 1, 0, 0), \sqrt{\frac{7}{117}}(2, 1, 0, 0, 0, 1), \sqrt{\frac{14}{117}}(2, 1, 0, 1, 0, 0)$
$600_{[31]\lambda}$	$\sqrt{\frac{7}{117}}(0, 0, 0, 1, 2, 1), \frac{1}{\sqrt{39}}(0, 0, 1, 0, 2, 0), \sqrt{\frac{10}{117}}(0, 0, 1, 1, 1, 1),$ $-\frac{2}{\sqrt{39}}(0, 0, 2, 0, 1, 0), \sqrt{\frac{7}{117}}(0, 0, 2, 1, 0, 1), -\sqrt{\frac{7}{39}}(0, 0, 3, 0, 0, 0),$ $\frac{1}{\sqrt{39}}(1, 0, 0, 0, 2, 0), \sqrt{\frac{2}{39}}(1, 0, 0, 1, 1, 1), \sqrt{\frac{2}{39}}(1, 0, 1, 1, 0, 1),$ $-\frac{1}{\sqrt{39}}(1, 0, 2, 0, 0, 0), \frac{2}{\sqrt{39}}(2, 0, 0, 0, 1, 0), \frac{1}{\sqrt{39}}(2, 0, 0, 1, 0, 1),$ $\frac{1}{\sqrt{39}}(2, 0, 1, 0, 0, 0), \sqrt{\frac{7}{39}}(3, 0, 0, 0, 0, 0)$
$600_{[31]\eta}$	$-\sqrt{\frac{14}{39}}(0, 0, 0, 0, 3, 0), -\sqrt{\frac{3}{26}}(0, 0, 1, 0, 2, 0), \sqrt{\frac{7}{78}}(0, 0, 3, 0, 0, 0),$ $-\frac{3}{\sqrt{26}}(1, 0, 0, 0, 2, 0), \frac{3}{\sqrt{26}}(1, 0, 2, 0, 0, 0), \sqrt{\frac{3}{26}}(2, 0, 1, 0, 0, 0),$ $\sqrt{\frac{7}{78}}(3, 0, 0, 0, 0, 0)$

Table B.7 (Continued) Normalized pentaquark (q^4 symmetry) spatial wave functions quantum number: $2N \ 0 \ 0$.

NLM	$C(n_\rho, l_\rho, n_\lambda, l_\lambda, n_\eta, l_\eta)$
$600_{[22]\rho}$	$\begin{aligned} & \sqrt{\frac{14}{117}}(0, 1, 0, 0, 2, 1), -\frac{1}{\sqrt{39}}(0, 1, 0, 1, 2, 0), \frac{2}{\sqrt{39}}(0, 1, 1, 0, 1, 1), \\ & -\sqrt{\frac{2}{39}}(0, 1, 1, 1, 1, 0), \sqrt{\frac{2}{39}}(0, 1, 2, 0, 0, 1), -\sqrt{\frac{7}{117}}(0, 1, 2, 1, 0, 0), \\ & \sqrt{\frac{20}{117}}(1, 1, 0, 0, 1, 1), -\sqrt{\frac{2}{39}}(1, 1, 0, 1, 1, 0), \frac{2}{\sqrt{39}}(1, 1, 1, 0, 0, 1), \\ & -\sqrt{\frac{10}{117}}(1, 1, 1, 1, 0, 0), \sqrt{\frac{14}{117}}(2, 1, 0, 0, 0, 1), -\sqrt{\frac{7}{117}}(2, 1, 0, 1, 0, 0) \end{aligned}$
$600_{[22]\lambda}$	$\begin{aligned} & \sqrt{\frac{14}{117}}(0, 0, 0, 1, 2, 1), \frac{1}{\sqrt{78}}(0, 0, 1, 0, 2, 0), \sqrt{\frac{20}{117}}(0, 0, 1, 1, 1, 1), \\ & \sqrt{\frac{2}{39}}(0, 0, 2, 0, 1, 0), \sqrt{\frac{14}{117}}(0, 0, 2, 1, 0, 1), \sqrt{\frac{7}{78}}(0, 0, 3, 0, 0, 0), \\ & -\frac{1}{\sqrt{78}}(1, 0, 0, 0, 2, 0), \frac{2}{\sqrt{39}}(1, 0, 0, 1, 1, 1), \frac{2}{\sqrt{39}}(1, 0, 1, 1, 0, 1), \\ & \frac{1}{\sqrt{78}}(1, 0, 2, 0, 0, 0), -\sqrt{\frac{2}{39}}(2, 0, 0, 0, 1, 0), \sqrt{\frac{2}{39}}(2, 0, 0, 1, 0, 1), \\ & -\frac{1}{\sqrt{78}}(2, 0, 1, 0, 0, 0), -\sqrt{\frac{7}{78}}(3, 0, 0, 0, 0, 0) \end{aligned}$
$800_{[4]S}$	$\begin{aligned} & \sqrt{\frac{7}{143}}(4, 0, 0, 0, 0, 0), \sqrt{\frac{7}{143}}(0, 0, 4, 0, 0, 0), \sqrt{\frac{7}{143}}(0, 0, 0, 0, 4, 0), \\ & \sqrt{\frac{28}{429}}(3, 0, 1, 0, 0, 0), \sqrt{\frac{28}{429}}(3, 0, 0, 0, 1, 0), \sqrt{\frac{28}{429}}(1, 0, 3, 0, 0, 0), \\ & \sqrt{\frac{28}{429}}(0, 0, 3, 0, 1, 0), \sqrt{\frac{28}{429}}(1, 0, 0, 0, 3, 0), \sqrt{\frac{28}{429}}(0, 0, 1, 0, 3, 0), \\ & \sqrt{\frac{10}{143}}(0, 0, 2, 0, 2, 0), \sqrt{\frac{10}{143}}(2, 0, 0, 0, 2, 0), \sqrt{\frac{10}{143}}(2, 0, 2, 0, 0, 0), \\ & \sqrt{\frac{12}{143}}(2, 0, 1, 0, 1, 0), \sqrt{\frac{12}{143}}(1, 0, 2, 0, 1, 0), \sqrt{\frac{12}{143}}(1, 0, 1, 0, 2, 0) \end{aligned}$
$800_{[31]\rho}$	$\begin{aligned} & \sqrt{\frac{7}{221}}(0, 1, 0, 0, 3, 1), \sqrt{\frac{14}{663}}(0, 1, 0, 1, 3, 0), \sqrt{\frac{7}{221}}(0, 1, 1, 0, 2, 1), \\ & \sqrt{\frac{10}{221}}(0, 1, 1, 1, 2, 0), \sqrt{\frac{5}{221}}(0, 1, 2, 0, 1, 1), \sqrt{\frac{14}{221}}(0, 1, 2, 1, 1, 0), \\ & \sqrt{\frac{7}{663}}(0, 1, 3, 0, 0, 1), \sqrt{\frac{14}{221}}(0, 1, 3, 1, 0, 0), \sqrt{\frac{35}{663}}(1, 1, 0, 0, 2, 1), \\ & \sqrt{\frac{10}{221}}(1, 1, 0, 1, 2, 0), \sqrt{\frac{10}{221}}(1, 1, 1, 0, 1, 1), \sqrt{\frac{20}{221}}(1, 1, 1, 1, 1, 0), \\ & \sqrt{\frac{5}{221}}(1, 1, 2, 0, 0, 1), \sqrt{\frac{70}{663}}(1, 1, 2, 1, 0, 0), \sqrt{\frac{35}{663}}(2, 1, 0, 0, 1, 1), \\ & \sqrt{\frac{14}{221}}(2, 1, 1, 0, 0, 1), \sqrt{\frac{7}{221}}(2, 1, 1, 0, 0, 1), \sqrt{\frac{70}{663}}(2, 1, 1, 1, 0, 0), \\ & \sqrt{\frac{7}{221}}(3, 1, 0, 0, 0, 1), \sqrt{\frac{14}{221}}(3, 1, 0, 1, 0, 0) \end{aligned}$
$800_{[31]\lambda}$	$\sqrt{\frac{7}{221}}(0, 0, 0, 1, 3, 1), \sqrt{\frac{7}{663}}(0, 0, 1, 0, 3, 0), \sqrt{\frac{35}{663}}(0, 0, 1, 1, 2, 1),$

Table B.7 (Continued) Normalized pentaquark (q^4 symmetry) spatial wave functions quantum number: $2N \ 0 \ 0$.

NLM	$C(n_\rho, l_\rho, n_\lambda, l_\lambda, n_\eta, l_\eta)$
	$-\sqrt{\frac{10}{221}}(0, 0, 2, 0, 2, 0), \sqrt{\frac{35}{663}}(0, 0, 2, 1, 1, 1), -\sqrt{\frac{21}{221}}(0, 0, 3, 0, 1, 0),$ $\sqrt{\frac{7}{221}}(0, 0, 3, 1, 0, 1), -\sqrt{\frac{28}{221}}(0, 0, 4, 0, 0, 0), \sqrt{\frac{7}{663}}(1, 0, 0, 0, 3, 0),$ $\sqrt{\frac{7}{221}}(1, 0, 0, 1, 2, 1), \sqrt{\frac{10}{221}}(1, 0, 1, 1, 1, 1), -\sqrt{\frac{3}{221}}(1, 0, 2, 0, 1, 0),$ $\sqrt{\frac{7}{221}}(1, 0, 2, 1, 0, 1), \sqrt{\frac{28}{663}}(1, 0, 3, 0, 0, 0), \sqrt{\frac{10}{221}}(2, 0, 0, 0, 2, 0),$ $\sqrt{\frac{5}{221}}(2, 0, 0, 1, 1, 1), \sqrt{\frac{3}{221}}(2, 0, 1, 0, 1, 0), \sqrt{\frac{5}{221}}(2, 0, 1, 1, 0, 1),$ $\sqrt{\frac{21}{221}}(3, 0, 0, 0, 1, 0), \sqrt{\frac{7}{663}}(3, 0, 0, 1, 0, 1), \sqrt{\frac{28}{663}}(3, 0, 1, 0, 0, 0),$ $\sqrt{\frac{28}{221}}(4, 0, 0, 0, 0, 0)$
$800_{[31]\eta}$	$-\sqrt{\frac{56}{221}}(0, 0, 0, 0, 4, 0), -\sqrt{\frac{175}{1326}}(0, 0, 1, 0, 3, 0), -\sqrt{\frac{5}{221}}(0, 0, 2, 0, 2, 0),$ $\sqrt{\frac{7}{1326}}(0, 0, 3, 0, 1, 0), \sqrt{\frac{14}{221}}(0, 0, 4, 0, 0, 0), -\sqrt{\frac{175}{1326}}(1, 0, 0, 0, 3, 0),$ $-\sqrt{\frac{6}{221}}(1, 0, 1, 0, 2, 0), \sqrt{\frac{3}{442}}(1, 0, 2, 0, 1, 0), \sqrt{\frac{56}{663}}(1, 0, 3, 0, 0, 0),$ $-\sqrt{\frac{5}{221}}(2, 0, 0, 0, 2, 0), \sqrt{\frac{3}{442}}(2, 0, 1, 0, 1, 0), \sqrt{\frac{20}{221}}(2, 0, 2, 0, 0, 0),$ $\sqrt{\frac{7}{1326}}(3, 0, 0, 0, 1, 0), \sqrt{\frac{56}{663}}(3, 0, 1, 0, 0, 0), \sqrt{\frac{14}{221}}(4, 0, 0, 0, 0, 0)$
$800_{[22]\rho}$	$\sqrt{\frac{14}{221}}(0, 1, 0, 0, 3, 1), -\sqrt{\frac{7}{663}}(0, 1, 0, 1, 3, 0), \sqrt{\frac{14}{221}}(0, 1, 1, 0, 2, 1),$ $-\sqrt{\frac{5}{221}}(0, 1, 1, 1, 2, 0), \sqrt{\frac{10}{221}}(0, 1, 2, 0, 1, 1), -\sqrt{\frac{7}{221}}(0, 1, 2, 1, 1, 0),$ $\sqrt{\frac{14}{663}}(0, 1, 3, 0, 0, 1), -\sqrt{\frac{7}{221}}(0, 1, 3, 1, 0, 0), \sqrt{\frac{70}{663}}(1, 1, 0, 0, 2, 1),$ $-\sqrt{\frac{5}{221}}(1, 1, 0, 1, 2, 0), \sqrt{\frac{20}{221}}(1, 1, 1, 0, 1, 1), -\sqrt{\frac{10}{221}}(1, 1, 1, 1, 1, 0),$ $\sqrt{\frac{10}{221}}(1, 1, 2, 0, 0, 1), -\sqrt{\frac{35}{663}}(1, 1, 2, 1, 0, 0), \sqrt{\frac{70}{663}}(2, 1, 0, 0, 1, 1),$ $-\sqrt{\frac{7}{221}}(2, 1, 1, 0, 0, 1), \sqrt{\frac{14}{221}}(2, 1, 1, 0, 0, 1), -\sqrt{\frac{35}{663}}(2, 1, 1, 1, 0, 0),$ $\sqrt{\frac{14}{221}}(3, 1, 0, 0, 0, 1), -\sqrt{\frac{7}{221}}(3, 1, 0, 1, 0, 0)$
$800_{[22]\lambda}$	$\sqrt{\frac{14}{221}}(0, 0, 0, 1, 3, 1), \sqrt{\frac{7}{1326}}(0, 0, 1, 0, 3, 0), \sqrt{\frac{70}{663}}(0, 0, 1, 1, 2, 1),$ $\sqrt{\frac{5}{221}}(0, 0, 2, 0, 2, 0), \sqrt{\frac{70}{663}}(0, 0, 2, 1, 1, 1), \sqrt{\frac{21}{442}}(0, 0, 3, 0, 1, 0),$ $\sqrt{\frac{14}{221}}(0, 0, 3, 1, 0, 1), \sqrt{\frac{14}{221}}(0, 0, 4, 0, 0, 0), -\sqrt{\frac{7}{1326}}(1, 0, 0, 0, 3, 0),$

Table B.7 (Continued) Normalized pentaquark (q^4 symmetry) spatial wave functions quantum number: $2N \ 0 \ 0$.

NLM	$C(n_\rho, l_\rho, n_\lambda, l_\lambda, n_\eta, l_\eta)$
	$\begin{aligned} & \sqrt{\frac{14}{221}}(1, 0, 0, 1, 2, 1), \sqrt{\frac{20}{221}}(1, 0, 1, 1, 1, 1), \sqrt{\frac{3}{442}}(1, 0, 2, 0, 1, 0), \\ & \sqrt{\frac{14}{221}}(1, 0, 2, 1, 0, 1), \sqrt{\frac{14}{663}}(1, 0, 3, 0, 0, 0), -\sqrt{\frac{5}{221}}(2, 0, 0, 0, 2, 0), \\ & \sqrt{\frac{10}{221}}(2, 0, 0, 1, 1, 1), -\sqrt{\frac{3}{442}}(2, 0, 1, 0, 1, 0), \sqrt{\frac{10}{221}}(2, 0, 1, 1, 0, 1), \\ & -\sqrt{\frac{21}{442}}(3, 0, 0, 0, 1, 0), \sqrt{\frac{14}{663}}(3, 0, 0, 1, 0, 1), -\sqrt{\frac{14}{663}}(3, 0, 1, 0, 0, 0), \\ & -\sqrt{\frac{14}{221}}(4, 0, 0, 0, 0, 0) \end{aligned}$
$1000_{[4]S}$	$\begin{aligned} & \sqrt{\frac{7}{221}}(5, 0, 0, 0, 0, 0), \sqrt{\frac{7}{221}}(0, 0, 5, 0, 0, 0), \sqrt{\frac{7}{221}}(0, 0, 0, 0, 5, 0), \\ & \sqrt{\frac{105}{2431}}(4, 0, 1, 0, 0, 0), \sqrt{\frac{105}{2431}}(4, 0, 0, 0, 1, 0), \sqrt{\frac{105}{2431}}(1, 0, 4, 0, 0, 0), \\ & \sqrt{\frac{105}{2431}}(0, 0, 4, 0, 1, 0), \sqrt{\frac{105}{2431}}(1, 0, 0, 0, 4, 0), \sqrt{\frac{105}{2431}}(0, 0, 1, 0, 4, 0), \\ & \sqrt{\frac{350}{7293}}(3, 0, 2, 0, 0, 0), \sqrt{\frac{350}{7293}}(3, 0, 0, 0, 2, 0), \sqrt{\frac{350}{7293}}(2, 0, 3, 0, 0, 0), \\ & \sqrt{\frac{350}{7293}}(0, 0, 3, 0, 2, 0), \sqrt{\frac{350}{7293}}(2, 0, 0, 0, 3, 0), \sqrt{\frac{350}{7293}}(0, 0, 2, 0, 3, 0), \\ & \sqrt{\frac{150}{2431}}(1, 0, 2, 0, 2, 0), \sqrt{\frac{150}{2431}}(2, 0, 1, 0, 2, 0), \sqrt{\frac{150}{2431}}(2, 0, 2, 0, 1, 0), \\ & \sqrt{\frac{12}{143}}(3, 0, 1, 0, 1, 0), \sqrt{\frac{12}{143}}(1, 0, 3, 0, 1, 0), \sqrt{\frac{12}{143}}(1, 0, 1, 0, 3, 0) \end{aligned}$
$1000_{[31]\rho}$	$\begin{aligned} & \sqrt{\frac{77}{4199}}(0, 1, 0, 0, 4, 1), \sqrt{\frac{42}{4199}}(0, 1, 0, 1, 4, 0), \sqrt{\frac{84}{4199}}(0, 1, 1, 0, 3, 1), \\ & \sqrt{\frac{280}{12597}}(0, 1, 1, 1, 3, 0), \sqrt{\frac{70}{4199}}(0, 1, 2, 0, 2, 1), \sqrt{\frac{140}{4199}}(0, 1, 2, 1, 2, 0), \\ & \sqrt{\frac{140}{12597}}(0, 1, 3, 0, 1, 1), \sqrt{\frac{168}{4199}}(0, 1, 3, 1, 1, 0), \sqrt{\frac{21}{4199}}(0, 1, 4, 0, 0, 1), \\ & \sqrt{\frac{154}{4199}}(0, 1, 4, 1, 0, 0), \sqrt{\frac{140}{4199}}(1, 1, 0, 0, 3, 1), \sqrt{\frac{280}{12597}}(1, 1, 0, 1, 3, 0), \\ & \sqrt{\frac{140}{4199}}(1, 1, 1, 0, 2, 1), \sqrt{\frac{200}{4199}}(1, 1, 1, 1, 2, 0), \sqrt{\frac{10}{4199}}(1, 1, 2, 0, 1, 1), \\ & \sqrt{\frac{280}{12597}}(1, 1, 2, 1, 1, 0), \sqrt{\frac{140}{4199}}(1, 1, 3, 0, 0, 1), \sqrt{\frac{280}{4199}}(1, 1, 3, 1, 0, 0), \\ & \sqrt{\frac{490}{12597}}(2, 1, 0, 0, 2, 1), \sqrt{\frac{140}{4199}}(2, 1, 0, 1, 2, 0), \sqrt{\frac{140}{4199}}(2, 1, 1, 0, 1, 1), \\ & \sqrt{\frac{280}{4199}}(2, 1, 1, 1, 1, 0), \sqrt{\frac{70}{4199}}(2, 1, 2, 0, 0, 1), \sqrt{\frac{980}{12597}}(2, 1, 2, 1, 0, 0), \\ & \sqrt{\frac{140}{4199}}(3, 1, 0, 0, 1, 1), \sqrt{\frac{168}{4199}}(3, 1, 0, 1, 1, 0), \sqrt{\frac{84}{4199}}(3, 1, 1, 0, 0, 1), \\ & \sqrt{\frac{280}{4199}}(3, 1, 1, 1, 0, 0), \sqrt{\frac{77}{4199}}(4, 1, 0, 0, 0, 1), \sqrt{\frac{154}{4199}}(4, 1, 0, 1, 0, 0) \end{aligned}$

Table B.7 (Continued) Normalized pentaquark (q^4 symmetry) spatial wave functions quantum number: $2N \ 0 \ 0$.

NLM	$C(n_\rho, l_\rho, n_\lambda, l_\lambda, n_\eta, l_\eta)$
$1000_{[31]\lambda}$	$\begin{aligned} & \sqrt{\frac{77}{4199}}(0, 0, 0, 1, 4, 1), -\sqrt{\frac{21}{4199}}(0, 0, 1, 0, 4, 0), \sqrt{\frac{140}{4199}}(0, 0, 1, 1, 3, 1), \\ & -\sqrt{\frac{280}{12597}}(0, 0, 2, 0, 3, 0), \sqrt{\frac{490}{12597}}(0, 0, 2, 1, 2, 1), -\sqrt{\frac{210}{4199}}(0, 0, 3, 0, 2, 0), \\ & \sqrt{\frac{140}{4199}}(0, 0, 3, 1, 1, 1), -\sqrt{\frac{336}{4199}}(0, 0, 4, 0, 1, 0), \sqrt{\frac{77}{4199}}(0, 0, 4, 1, 0, 1), \\ & -\sqrt{\frac{385}{4199}}(0, 0, 5, 0, 0, 0), \sqrt{\frac{21}{4199}}(1, 0, 0, 0, 4, 0), \sqrt{\frac{84}{4199}}(1, 0, 0, 1, 3, 1), \\ & \sqrt{\frac{140}{4199}}(1, 0, 1, 1, 2, 1), -\sqrt{\frac{30}{4199}}(1, 0, 2, 0, 2, 0), \frac{140}{\sqrt{4199}}(1, 1, 2, 1, 1, 1), \\ & -\sqrt{\frac{112}{4199}}(1, 0, 3, 0, 1, 0), \sqrt{\frac{84}{4199}}(1, 0, 3, 1, 0, 1), -\sqrt{\frac{189}{4199}}(1, 0, 4, 0, 0, 0), \\ & \sqrt{\frac{280}{12597}}(2, 0, 0, 0, 3, 0), \sqrt{\frac{70}{4199}}(2, 0, 0, 1, 2, 1), \sqrt{\frac{30}{4199}}(2, 0, 1, 1, 1, 1), \\ & \frac{10}{\sqrt{4199}}(2, 0, 1, 1, 1, 1), \sqrt{\frac{70}{4199}}(2, 0, 2, 1, 0, 1), -\sqrt{\frac{70}{12597}}(2, 0, 3, 0, 0, 0), \\ & \sqrt{\frac{210}{4199}}(3, 0, 0, 0, 2, 0), \sqrt{\frac{140}{12597}}(3, 0, 0, 1, 1, 1), \sqrt{\frac{112}{4199}}(3, 0, 1, 0, 1, 0), \\ & \sqrt{\frac{140}{12597}}(3, 0, 1, 1, 0, 1), \sqrt{\frac{70}{12597}}(3, 0, 2, 0, 0, 0), \sqrt{\frac{336}{4199}}(4, 0, 0, 0, 1, 0), \\ & \sqrt{\frac{21}{4199}}(4, 0, 0, 1, 0, 1), \sqrt{\frac{189}{4199}}(4, 0, 1, 0, 0, 0), \sqrt{\frac{385}{4199}}(5, 0, 0, 0, 0, 0) \end{aligned}$
$1000_{[31]\eta}$	$\begin{aligned} & -\sqrt{\frac{770}{4199}}(0, 0, 0, 0, 5, 0), -\sqrt{\frac{1029}{8398}}(0, 0, 1, 0, 4, 0), -\sqrt{\frac{560}{12597}}(0, 0, 2, 0, 3, 0), \\ & -\sqrt{\frac{35}{12597}}(0, 0, 3, 0, 2, 0), \sqrt{\frac{42}{4199}}(0, 0, 4, 0, 1, 0), \sqrt{\frac{385}{8398}}(0, 0, 5, 0, 0, 0), \\ & -\sqrt{\frac{1029}{8398}}(1, 0, 0, 0, 4, 0), -\sqrt{\frac{224}{4199}}(1, 0, 1, 0, 3, 0), -\sqrt{\frac{15}{4199}}(1, 0, 2, 0, 2, 0), \\ & \sqrt{\frac{56}{4199}}(1, 0, 3, 0, 1, 0), \sqrt{\frac{525}{8398}}(1, 0, 4, 0, 0, 0), -\sqrt{\frac{560}{12597}}(2, 0, 0, 0, 3, 0), \\ & -\sqrt{\frac{15}{4199}}(2, 0, 1, 0, 2, 0), \sqrt{\frac{60}{4199}}(2, 0, 2, 0, 1, 0), \sqrt{\frac{875}{12597}}(2, 0, 3, 0, 0, 0), \\ & -\sqrt{\frac{35}{12597}}(3, 0, 0, 0, 2, 0), \sqrt{\frac{56}{4199}}(3, 0, 1, 0, 1, 0), \sqrt{\frac{875}{12597}}(3, 0, 2, 0, 0, 0), \\ & \sqrt{\frac{42}{4199}}(4, 0, 0, 0, 1, 0), \sqrt{\frac{525}{8398}}(4, 0, 1, 0, 0, 0), \sqrt{\frac{385}{8398}}(5, 0, 0, 0, 0, 0) \end{aligned}$
$1000_{[22]\rho}$	$\begin{aligned} & \sqrt{\frac{154}{4199}}(0, 1, 0, 0, 4, 1), -\sqrt{\frac{21}{4199}}(0, 1, 0, 1, 4, 0), \sqrt{\frac{168}{4199}}(0, 1, 1, 0, 3, 1), \\ & -\sqrt{\frac{140}{12597}}(0, 1, 1, 1, 3, 0), \sqrt{\frac{140}{4199}}(0, 1, 2, 0, 2, 1), -\sqrt{\frac{70}{4199}}(0, 1, 2, 1, 2, 0), \\ & \sqrt{\frac{280}{12597}}(0, 1, 3, 0, 1, 1), -\sqrt{\frac{84}{4199}}(0, 1, 3, 1, 1, 0), \sqrt{\frac{42}{4199}}(0, 1, 4, 0, 0, 1), \\ & -\sqrt{\frac{77}{4199}}(0, 1, 4, 1, 0, 0), \sqrt{\frac{70}{4199}}(1, 1, 0, 0, 3, 1), -\sqrt{\frac{140}{12597}}(1, 1, 0, 1, 3, 0), \end{aligned}$

Table B.7 (Continued) Normalized pentaquark (q^4 symmetry) spatial wave functions quantum number: $2N \ 0 \ 0$.

NLM	$C(n_\rho, l_\rho, n_\lambda, l_\lambda, n_\eta, l_\eta)$
	$\sqrt{\frac{280}{4199}}(1, 1, 1, 0, 2, 1), -\frac{10}{\sqrt{4199}}(1, 1, 1, 1, 2, 0), \sqrt{\frac{200}{4199}}(1, 1, 2, 0, 1, 1),$ $-\sqrt{\frac{140}{12597}}(1, 1, 2, 1, 1, 0), \sqrt{\frac{280}{4199}}(1, 1, 3, 0, 0, 1), -\sqrt{\frac{140}{4199}}(1, 1, 3, 1, 0, 0),$ $\sqrt{\frac{980}{12597}}(2, 1, 0, 0, 2, 1), -\sqrt{\frac{70}{4199}}(2, 1, 0, 1, 2, 0), \sqrt{\frac{280}{4199}}(2, 1, 1, 0, 1, 1),$ $-\sqrt{\frac{140}{4199}}(2, 1, 1, 1, 1, 0), \sqrt{\frac{140}{4199}}(2, 1, 2, 0, 0, 1), -\sqrt{\frac{490}{12597}}(2, 1, 2, 1, 0, 0),$ $\sqrt{\frac{280}{4199}}(3, 1, 0, 0, 1, 1), -\sqrt{\frac{84}{4199}}(3, 1, 0, 1, 1, 0), \sqrt{\frac{168}{4199}}(3, 1, 1, 0, 0, 1),$ $-\sqrt{\frac{140}{4199}}(3, 1, 1, 1, 0, 0), \sqrt{\frac{154}{4199}}(4, 1, 0, 0, 0, 1), -\sqrt{\frac{77}{4199}}(4, 1, 0, 1, 0, 0)$
$1000_{[22]\lambda}$	$\sqrt{\frac{154}{4199}}(0, 0, 0, 1, 4, 1), \sqrt{\frac{21}{8398}}(0, 0, 1, 0, 4, 0), \sqrt{\frac{280}{4199}}(0, 0, 1, 1, 3, 1),$ $\sqrt{\frac{140}{12597}}(0, 0, 2, 0, 3, 0), \sqrt{\frac{980}{12597}}(0, 0, 2, 1, 2, 1), \sqrt{\frac{105}{4199}}(0, 0, 3, 0, 2, 0),$ $\sqrt{\frac{280}{4199}}(0, 0, 3, 1, 1, 1), \sqrt{\frac{168}{4199}}(0, 0, 4, 0, 1, 0), \sqrt{\frac{154}{4199}}(0, 0, 4, 1, 0, 1),$ $\sqrt{\frac{385}{8398}}(0, 0, 5, 0, 0, 0), -\sqrt{\frac{21}{8398}}(1, 0, 0, 0, 4, 0), \sqrt{\frac{168}{4199}}(1, 0, 0, 1, 3, 1),$ $\sqrt{\frac{280}{4199}}(1, 0, 1, 1, 2, 1), \sqrt{\frac{15}{4199}}(1, 0, 2, 0, 2, 0), \frac{280}{\sqrt{4199}}(1, 1, 2, 1, 1, 1),$ $\sqrt{\frac{56}{4199}}(1, 0, 3, 0, 1, 0), \sqrt{\frac{168}{4199}}(1, 0, 3, 1, 0, 1), \sqrt{\frac{189}{8398}}(1, 0, 4, 0, 0, 0),$ $-\sqrt{\frac{140}{12597}}(2, 0, 0, 0, 3, 0), \sqrt{\frac{140}{4199}}(2, 0, 0, 1, 2, 1), -\sqrt{\frac{15}{4199}}(2, 0, 1, 1, 1, 1),$ $\sqrt{\frac{200}{4199}}(2, 0, 1, 1, 1, 1), \sqrt{\frac{140}{4199}}(2, 0, 2, 1, 0, 1), \sqrt{\frac{35}{12597}}(2, 0, 3, 0, 0, 0),$ $-\sqrt{\frac{105}{4199}}(3, 0, 0, 0, 2, 0), \sqrt{\frac{280}{12597}}(3, 0, 0, 1, 1, 1), -\sqrt{\frac{56}{4199}}(3, 0, 1, 0, 1, 0),$ $\sqrt{\frac{280}{12597}}(3, 0, 1, 1, 0, 1), -\sqrt{\frac{35}{12597}}(3, 0, 2, 0, 0, 0), -\sqrt{\frac{168}{4199}}(4, 0, 0, 0, 1, 0),$ $\sqrt{\frac{42}{4199}}(4, 0, 0, 1, 0, 1), -\sqrt{\frac{189}{8398}}(4, 0, 1, 0, 0, 0), -\sqrt{\frac{385}{8398}}(5, 0, 0, 0, 0, 0)$
$1200_{[4]S}$	$\sqrt{\frac{7}{323}}(6, 0, 0, 0, 0, 0), \sqrt{\frac{7}{323}}(0, 0, 6, 0, 0, 0), \sqrt{\frac{7}{323}}(0, 0, 0, 0, 6, 0),$ $\sqrt{\frac{126}{4199}}(5, 0, 1, 0, 0, 0), \sqrt{\frac{126}{4199}}(5, 0, 0, 0, 1, 0), \sqrt{\frac{126}{4199}}(1, 0, 5, 0, 0, 0),$ $\sqrt{\frac{126}{4199}}(0, 0, 5, 0, 1, 0), \sqrt{\frac{126}{4199}}(1, 0, 0, 0, 5, 0), \sqrt{\frac{126}{4199}}(0, 0, 1, 0, 5, 0),$ $\sqrt{\frac{1575}{46189}}(4, 0, 2, 0, 0, 0), \sqrt{\frac{1575}{46189}}(4, 0, 0, 0, 2, 0), \sqrt{\frac{1575}{46189}}(2, 0, 4, 0, 0, 0),$ $\sqrt{\frac{1575}{46189}}(0, 0, 4, 0, 2, 0), \sqrt{\frac{1575}{46189}}(2, 0, 0, 0, 4, 0), \sqrt{\frac{1575}{46189}}(0, 0, 2, 0, 4, 0),$

Table B.7 (Continued) Normalized pentaquark (q^4 symmetry) spatial wave functions quantum number: $2N \ 0 \ 0$.

NLM	$C(n_\rho, l_\rho, n_\lambda, l_\lambda, n_\eta, l_\eta)$
	$\frac{70}{\sqrt{138567}}(0, 0, 3, 0, 3, 0), \frac{70}{\sqrt{138567}}(3, 0, 0, 0, 3, 0), \frac{70}{\sqrt{138567}}(3, 0, 3, 0, 0, 0),$ $\sqrt{\frac{2100}{46189}}(3, 0, 1, 0, 2, 0), \sqrt{\frac{2100}{46189}}(3, 0, 2, 0, 1, 0), \sqrt{\frac{2100}{46189}}(1, 0, 3, 0, 2, 0),$ $\sqrt{\frac{2100}{46189}}(2, 0, 3, 0, 1, 0), \sqrt{\frac{2100}{46189}}(1, 0, 2, 0, 3, 0), \sqrt{\frac{2100}{46189}}(2, 0, 1, 0, 3, 0),$ $\sqrt{\frac{1890}{46189}}(4, 0, 1, 0, 1, 0), \sqrt{\frac{1890}{46189}}(1, 0, 4, 0, 1, 0), \sqrt{\frac{1890}{46189}}(1, 0, 1, 0, 4, 0),$ $\sqrt{\frac{2250}{46189}}(2, 0, 2, 0, 2, 0)$
1400 _{[4]S}	$\sqrt{\frac{5}{323}}(7, 0, 0, 0, 0, 0), \sqrt{\frac{5}{323}}(0, 0, 7, 0, 0, 0), \sqrt{\frac{5}{323}}(0, 0, 0, 0, 7, 0),$ $\sqrt{\frac{7}{323}}(6, 0, 1, 0, 0, 0), \sqrt{\frac{7}{323}}(6, 0, 0, 0, 1, 0), \sqrt{\frac{7}{323}}(1, 0, 6, 0, 0, 0),$ $\sqrt{\frac{7}{323}}(0, 0, 6, 0, 1, 0), \sqrt{\frac{7}{323}}(1, 0, 0, 0, 6, 0), \sqrt{\frac{7}{323}}(0, 0, 1, 0, 6, 0),$ $\sqrt{\frac{105}{4199}}(5, 0, 2, 0, 0, 0), \sqrt{\frac{105}{4199}}(5, 0, 0, 0, 2, 0), \sqrt{\frac{105}{4199}}(2, 0, 5, 0, 0, 0),$ $\sqrt{\frac{105}{4199}}(0, 0, 5, 0, 2, 0), \sqrt{\frac{105}{4199}}(2, 0, 0, 0, 5, 0), \sqrt{\frac{105}{4199}}(0, 0, 2, 0, 5, 0),$ $\sqrt{\frac{126}{4199}}(5, 0, 1, 0, 1, 0), \sqrt{\frac{126}{4199}}(1, 0, 5, 0, 1, 0), \sqrt{\frac{126}{4199}}(1, 0, 1, 0, 5, 0),$ $\frac{35}{\sqrt{46189}}(0, 0, 4, 0, 3, 0), \frac{35}{\sqrt{46189}}(0, 0, 3, 0, 4, 0), \frac{35}{\sqrt{46189}}(4, 0, 0, 0, 3, 0),$ $\frac{35}{\sqrt{46189}}(3, 0, 0, 0, 4, 0), \frac{35}{\sqrt{46189}}(4, 0, 3, 0, 0, 0), \frac{35}{\sqrt{46189}}(3, 0, 4, 0, 0, 0),$ $\sqrt{\frac{1575}{46189}}(4, 0, 1, 0, 2, 0), \sqrt{\frac{1575}{46189}}(4, 0, 2, 0, 1, 0), \sqrt{\frac{1575}{46189}}(1, 0, 4, 0, 2, 0),$ $\sqrt{\frac{1575}{46189}}(2, 0, 4, 0, 1, 0), \sqrt{\frac{1575}{46189}}(1, 0, 2, 0, 4, 0), \sqrt{\frac{1575}{46189}}(2, 0, 1, 0, 4, 0),$ $\frac{70}{\sqrt{138567}}(1, 0, 3, 0, 3, 0), \frac{70}{\sqrt{138567}}(3, 0, 1, 0, 3, 0), \frac{70}{\sqrt{138567}}(3, 0, 3, 0, 1, 0),$ $\sqrt{\frac{1750}{46189}}(3, 0, 2, 0, 2, 0), \sqrt{\frac{1750}{46189}}(2, 0, 3, 0, 2, 0), \sqrt{\frac{1750}{46189}}(2, 0, 2, 0, 3, 0)$
1600 _{[4]S}	$\sqrt{\frac{5}{437}}(8, 0, 0, 0, 0, 0), \sqrt{\frac{5}{437}}(0, 0, 8, 0, 0, 0), \sqrt{\frac{5}{437}}(0, 0, 0, 0, 8, 0),$ $\sqrt{\frac{120}{7429}}(7, 0, 1, 0, 0, 0), \sqrt{\frac{120}{7429}}(7, 0, 0, 0, 1, 0), \sqrt{\frac{120}{7429}}(1, 0, 7, 0, 0, 0),$ $\sqrt{\frac{120}{7429}}(0, 0, 7, 0, 1, 0), \sqrt{\frac{120}{7429}}(1, 0, 0, 0, 7, 0), \sqrt{\frac{120}{7429}}(0, 0, 1, 0, 7, 0),$ $\sqrt{\frac{140}{7429}}(6, 0, 2, 0, 0, 0), \sqrt{\frac{140}{7429}}(6, 0, 0, 0, 2, 0), \sqrt{\frac{140}{7429}}(2, 0, 6, 0, 0, 0),$ $\sqrt{\frac{140}{7429}}(0, 0, 6, 0, 2, 0), \sqrt{\frac{140}{7429}}(2, 0, 0, 0, 6, 0), \sqrt{\frac{140}{7429}}(0, 0, 2, 0, 6, 0),$

Table B.7 (Continued) Normalized pentaquark (q^4 symmetry) spatial wave functions quantum number: $2N \ 0 \ 0$.

NLM	$C(n_\rho, l_\rho, n_\lambda, l_\lambda, n_\eta, l_\eta)$
	$\sqrt{\frac{168}{7429}}(6, 0, 1, 0, 1, 0), \sqrt{\frac{168}{7429}}(1, 0, 6, 0, 1, 0), \sqrt{\frac{168}{7429}}(1, 0, 1, 0, 6, 0),$ $\sqrt{\frac{1960}{96577}}(0, 0, 5, 0, 3, 0), \sqrt{\frac{1960}{96577}}(0, 0, 3, 0, 5, 0), \sqrt{\frac{1960}{96577}}(5, 0, 0, 0, 3, 0),$ $\sqrt{\frac{1960}{96577}}(3, 0, 0, 0, 5, 0), \sqrt{\frac{1960}{96577}}(5, 0, 3, 0, 0, 0), \sqrt{\frac{1960}{96577}}(3, 0, 5, 0, 0, 0),$ $\sqrt{\frac{2520}{96577}}(5, 0, 1, 0, 2, 0), \sqrt{\frac{2520}{96577}}(5, 0, 2, 0, 1, 0), \sqrt{\frac{2520}{96577}}(1, 0, 5, 0, 2, 0),$ $\sqrt{\frac{2520}{96577}}(2, 0, 5, 0, 1, 0), \sqrt{\frac{2520}{96577}}(1, 0, 2, 0, 5, 0), \sqrt{\frac{2520}{96577}}(2, 0, 1, 0, 5, 0),$ $\sqrt{\frac{22050}{1062347}}(0, 0, 4, 0, 4, 0), \sqrt{\frac{22050}{1062347}}(4, 0, 0, 0, 4, 0), \sqrt{\frac{22050}{1062347}}(4, 0, 4, 0, 0, 0),$ $\sqrt{\frac{29400}{1062347}}(4, 0, 1, 0, 3, 0), \sqrt{\frac{29400}{1062347}}(4, 0, 3, 0, 1, 0), \sqrt{\frac{29400}{1062347}}(1, 0, 4, 0, 3, 0),$ $\sqrt{\frac{29400}{1062347}}(3, 0, 4, 0, 1, 0), \sqrt{\frac{29400}{1062347}}(1, 0, 3, 0, 4, 0), \sqrt{\frac{29400}{1062347}}(3, 0, 1, 0, 4, 0),$ $\sqrt{\frac{31500}{1062347}}(4, 0, 2, 0, 2, 0), \sqrt{\frac{31500}{1062347}}(2, 0, 4, 0, 2, 0), \sqrt{\frac{31500}{1062347}}(2, 0, 2, 0, 4, 0),$ $\sqrt{\frac{98000}{3187041}}(2, 0, 3, 0, 3, 0), \sqrt{\frac{98000}{3187041}}(3, 0, 2, 0, 3, 0), \sqrt{\frac{98000}{3187041}}(3, 0, 3, 0, 2, 0)$
$1800_{[4]S}$	$\frac{1}{\sqrt{105}}(9, 0, 0, 0, 0, 0), \frac{1}{\sqrt{105}}(0, 0, 9, 0, 0, 0), \frac{1}{\sqrt{105}}(0, 0, 0, 0, 9, 0),$ $\sqrt{\frac{27}{2185}}(8, 0, 1, 0, 0, 0), \sqrt{\frac{27}{2185}}(8, 0, 0, 0, 1, 0), \sqrt{\frac{27}{2185}}(1, 0, 8, 0, 0, 0),$ $\sqrt{\frac{27}{2185}}(0, 0, 8, 0, 1, 0), \sqrt{\frac{27}{2185}}(1, 0, 0, 0, 8, 0), \sqrt{\frac{27}{2185}}(0, 0, 1, 0, 8, 0),$ $\sqrt{\frac{108}{7429}}(7, 0, 2, 0, 0, 0), \sqrt{\frac{108}{7429}}(7, 0, 0, 0, 2, 0), \sqrt{\frac{108}{7429}}(2, 0, 7, 0, 0, 0),$ $\sqrt{\frac{108}{7429}}(0, 0, 7, 0, 2, 0), \sqrt{\frac{108}{7429}}(2, 0, 0, 0, 7, 0), \sqrt{\frac{108}{7429}}(0, 0, 2, 0, 7, 0),$ $\sqrt{\frac{648}{37145}}(7, 0, 1, 0, 1, 0), \sqrt{\frac{648}{37145}}(1, 0, 7, 0, 1, 0), \sqrt{\frac{648}{37145}}(1, 0, 1, 0, 7, 0),$ $\sqrt{\frac{588}{37145}}(0, 0, 6, 0, 3, 0), \sqrt{\frac{588}{37145}}(0, 0, 3, 0, 6, 0), \sqrt{\frac{588}{37145}}(6, 0, 0, 0, 3, 0),$ $\sqrt{\frac{588}{37145}}(3, 0, 0, 0, 6, 0), \sqrt{\frac{588}{37145}}(6, 0, 3, 0, 0, 0), \sqrt{\frac{588}{37145}}(3, 0, 6, 0, 0, 0),$ $\sqrt{\frac{756}{37145}}(6, 0, 1, 0, 2, 0), \sqrt{\frac{756}{37145}}(6, 0, 2, 0, 1, 0), \sqrt{\frac{756}{37145}}(1, 0, 6, 0, 2, 0),$ $\sqrt{\frac{756}{37145}}(2, 0, 6, 0, 1, 0), \sqrt{\frac{756}{37145}}(1, 0, 2, 0, 6, 0), \sqrt{\frac{756}{37145}}(2, 0, 1, 0, 6, 0),$ $\sqrt{\frac{7938}{482885}}(0, 0, 5, 0, 4, 0), \sqrt{\frac{7938}{482885}}(0, 0, 4, 0, 5, 0), \sqrt{\frac{7938}{482885}}(5, 0, 0, 0, 4, 0),$ $\sqrt{\frac{7938}{482885}}(4, 0, 0, 0, 5, 0), \sqrt{\frac{7938}{482885}}(5, 0, 4, 0, 0, 0), \sqrt{\frac{7938}{482885}}(4, 0, 5, 0, 0, 0),$

Table B.7 (Continued) Normalized pentaquark (q^4 symmetry) spatial wave functions quantum number: $2N \ 0 \ 0$.

NLM	$C(n_\rho, l_\rho, n_\lambda, l_\lambda, n_\eta, l_\eta)$
	$\sqrt{\frac{10584}{482885}}(5, 0, 1, 0, 3, 0), \sqrt{\frac{10584}{482885}}(5, 0, 3, 0, 1, 0), \sqrt{\frac{10584}{482885}}(1, 0, 5, 0, 3, 0),$ $\sqrt{\frac{10584}{482885}}(3, 0, 5, 0, 1, 0), \sqrt{\frac{10584}{482885}}(1, 0, 3, 0, 5, 0), \sqrt{\frac{10584}{482885}}(3, 0, 1, 0, 5, 0),$ $\sqrt{\frac{2268}{96577}}(5, 0, 2, 0, 2, 0), \sqrt{\frac{2268}{96577}}(2, 0, 5, 0, 2, 0), \sqrt{\frac{2268}{96577}}(2, 0, 2, 0, 5, 0),$ $\sqrt{\frac{23814}{1062347}}(1, 0, 4, 0, 4, 0), \sqrt{\frac{23814}{1062347}}(4, 0, 1, 0, 4, 0), \sqrt{\frac{23814}{1062347}}(4, 0, 4, 0, 1, 0),$ $\sqrt{\frac{26460}{1062347}}(4, 0, 2, 0, 3, 0), \sqrt{\frac{26460}{1062347}}(4, 0, 3, 0, 2, 0), \sqrt{\frac{26460}{1062347}}(2, 0, 4, 0, 3, 0),$ $\sqrt{\frac{26460}{1062347}}(3, 0, 4, 0, 2, 0), \sqrt{\frac{26460}{1062347}}(2, 0, 3, 0, 4, 0), \sqrt{\frac{26460}{1062347}}(3, 0, 2, 0, 4, 0),$ $\sqrt{\frac{2250}{46189}}(3, 0, 3, 0, 3, 0)$
$2000_{[4]S}$	$\sqrt{\frac{7}{1035}}(10, 0, 0, 0, 0, 0), \sqrt{\frac{7}{1035}}(0, 0, 10, 0, 0, 0), \sqrt{\frac{7}{1035}}(0, 0, 0, 0, 10, 0),$ $\sqrt{\frac{2}{207}}(9, 0, 1, 0, 0, 0), \sqrt{\frac{2}{207}}(9, 0, 0, 0, 1, 0), \sqrt{\frac{2}{207}}(1, 0, 9, 0, 0, 0),$ $\sqrt{\frac{2}{207}}(0, 0, 9, 0, 1, 0), \sqrt{\frac{2}{207}}(1, 0, 0, 0, 9, 0), \sqrt{\frac{2}{207}}(0, 0, 1, 0, 9, 0),$ $\sqrt{\frac{5}{437}}(8, 0, 2, 0, 0, 0), \sqrt{\frac{5}{437}}(8, 0, 0, 0, 2, 0), \sqrt{\frac{5}{437}}(2, 0, 8, 0, 0, 0),$ $\sqrt{\frac{5}{437}}(0, 0, 8, 0, 2, 0), \sqrt{\frac{5}{437}}(2, 0, 0, 0, 8, 0), \sqrt{\frac{5}{437}}(0, 0, 2, 0, 8, 0),$ $\sqrt{\frac{6}{437}}(8, 0, 1, 0, 1, 0), \sqrt{\frac{6}{437}}(1, 0, 8, 0, 1, 0), \sqrt{\frac{6}{437}}(1, 0, 1, 0, 8, 0),$ $\sqrt{\frac{280}{22287}}(0, 0, 7, 0, 3, 0), \sqrt{\frac{280}{22287}}(0, 0, 3, 0, 7, 0), \sqrt{\frac{280}{22287}}(7, 0, 0, 0, 3, 0),$ $\sqrt{\frac{280}{22287}}(3, 0, 0, 0, 7, 0), \sqrt{\frac{280}{22287}}(7, 0, 3, 0, 0, 0), \sqrt{\frac{280}{22287}}(3, 0, 7, 0, 0, 0),$ $\sqrt{\frac{120}{7429}}(7, 0, 1, 0, 2, 0), \sqrt{\frac{120}{7429}}(7, 0, 2, 0, 1, 0), \sqrt{\frac{120}{7429}}(1, 0, 7, 0, 2, 0),$ $\sqrt{\frac{120}{7429}}(2, 0, 7, 0, 1, 0), \sqrt{\frac{120}{7429}}(1, 0, 2, 0, 7, 0), \sqrt{\frac{120}{7429}}(2, 0, 1, 0, 7, 0),$ $\sqrt{\frac{56}{7429}}(0, 0, 6, 0, 4, 0), \sqrt{\frac{56}{7429}}(0, 0, 4, 0, 6, 0), \sqrt{\frac{56}{7429}}(6, 0, 0, 0, 4, 0),$ $\sqrt{\frac{56}{7429}}(4, 0, 0, 0, 6, 0), \sqrt{\frac{56}{7429}}(6, 0, 4, 0, 0, 0), \sqrt{\frac{56}{7429}}(4, 0, 6, 0, 0, 0),$ $\sqrt{\frac{392}{22287}}(6, 0, 1, 0, 3, 0), \sqrt{\frac{392}{22287}}(6, 0, 3, 0, 1, 0), \sqrt{\frac{392}{22287}}(1, 0, 6, 0, 3, 0),$ $\sqrt{\frac{392}{22287}}(3, 0, 6, 0, 1, 0), \sqrt{\frac{392}{22287}}(1, 0, 3, 0, 6, 0), \sqrt{\frac{392}{22287}}(3, 0, 1, 0, 6, 0),$ $\sqrt{\frac{140}{7429}}(6, 0, 2, 0, 2, 0), \sqrt{\frac{140}{7429}}(2, 0, 6, 0, 2, 0), \sqrt{\frac{140}{7429}}(2, 0, 2, 0, 6, 0),$

Table B.7 (Continued) Normalized pentaquark (q^4 symmetry) spatial wave functions quantum number: $2N \ 0 \ 0$.

NLM	$C(n_\rho, l_\rho, n_\lambda, l_\lambda, n_\eta, l_\eta)$
	$\sqrt{\frac{6468}{482885}}(0, 0, 5, 0, 5, 0), \sqrt{\frac{6468}{482885}}(5, 0, 0, 0, 5, 0), \sqrt{\frac{6468}{482885}}(5, 0, 5, 0, 0, 0),$ $\frac{42}{\sqrt{96577}}(5, 0, 1, 0, 4, 0), \frac{42}{\sqrt{96577}}(5, 0, 4, 0, 1, 0), \frac{42}{\sqrt{96577}}(1, 0, 5, 0, 4, 0),$ $\frac{42}{\sqrt{96577}}(4, 0, 5, 0, 1, 0), \frac{42}{\sqrt{96577}}(1, 0, 4, 0, 5, 0), \frac{42}{\sqrt{96577}}(4, 0, 1, 0, 5, 0),$ $\sqrt{\frac{1960}{96577}}(5, 0, 2, 0, 3, 0), \sqrt{\frac{1960}{96577}}(5, 0, 3, 0, 2, 0), \sqrt{\frac{1960}{96577}}(2, 0, 5, 0, 3, 0),$ $\sqrt{\frac{1960}{96577}}(3, 0, 5, 0, 2, 0), \sqrt{\frac{1960}{96577}}(2, 0, 3, 0, 5, 0), \sqrt{\frac{1960}{96577}}(3, 0, 2, 0, 5, 0),$ $\sqrt{\frac{22050}{1062347}}(2, 0, 4, 0, 4, 0), \sqrt{\frac{22050}{1062347}}(4, 0, 2, 0, 4, 0), \sqrt{\frac{22050}{1062347}}(4, 0, 4, 0, 2, 0),$ $\sqrt{\frac{68600}{3187041}}(4, 0, 3, 0, 3, 0), \sqrt{\frac{68600}{3187041}}(3, 0, 4, 0, 3, 0), \sqrt{\frac{68600}{3187041}}(3, 0, 3, 0, 4, 0)$
$2200_{[4]S}$	$\sqrt{\frac{7}{1305}}(11, 0, 0, 0, 0, 0), \sqrt{\frac{7}{1305}}(0, 0, 11, 0, 0, 0), \sqrt{\frac{7}{1305}}(0, 0, 0, 0, 11, 0),$ $\sqrt{\frac{77}{10005}}(10, 0, 1, 0, 0, 0), \sqrt{\frac{77}{10005}}(10, 0, 0, 0, 1, 0), \sqrt{\frac{77}{10005}}(1, 0, 10, 0, 0, 0),$ $\sqrt{\frac{77}{10005}}(0, 0, 10, 0, 1, 0), \sqrt{\frac{77}{10005}}(1, 0, 0, 0, 10, 0), \sqrt{\frac{77}{10005}}(0, 0, 1, 0, 10, 0),$ $\sqrt{\frac{55}{6003}}(9, 0, 2, 0, 0, 0), \sqrt{\frac{55}{6003}}(9, 0, 0, 0, 2, 0), \sqrt{\frac{55}{6003}}(2, 0, 9, 0, 0, 0),$ $\sqrt{\frac{55}{6003}}(0, 0, 9, 0, 2, 0), \sqrt{\frac{55}{6003}}(2, 0, 0, 0, 9, 0), \sqrt{\frac{55}{6003}}(0, 0, 2, 0, 9, 0),$ $\sqrt{\frac{22}{2001}}(9, 0, 1, 0, 1, 0), \sqrt{\frac{22}{2001}}(1, 0, 9, 0, 1, 0), \sqrt{\frac{22}{2001}}(1, 0, 1, 0, 9, 0),$ $\sqrt{\frac{385}{38019}}(0, 0, 8, 0, 3, 0), \sqrt{\frac{385}{38019}}(0, 0, 3, 0, 8, 0), \sqrt{\frac{385}{38019}}(8, 0, 0, 0, 3, 0),$ $\sqrt{\frac{385}{38019}}(3, 0, 0, 0, 8, 0), \sqrt{\frac{385}{38019}}(8, 0, 3, 0, 0, 0), \sqrt{\frac{385}{38019}}(3, 0, 8, 0, 0, 0),$ $\sqrt{\frac{165}{12673}}(8, 0, 1, 0, 2, 0), \sqrt{\frac{165}{12673}}(8, 0, 2, 0, 1, 0), \sqrt{\frac{165}{12673}}(1, 0, 8, 0, 2, 0),$ $\sqrt{\frac{165}{12673}}(2, 0, 8, 0, 1, 0), \sqrt{\frac{165}{12673}}(1, 0, 2, 0, 8, 0), \sqrt{\frac{165}{12673}}(2, 0, 1, 0, 8, 0),$ $\sqrt{\frac{2310}{215441}}(0, 0, 7, 0, 4, 0), \sqrt{\frac{2310}{215441}}(0, 0, 4, 0, 7, 0), \sqrt{\frac{2310}{215441}}(7, 0, 0, 0, 4, 0),$ $\sqrt{\frac{2310}{215441}}(4, 0, 0, 0, 7, 0), \sqrt{\frac{2310}{215441}}(7, 0, 4, 0, 0, 0), \sqrt{\frac{2310}{215441}}(4, 0, 7, 0, 0, 0),$ $\sqrt{\frac{3080}{215441}}(7, 0, 1, 0, 3, 0), \sqrt{\frac{3080}{215441}}(7, 0, 3, 0, 1, 0), \sqrt{\frac{3080}{215441}}(1, 0, 7, 0, 3, 0),$ $\sqrt{\frac{3080}{215441}}(3, 0, 7, 0, 1, 0), \sqrt{\frac{3080}{215441}}(1, 0, 3, 0, 7, 0), \sqrt{\frac{3080}{215441}}(3, 0, 1, 0, 7, 0),$ $\sqrt{\frac{3300}{215441}}(7, 0, 2, 0, 2, 0), \sqrt{\frac{3300}{215441}}(2, 0, 7, 0, 2, 0), \sqrt{\frac{3300}{215441}}(2, 0, 2, 0, 7, 0),$

Table B.7 (Continued) Normalized pentaquark (q^4 symmetry) spatial wave functions quantum number: $2N \ 0 \ 0$.

NLM	$C(n_\rho, l_\rho, n_\lambda, l_\lambda, n_\eta, l_\eta)$
	$\sqrt{\frac{11858}{1077205}}(0, 0, 5, 0, 6, 0), \sqrt{\frac{11858}{1077205}}(0, 0, 6, 0, 5, 0), \sqrt{\frac{11858}{1077205}}(5, 0, 0, 0, 6, 0),$
	$\sqrt{\frac{11858}{1077205}}(6, 0, 0, 0, 5, 0), \sqrt{\frac{11858}{1077205}}(5, 0, 6, 0, 0, 0), \sqrt{\frac{11858}{1077205}}(6, 0, 5, 0, 0, 0),$
	$\sqrt{\frac{3234}{215441}}(6, 0, 1, 0, 4, 0), \sqrt{\frac{3234}{215441}}(6, 0, 4, 0, 1, 0), \sqrt{\frac{3234}{215441}}(1, 0, 6, 0, 4, 0),$
	$\sqrt{\frac{3234}{215441}}(4, 0, 6, 0, 1, 0), \sqrt{\frac{3234}{215441}}(1, 0, 4, 0, 6, 0), \sqrt{\frac{3234}{215441}}(4, 0, 1, 0, 6, 0),$
	$\sqrt{\frac{10780}{646323}}(6, 0, 2, 0, 3, 0), \sqrt{\frac{10780}{646323}}(6, 0, 3, 0, 2, 0), \sqrt{\frac{10780}{646323}}(2, 0, 6, 0, 3, 0),$
	$\sqrt{\frac{10780}{646323}}(3, 0, 6, 0, 2, 0), \sqrt{\frac{10780}{646323}}(2, 0, 3, 0, 6, 0), \sqrt{\frac{10780}{646323}}(3, 0, 2, 0, 6, 0),$
	$\frac{462}{\sqrt{14003665}}(1, 0, 5, 0, 5, 0), \frac{462}{\sqrt{14003665}}(5, 0, 1, 0, 5, 0),$
	$\frac{462}{\sqrt{14003665}}(5, 0, 5, 0, 1, 0), \sqrt{\frac{48510}{2800733}}(5, 0, 2, 0, 4, 0),$
	$\sqrt{\frac{48510}{2800733}}(5, 0, 4, 0, 2, 0), \sqrt{\frac{48510}{2800733}}(2, 0, 5, 0, 4, 0),$
	$\sqrt{\frac{48510}{2800733}}(4, 0, 5, 0, 2, 0), \sqrt{\frac{48510}{2800733}}(2, 0, 4, 0, 5, 0), \sqrt{\frac{48510}{2800733}}(4, 0, 2, 0, 5, 0),$
	$\sqrt{\frac{150920}{8402199}}(5, 0, 3, 0, 3, 0), \sqrt{\frac{150920}{8402199}}(3, 0, 5, 0, 3, 0), \sqrt{\frac{150920}{8402199}}(3, 0, 3, 0, 5, 0),$
	$\sqrt{\frac{51450}{2800733}}(3, 0, 4, 0, 4, 0), \sqrt{\frac{51450}{2800733}}(4, 0, 3, 0, 4, 0), \sqrt{\frac{51450}{2800733}}(4, 0, 4, 0, 3, 0)$

Table B.8 Normalized pentaquark (q^4 symmetry) spatial wave functions quantum number: $2N + 1 \ 1 \ 0$.

NLM	$C(n_\rho, l_\rho, n_\lambda, l_\lambda, n_\eta, l_\eta)$
$110_{[31]\rho}$	$(0, 1, 0, 0, 0, 0)$
$110_{[31]\lambda}$	$(0, 0, 0, 1, 0, 0)$
$110_{[31]\eta}$	$(0, 0, 0, 0, 0, 1)$
$310_{[31]\rho}$	$\sqrt{\frac{5}{33}}(1, 1, 0, 0, 0, 0), \frac{1}{\sqrt{11}}(0, 1, 1, 0, 0, 0), \frac{1}{\sqrt{11}}(0, 1, 0, 0, 1, 0)$
$310_{[31]\lambda}$	$\sqrt{\frac{5}{33}}(0, 0, 1, 1, 0, 0), \frac{1}{\sqrt{11}}(1, 0, 0, 1, 0, 0), \frac{1}{\sqrt{11}}(0, 0, 0, 1, 1, 0)$
$310_{[31]\eta}$	$\sqrt{\frac{5}{33}}(0, 0, 0, 0, 1, 1), \frac{1}{\sqrt{11}}(1, 0, 0, 0, 0, 1), \frac{1}{\sqrt{11}}(0, 0, 1, 0, 0, 1)$

Table B.8 (Continued) Normalized pentaquark (q^4 symmetry) spatial wave functions quantum number: $2N + 1 \ 1 \ 0$.

NLM	$C(n_\rho, l_\rho, n_\lambda, l_\lambda, n_\eta, l_\eta)$
$510_{[31]\rho}$	$\sqrt{\frac{35}{429}}(2, 1, 0, 0, 0, 0), \sqrt{\frac{5}{143}}(0, 1, 2, 0, 0, 0), \sqrt{\frac{5}{143}}(0, 1, 0, 0, 2, 0),$ $\sqrt{\frac{10}{143}}(1, 1, 1, 0, 0, 0), \sqrt{\frac{10}{143}}(1, 1, 0, 0, 1, 0), \sqrt{\frac{6}{143}}(0, 1, 1, 0, 1, 0)$
$510_{[31]\lambda}$	$\sqrt{\frac{35}{429}}(0, 0, 2, 1, 0, 0), \sqrt{\frac{5}{143}}(2, 0, 0, 1, 0, 0), \sqrt{\frac{5}{143}}(0, 0, 0, 1, 2, 0),$ $\sqrt{\frac{10}{143}}(1, 0, 1, 1, 0, 0), \sqrt{\frac{10}{143}}(0, 0, 1, 1, 1, 0), \sqrt{\frac{6}{143}}(1, 0, 0, 1, 1, 0)$
$510_{[31]\eta}$	$\sqrt{\frac{35}{429}}(0, 0, 0, 0, 2, 1), \sqrt{\frac{5}{143}}(0, 0, 2, 0, 0, 1), \sqrt{\frac{5}{143}}(2, 0, 0, 0, 0, 1),$ $\sqrt{\frac{10}{143}}(1, 0, 0, 0, 1, 1), \sqrt{\frac{10}{143}}(0, 0, 1, 0, 1, 1), \sqrt{\frac{6}{143}}(1, 0, 1, 0, 0, 1)$
$710_{[31]\rho}$	$\sqrt{\frac{7}{429}}(0, 1, 3, 0, 0, 0), \sqrt{\frac{3}{143}}(0, 1, 2, 0, 1, 0), \sqrt{\frac{3}{143}}(0, 1, 1, 0, 2, 0),$ $\sqrt{\frac{5}{143}}(1, 1, 2, 0, 0, 0), \sqrt{\frac{7}{429}}(0, 1, 0, 0, 3, 0), \sqrt{\frac{6}{143}}(1, 1, 1, 0, 1, 0),$ $\sqrt{\frac{5}{143}}(1, 1, 0, 0, 2, 0), \sqrt{\frac{7}{143}}(2, 1, 1, 0, 0, 0), \sqrt{\frac{7}{143}}(2, 1, 0, 0, 1, 0),$ $\sqrt{\frac{7}{143}}(3, 1, 0, 0, 0, 0)$
$710_{[31]\lambda}$	$\sqrt{\frac{7}{429}}(3, 0, 0, 1, 0, 0), \sqrt{\frac{3}{143}}(2, 0, 0, 1, 1, 0), \sqrt{\frac{3}{143}}(1, 0, 0, 1, 2, 0),$ $\sqrt{\frac{5}{143}}(2, 0, 1, 1, 0, 0), \sqrt{\frac{7}{429}}(0, 0, 0, 1, 3, 0), \sqrt{\frac{6}{143}}(1, 0, 1, 1, 1, 0),$ $\sqrt{\frac{5}{143}}(0, 0, 1, 1, 2, 0), \sqrt{\frac{7}{143}}(1, 0, 2, 1, 0, 0), \sqrt{\frac{7}{143}}(0, 0, 2, 1, 1, 0),$ $\sqrt{\frac{7}{143}}(0, 0, 3, 1, 0, 0)$
$710_{[31]\eta}$	$\sqrt{\frac{7}{429}}(3, 0, 0, 0, 0, 1), \sqrt{\frac{3}{143}}(2, 0, 1, 0, 0, 1), \sqrt{\frac{3}{143}}(1, 0, 2, 0, 0, 1),$ $\sqrt{\frac{5}{143}}(2, 0, 0, 0, 1, 1), \sqrt{\frac{7}{429}}(0, 0, 3, 0, 0, 1), \sqrt{\frac{6}{143}}(1, 0, 1, 0, 1, 1),$ $\sqrt{\frac{5}{143}}(0, 0, 2, 0, 1, 1), \sqrt{\frac{7}{143}}(1, 0, 0, 0, 2, 1), \sqrt{\frac{7}{143}}(0, 0, 1, 0, 2, 1),$ $\sqrt{\frac{7}{143}}(0, 0, 0, 0, 3, 1)$
$910_{[31]\rho}$	$\sqrt{\frac{21}{2431}}(0, 1, 0, 0, 4, 0), \sqrt{\frac{28}{2431}}(0, 1, 1, 0, 3, 0), \sqrt{\frac{30}{2431}}(0, 1, 2, 0, 2, 0),$ $\sqrt{\frac{28}{2431}}(0, 1, 3, 0, 1, 0), \sqrt{\frac{21}{2431}}(0, 1, 4, 0, 0, 0), \sqrt{\frac{140}{7293}}(1, 1, 0, 0, 3, 0),$ $\sqrt{\frac{60}{2431}}(1, 1, 1, 0, 2, 0), \sqrt{\frac{60}{2431}}(1, 1, 2, 0, 1, 0), \sqrt{\frac{140}{7293}}(1, 1, 3, 0, 0, 0),$ $\sqrt{\frac{70}{2431}}(2, 1, 0, 0, 2, 0), \sqrt{\frac{84}{2431}}(2, 1, 1, 0, 1, 0), \sqrt{\frac{70}{2431}}(2, 1, 2, 0, 0, 0),$

Table B.8 (Continued) Normalized pentaquark (q^4 symmetry) spatial wave functions quantum number: $2N + 1 \ 1 \ 0$.

NLM	$C(n_\rho, l_\rho, n_\lambda, l_\lambda, n_\eta, l_\eta)$	
$910_{[31]\lambda}$	$\sqrt{\frac{84}{2431}}(3, 1, 0, 0, 1, 0), \sqrt{\frac{84}{2431}}(3, 1, 1, 0, 0, 0), \sqrt{\frac{7}{221}}(4, 1, 0, 0, 0, 0)$	
	$\sqrt{\frac{21}{2431}}(0, 0, 0, 1, 4, 0), \sqrt{\frac{28}{2431}}(1, 0, 0, 1, 3, 0), \sqrt{\frac{30}{2431}}(2, 0, 0, 1, 2, 0),$	
	$\sqrt{\frac{28}{2431}}(3, 0, 0, 1, 1, 0), \sqrt{\frac{21}{2431}}(4, 0, 0, 1, 0, 0), \sqrt{\frac{140}{7293}}(0, 0, 1, 1, 3, 0),$	
	$\sqrt{\frac{60}{2431}}(1, 0, 1, 1, 2, 0), \sqrt{\frac{60}{2431}}(2, 0, 1, 1, 1, 0), \sqrt{\frac{140}{7293}}(3, 0, 1, 1, 0, 0),$	
	$\sqrt{\frac{70}{2431}}(0, 0, 2, 1, 2, 0), \sqrt{\frac{84}{2431}}(1, 0, 2, 1, 1, 0), \sqrt{\frac{70}{2431}}(2, 0, 2, 1, 0, 0),$	
	$\sqrt{\frac{84}{2431}}(0, 0, 3, 1, 1, 0), \sqrt{\frac{84}{2431}}(1, 0, 3, 1, 0, 0), \sqrt{\frac{7}{221}}(0, 0, 4, 1, 0, 0)$	
$910_{[31]\eta}$	$\sqrt{\frac{21}{2431}}(0, 0, 4, 0, 0, 1), \sqrt{\frac{28}{2431}}(1, 0, 3, 0, 0, 1), \sqrt{\frac{30}{2431}}(2, 0, 2, 0, 0, 1),$	
	$\sqrt{\frac{28}{2431}}(3, 0, 1, 0, 0, 1), \sqrt{\frac{21}{2431}}(4, 0, 0, 0, 0, 1), \sqrt{\frac{140}{7293}}(0, 0, 3, 0, 1, 1),$	
	$\sqrt{\frac{60}{2431}}(1, 0, 2, 0, 1, 1), \sqrt{\frac{60}{2431}}(2, 0, 1, 0, 1, 1), \sqrt{\frac{140}{7293}}(3, 0, 0, 0, 1, 1),$	
	$\sqrt{\frac{70}{2431}}(2, 0, 0, 0, 2, 1), \sqrt{\frac{84}{2431}}(1, 0, 1, 0, 2, 1), \sqrt{\frac{70}{2431}}(0, 0, 2, 0, 2, 1),$	
	$\sqrt{\frac{84}{2431}}(0, 0, 1, 0, 3, 1), \sqrt{\frac{84}{2431}}(1, 0, 0, 0, 3, 1), \sqrt{\frac{7}{221}}(0, 0, 0, 0, 4, 1)$	
	$1110_{[31]\rho}$	$\sqrt{\frac{21}{4199}}(0, 1, 0, 0, 5, 0), \sqrt{\frac{315}{46189}}(0, 1, 1, 0, 4, 0), \sqrt{\frac{350}{46189}}(0, 1, 2, 0, 3, 0),$
$\sqrt{\frac{350}{46189}}(0, 1, 3, 0, 2, 0), \sqrt{\frac{315}{46189}}(0, 1, 4, 0, 1, 0), \sqrt{\frac{21}{4199}}(0, 1, 5, 0, 0, 0),$		
$\sqrt{\frac{525}{46189}}(1, 1, 0, 0, 4, 0), \sqrt{\frac{700}{46189}}(1, 1, 1, 0, 3, 0), \sqrt{\frac{750}{46189}}(1, 1, 2, 0, 2, 0),$		
$\sqrt{\frac{700}{46189}}(1, 1, 3, 0, 1, 0), \sqrt{\frac{525}{46189}}(1, 1, 4, 0, 0, 0), \sqrt{\frac{2450}{138567}}(2, 1, 3, 0, 0, 0),$		
$\sqrt{\frac{1050}{46189}}(2, 1, 1, 0, 2, 0), \sqrt{\frac{1050}{46189}}(2, 1, 2, 0, 1, 0), \sqrt{\frac{2450}{138567}}(2, 1, 0, 0, 3, 0),$		
$\sqrt{\frac{1050}{46189}}(3, 1, 0, 0, 2, 0), \sqrt{\frac{1260}{46189}}(3, 1, 1, 0, 1, 0), \sqrt{\frac{1050}{46189}}(3, 1, 2, 0, 0, 0),$		
$\sqrt{\frac{105}{4199}}(4, 1, 0, 0, 1, 0), \sqrt{\frac{105}{4199}}(4, 1, 1, 0, 0, 0), \sqrt{\frac{7}{323}}(5, 1, 0, 0, 0, 0)$		
$1110_{[31]\lambda}$		$\sqrt{\frac{21}{4199}}(0, 0, 0, 1, 5, 0), \sqrt{\frac{315}{46189}}(1, 0, 0, 1, 4, 0), \sqrt{\frac{350}{46189}}(2, 0, 0, 1, 3, 0),$
		$\sqrt{\frac{350}{46189}}(3, 0, 0, 1, 2, 0), \sqrt{\frac{315}{46189}}(4, 0, 0, 1, 1, 0), \sqrt{\frac{21}{4199}}(5, 0, 0, 1, 0, 0),$
		$\sqrt{\frac{525}{46189}}(0, 0, 1, 1, 4, 0), \sqrt{\frac{700}{46189}}(1, 0, 1, 1, 3, 0), \sqrt{\frac{750}{46189}}(2, 0, 1, 1, 2, 0),$
	$\sqrt{\frac{700}{46189}}(3, 0, 1, 1, 1, 0), \sqrt{\frac{525}{46189}}(4, 0, 1, 1, 0, 0), \sqrt{\frac{2450}{138567}}(3, 0, 2, 1, 0, 0),$	

Table B.8 (Continued) Normalized pentaquark (q^4 symmetry) spatial wave functions quantum number: $2N + 1 \ 1 \ 0$.

NLM	$C(n_\rho, l_\rho, n_\lambda, l_\lambda, n_\eta, l_\eta)$
$1110_{[31]\eta}$	$\sqrt{\frac{1050}{46189}}(1, 0, 2, 1, 2, 0), \sqrt{\frac{1050}{46189}}(2, 0, 2, 1, 1, 0), \sqrt{\frac{2450}{138567}}(0, 0, 2, 1, 3, 0),$
	$\sqrt{\frac{1050}{46189}}(0, 0, 3, 1, 2, 0), \sqrt{\frac{1260}{46189}}(1, 0, 3, 1, 1, 0), \sqrt{\frac{1050}{46189}}(2, 0, 3, 1, 0, 0),$
	$\sqrt{\frac{105}{4199}}(0, 0, 4, 1, 1, 0), \sqrt{\frac{105}{4199}}(1, 0, 4, 1, 0, 0), \sqrt{\frac{7}{323}}(0, 0, 5, 1, 0, 0)$
	$\sqrt{\frac{21}{4199}}(5, 0, 0, 0, 0, 1), \sqrt{\frac{315}{46189}}(4, 0, 1, 0, 0, 1), \sqrt{\frac{350}{46189}}(3, 0, 2, 0, 0, 1),$
	$\sqrt{\frac{350}{46189}}(2, 0, 3, 0, 0, 1), \sqrt{\frac{315}{46189}}(1, 0, 4, 0, 0, 1), \sqrt{\frac{21}{4199}}(0, 0, 5, 0, 0, 1),$
	$\sqrt{\frac{525}{46189}}(4, 0, 0, 0, 1, 1), \sqrt{\frac{700}{46189}}(1, 0, 3, 0, 1, 1), \sqrt{\frac{750}{46189}}(2, 0, 2, 0, 1, 1),$
	$\sqrt{\frac{700}{46189}}(3, 0, 1, 0, 1, 1), \sqrt{\frac{525}{46189}}(0, 0, 4, 0, 1, 1), \sqrt{\frac{2450}{138567}}(0, 0, 3, 0, 2, 1),$
	$\sqrt{\frac{1050}{46189}}(2, 0, 1, 0, 2, 1), \sqrt{\frac{1050}{46189}}(1, 0, 2, 0, 2, 1), \sqrt{\frac{2450}{138567}}(3, 0, 0, 0, 2, 1),$
	$\sqrt{\frac{1050}{46189}}(2, 0, 0, 0, 3, 1), \sqrt{\frac{1260}{46189}}(1, 0, 1, 0, 3, 1), \sqrt{\frac{1050}{46189}}(0, 0, 2, 0, 3, 1),$
	$\sqrt{\frac{105}{4199}}(1, 0, 0, 0, 4, 1), \sqrt{\frac{105}{4199}}(0, 0, 1, 0, 4, 1), \sqrt{\frac{7}{323}}(0, 0, 0, 0, 5, 1)$

Table B.9 Normalized pentaquark (q^4 symmetry) spatial wave functions quantum number: $2N \ 1 \ 0$.

NLM	$C(n_\rho, l_\rho, n_\lambda, l_\lambda, n_\eta, l_\eta)$
$210_{[211]\rho}$	$(0, 1, 0, 0, 0, 1)$
$210_{[211]\lambda}$	$(0, 0, 0, 1, 0, 1)$
$210_{[211]\eta}$	$(0, 1, 0, 1, 0, 0)$
$410_{[211]\rho}$	$\sqrt{\frac{5}{39}}(0, 1, 0, 0, 1, 1), \frac{1}{\sqrt{13}}(0, 1, 1, 0, 0, 1), \sqrt{\frac{5}{39}}(1, 1, 0, 0, 0, 1)$
$410_{[211]\lambda}$	$\sqrt{\frac{5}{39}}(0, 0, 0, 1, 1, 1), \frac{1}{\sqrt{13}}(1, 0, 0, 1, 0, 1), \sqrt{\frac{5}{39}}(0, 0, 1, 1, 0, 1)$
$410_{[211]\eta}$	$\sqrt{\frac{5}{39}}(0, 1, 1, 1, 0, 0), \frac{1}{\sqrt{13}}(0, 1, 0, 1, 1, 0), \sqrt{\frac{5}{39}}(1, 1, 0, 1, 0, 0)$
$610_{[211]\rho}$	$\sqrt{\frac{7}{117}}(0, 1, 0, 0, 2, 1), \sqrt{\frac{2}{39}}(0, 1, 1, 0, 1, 1), \frac{1}{\sqrt{39}}(0, 1, 2, 0, 0, 1),$ $\sqrt{\frac{10}{117}}(1, 1, 0, 0, 1, 1), \sqrt{\frac{2}{39}}(1, 1, 1, 0, 0, 1), \sqrt{\frac{7}{117}}(2, 1, 0, 0, 0, 1)$

Table B.9 (Continued) Normalized pentaquark (q^4 symmetry) spatial wave functions quantum number: $2N-10$.

NLM	$C(n_\rho, l_\rho, n_\lambda, l_\lambda, n_\eta, l_\eta)$
$610_{[211]\lambda}$	$\sqrt{\frac{7}{117}}(0, 0, 0, 1, 2, 1), \sqrt{\frac{2}{39}}(1, 0, 0, 1, 1, 1), \frac{1}{\sqrt{39}}(2, 0, 0, 1, 0, 1),$ $\sqrt{\frac{10}{117}}(0, 0, 1, 1, 1, 1), \sqrt{\frac{2}{39}}(1, 0, 1, 1, 0, 1), \sqrt{\frac{7}{117}}(0, 0, 2, 1, 0, 1)$
$610_{[211]\eta}$	$\sqrt{\frac{7}{117}}(0, 1, 2, 1, 0, 0), \sqrt{\frac{2}{39}}(0, 1, 1, 1, 1, 0), \frac{1}{\sqrt{39}}(0, 1, 0, 1, 2, 0),$ $\sqrt{\frac{10}{117}}(1, 1, 1, 1, 0, 0), \sqrt{\frac{2}{39}}(1, 1, 0, 1, 1, 0), \sqrt{\frac{7}{117}}(2, 1, 0, 1, 0, 0)$
$810_{[211]\rho}$	$\sqrt{\frac{7}{221}}(0, 1, 0, 0, 3, 1), \sqrt{\frac{7}{221}}(0, 1, 1, 0, 2, 1), \sqrt{\frac{5}{221}}(0, 1, 2, 0, 1, 1),$ $\sqrt{\frac{7}{663}}(0, 1, 3, 0, 0, 1), \sqrt{\frac{35}{663}}(1, 1, 0, 0, 2, 1), \sqrt{\frac{10}{221}}(1, 1, 1, 0, 1, 1),$ $\sqrt{\frac{5}{221}}(1, 1, 2, 0, 0, 1), \sqrt{\frac{35}{663}}(2, 1, 0, 0, 1, 1), \sqrt{\frac{7}{221}}(2, 1, 1, 0, 0, 1),$ $\sqrt{\frac{7}{221}}(3, 1, 0, 0, 0, 1)$
$810_{[211]\lambda}$	$\sqrt{\frac{7}{221}}(0, 0, 0, 1, 3, 1), \sqrt{\frac{7}{221}}(1, 0, 0, 1, 2, 1), \sqrt{\frac{5}{221}}(2, 0, 0, 1, 1, 1),$ $\sqrt{\frac{7}{663}}(3, 0, 0, 1, 0, 1), \sqrt{\frac{35}{663}}(0, 0, 1, 1, 2, 1), \sqrt{\frac{10}{221}}(1, 0, 1, 1, 1, 1),$ $\sqrt{\frac{5}{221}}(2, 0, 1, 1, 0, 1), \sqrt{\frac{35}{663}}(0, 0, 2, 1, 1, 1), \sqrt{\frac{7}{221}}(1, 0, 2, 1, 0, 1),$ $\sqrt{\frac{7}{221}}(0, 0, 3, 1, 0, 1)$
$810_{[211]\eta}$	$\sqrt{\frac{7}{221}}(3, 1, 0, 1, 0, 0), \sqrt{\frac{7}{221}}(2, 1, 0, 1, 1, 0), \sqrt{\frac{5}{221}}(1, 1, 0, 1, 2, 0),$ $\sqrt{\frac{7}{663}}(0, 1, 0, 1, 3, 0), \sqrt{\frac{35}{663}}(2, 1, 1, 1, 0, 0), \sqrt{\frac{10}{221}}(1, 1, 1, 1, 1, 0),$ $\sqrt{\frac{5}{221}}(0, 1, 1, 1, 2, 0), \sqrt{\frac{35}{663}}(1, 1, 2, 1, 0, 0), \sqrt{\frac{7}{221}}(0, 1, 2, 1, 1, 0),$ $\sqrt{\frac{7}{221}}(0, 1, 3, 1, 0, 0)$
$1010_{[211]\rho}$	$\sqrt{\frac{77}{4199}}(0, 1, 0, 0, 4, 1), \sqrt{\frac{84}{4199}}(0, 1, 1, 0, 3, 1), \sqrt{\frac{70}{4199}}(0, 1, 2, 0, 2, 1),$ $\sqrt{\frac{140}{12597}}(0, 1, 3, 0, 1, 1), \sqrt{\frac{21}{4199}}(0, 1, 4, 0, 0, 1), \sqrt{\frac{140}{4199}}(1, 1, 0, 0, 3, 1),$ $\sqrt{\frac{140}{4199}}(1, 1, 1, 0, 2, 1), \frac{10}{\sqrt{4199}}(1, 1, 2, 0, 1, 1), \sqrt{\frac{140}{12597}}(1, 1, 3, 0, 0, 1),$ $\sqrt{\frac{700}{12597}}(2, 1, 0, 0, 2, 1), \sqrt{\frac{140}{4199}}(2, 1, 1, 0, 1, 1), \sqrt{\frac{70}{4199}}(2, 1, 2, 0, 0, 1),$ $\sqrt{\frac{140}{4199}}(3, 1, 0, 0, 1, 1), \sqrt{\frac{84}{4199}}(3, 1, 1, 0, 0, 1), \sqrt{\frac{77}{4199}}(4, 1, 0, 0, 0, 1)$
$1010_{[211]\lambda}$	$\sqrt{\frac{77}{4199}}(0, 0, 0, 1, 4, 1), \sqrt{\frac{84}{4199}}(1, 0, 0, 1, 3, 1), \sqrt{\frac{70}{4199}}(2, 0, 0, 1, 2, 1),$

Table B.9 (Continued) Normalized pentaquark (q^4 symmetry) spatial wave functions quantum number: $2N-10$.

NLM	$C(n_\rho, l_\rho, n_\lambda, l_\lambda, n_\eta, l_\eta)$
1010 _{[211]η}	$\sqrt{\frac{140}{12597}}(3, 0, 0, 1, 1, 1), \sqrt{\frac{21}{4199}}(4, 0, 0, 1, 0, 1), \sqrt{\frac{140}{4199}}(0, 0, 1, 1, 3, 1),$
	$\sqrt{\frac{140}{4199}}(1, 0, 1, 1, 2, 1), \sqrt{\frac{10}{4199}}(2, 0, 1, 1, 1, 1), \sqrt{\frac{140}{12597}}(3, 0, 1, 1, 0, 1),$
	$\sqrt{\frac{700}{12597}}(0, 0, 2, 1, 2, 1), \sqrt{\frac{140}{4199}}(1, 0, 2, 1, 1, 1), \sqrt{\frac{70}{4199}}(2, 0, 2, 1, 0, 1),$
	$\sqrt{\frac{140}{4199}}(0, 0, 3, 1, 1, 1), \sqrt{\frac{84}{4199}}(1, 0, 3, 1, 0, 1), \sqrt{\frac{77}{4199}}(0, 0, 4, 1, 0, 1)$
	$\sqrt{\frac{77}{4199}}(0, 1, 4, 1, 0, 0), \sqrt{\frac{84}{4199}}(0, 1, 3, 1, 1, 0), \sqrt{\frac{70}{4199}}(0, 1, 2, 1, 2, 0),$
	$\sqrt{\frac{140}{12597}}(0, 1, 1, 1, 3, 0), \sqrt{\frac{21}{4199}}(0, 1, 0, 1, 4, 0), \sqrt{\frac{140}{4199}}(1, 1, 3, 1, 0, 0),$
	$\sqrt{\frac{140}{4199}}(1, 1, 2, 1, 1, 0), \sqrt{\frac{10}{4199}}(1, 1, 1, 1, 2, 0), \sqrt{\frac{140}{12597}}(1, 1, 0, 1, 3, 0),$
	$\sqrt{\frac{700}{12597}}(2, 1, 2, 1, 0, 0), \sqrt{\frac{140}{4199}}(2, 1, 1, 1, 1, 0), \sqrt{\frac{70}{4199}}(2, 1, 0, 1, 2, 0),$
	$\sqrt{\frac{140}{4199}}(3, 1, 1, 1, 0, 0), \sqrt{\frac{84}{4199}}(3, 1, 0, 1, 1, 0), \sqrt{\frac{77}{4199}}(4, 1, 0, 1, 0, 0)$



APPENDIX C

PENTAQUARK WAVE FUNCTION

Example 1: in the q^4 , we can construct the fully antisymmetric wave function of the spatial-spin-flavor-color part $[1111]_{OSFC}$ consisting of 2 wave functions spatial-spin-flavor $[31]_{OSF}$ and color $[211]_C$ as

$$\begin{aligned}
 \psi_{[1111]}^{OSFC} &= \sum_{i,j=\{\rho,\lambda,\eta\}} C_{[31]_i[211]_j}^{[1111]} \psi_{[31]_i}^{OSF} \psi_{[211]_j}^C \\
 &= \frac{1}{\sqrt{3}} \left(\psi_{[31]_\rho}^{OSF} \psi_{[211]_\lambda}^C - \psi_{[31]_\lambda}^{OSF} \psi_{[211]_\rho}^C + \psi_{[31]_\eta}^{OSF} \psi_{[211]_\eta}^C \right) \quad (C.1)
 \end{aligned}$$

where we use the coefficients $C_{[31]_i[211]_j}^{[1111]}$ from the Table D.1.

Example 2: we will construct a $\frac{1}{2}^-$ pentaquark for $[31]_{FS}[22]_F[31]_S$ configuration. From Eq. (2.5), we will get

$$\Psi_{\text{total}}^{q^4} = \sum_{i,j,w,x,y,z=\{S,A,\rho,\lambda,\eta\}} C_{[31]_i[211]_j}^{[1111]} C_{[4]_{[31]_x}}^{[31]_i} C_{[31]_y[22]_z}^{[31]_x} \psi_{[4]}^O \psi_{[211]_j}^C \psi_{[31]_y}^S \psi_{[22]_z}^F. \quad (C.2)$$

APPENDIX D

Coefficient $C_{[X]_x[Y]_y}^{[Z]_z}$

Table D.1 The $C_{[31]_i[211]_j}^{[1111]}$ coefficients.

$[1111]$	$[211]_j$		
	λ	ρ	η
$[31]_i$	λ	$-\frac{1}{\sqrt{3}}$	
	ρ	$\frac{1}{\sqrt{3}}$	
	η		$\frac{1}{\sqrt{3}}$

Table D.2 The $C_{[4][31]_j}^{[31]_k}$ coefficients for λ -type, ρ -type, and η -type, respectively.

$[31]_\lambda$	$[31]_j$			$[31]_\rho$	$[31]_j$			$[31]_\eta$	$[31]_j$		
	λ	ρ	η		λ	ρ	η		λ	ρ	η
$[4]$	S	1		$[4]$	S	1		$[4]$	S	1	

Table D.3 The $C_{[31]_i[22]_j}^{[31]_k}$ coefficients for λ -type, ρ -type, and η -type, respectively.

$[31]_\lambda$	$[22]_j$			$[31]_\rho$	$[22]_j$			$[31]_\eta$	$[22]_j$		
	λ	$-\frac{1}{2}$	ρ		λ	ρ	$\frac{1}{2}$		λ	$-\frac{1}{\sqrt{2}}$	ρ
$[31]_i$	ρ	$\frac{1}{2}$		$[31]_i$	ρ	$\frac{1}{2}$		$[31]_i$	ρ	$-\frac{1}{\sqrt{2}}$	
	η	$-\frac{1}{\sqrt{2}}$			η	$-\frac{1}{\sqrt{2}}$			η		

Table D.4 The $C_{[31]_i[31]_j}^{[31]_k}$ coefficients for λ -type, ρ -type, and η -type, respectively.

$[31]_\lambda$	$[31]_j$		
	λ	ρ	η
$[31]_i$	λ	$-\frac{1}{\sqrt{3}}$	$\frac{1}{\sqrt{3}}$
	ρ		$\frac{1}{\sqrt{6}}$
	η		$\frac{1}{\sqrt{6}}$

$[31]_\rho$	$[31]_j$		
	λ	ρ	η
$[31]_i$	λ	$\frac{1}{\sqrt{3}}$	
	ρ	$\frac{1}{\sqrt{3}}$	$\frac{1}{\sqrt{6}}$
	η	$\frac{1}{\sqrt{6}}$	

$[31]_\eta$	$[31]_j$		
	λ	ρ	η
$[31]_i$	λ	$\frac{1}{\sqrt{6}}$	
	ρ	$\frac{1}{\sqrt{6}}$	
	η		$-\frac{2}{\sqrt{6}}$

Table D.5 The $C_{[22]_i[31]_j}^{[31]_k}$ coefficients for λ -type, ρ -type, and η -type, respectively.

$[31]_\lambda$	$[31]_j$		
	λ	ρ	η
$[22]_i$	λ	$-\frac{1}{\sqrt{3}}$	$\frac{1}{\sqrt{3}}$
	ρ		$\frac{1}{\sqrt{6}}$

$[31]_\lambda$	$[31]_j$		
	λ	ρ	η
$[22]_i$	λ	$-\frac{1}{\sqrt{3}}$	$\frac{1}{\sqrt{3}}$
	ρ		$\frac{1}{\sqrt{6}}$

$[31]_\lambda$	$[31]_j$		
	λ	ρ	η
$[22]_i$	λ	$-\frac{1}{\sqrt{3}}$	$\frac{1}{\sqrt{3}}$
	ρ		$\frac{1}{\sqrt{6}}$

Table D.6 The $C_{[31]_i[4]}^{[31]_k}$ coefficients for λ -type, ρ -type, and η -type, respectively.

$[31]_\lambda$	$\frac{[4]}{S}$	
	λ	1
$[31]_i$	ρ	
	η	

$[31]_\rho$	$\frac{[4]}{S}$	
	λ	1
$[31]_i$	ρ	1
	η	

$[31]_\eta$	$\frac{[4]}{S}$	
	λ	1
$[31]_i$	ρ	
	η	1

APPENDIX E

SPIN WAVE FUNCTION OF PENTAQUARK

The list of explicit form of spin and flavor wave functions are shown in Eq.

(E.1)

$$\begin{aligned}
 \psi_{[4]}^S(2, s_{q^4}) &\rightarrow \left| \begin{array}{|c|c|c|c|} \hline 1 & 2 & 3 & 4 \\ \hline \end{array}, s_1 s_2 s_3 s_4 \right\rangle \\
 &\rightarrow [[[[S_1 \otimes S_2]_{1, s_{12}} \otimes S_3]_{\frac{3}{2}, s_{123}} \otimes S_4]_{2, s_{q^4}} \\
 &= \sum_{s_1, s_2, s_3, s_4, s_{12}, s_{123}} C\left(\frac{1}{2}, s_1; \frac{1}{2}, s_2; 1, s_{12}\right) C\left(1, s_{12}; \frac{1}{2}, s_3; \frac{3}{2}, s_{123}\right) \\
 &\quad \times C\left(\frac{3}{2}, s_{123}; \frac{1}{2}, s_4; 2, s_{q^4}\right) \chi_{s_1} \chi_{s_2} \chi_{s_3} \chi_{s_4} \\
 \psi_{[31]_\lambda}^S(1, s_{q^4}) &\rightarrow \left| \begin{array}{|c|c|c|} \hline 1 & 2 & 4 \\ \hline 3 & & \\ \hline \end{array}, s_1 s_2 s_3 s_4 \right\rangle \\
 &\rightarrow [[[[S_1 \otimes S_2]_{1, s_{12}} \otimes S_3]_{\frac{1}{2}, s_{123}} \otimes S_4]_{1, s_{q^4}} \\
 &= \sum_{s_1, s_2, s_3, s_4, s_{12}, s_{123}} C\left(\frac{1}{2}, s_1; \frac{1}{2}, s_2; 1, s_{12}\right) C\left(1, s_{12}; \frac{1}{2}, s_3; \frac{1}{2}, s_{123}\right) \\
 &\quad \times C\left(\frac{1}{2}, s_{123}; \frac{1}{2}, s_4; 1, s_{q^4}\right) \chi_{s_1} \chi_{s_2} \chi_{s_3} \chi_{s_4} \\
 \psi_{[31]_\rho}^S(1, s_{q^4}) &\rightarrow \left| \begin{array}{|c|c|c|} \hline 1 & 3 & 4 \\ \hline 2 & & \\ \hline \end{array}, s_1 s_2 s_3 s_4 \right\rangle \\
 &\rightarrow [[[[S_1 \otimes S_2]_{0, s_{12}} \otimes S_3]_{\frac{1}{2}, s_{123}} \otimes S_4]_{1, s_{q^4}}
 \end{aligned}$$

$$\begin{aligned}
&= \sum_{s_1, s_2, s_3, s_4, s_{12}, s_{123}} C\left(\frac{1}{2}, s_1; \frac{1}{2}, s_2; 0, s_{12}\right) C\left(1, s_{12}; \frac{1}{2}, s_3; \frac{1}{2}, s_{123}\right) \\
&\quad \times C\left(\frac{1}{2}, s_{123}; \frac{1}{2}, s_4; 1, s_{q^4}\right) \chi_{s_1} \chi_{s_2} \chi_{s_3} \chi_{s_4} \\
\psi_{[31]_n}^S(1, s_{q^4}) &\rightarrow \left| \begin{array}{|c|c|c|} \hline 1 & 2 & 3 \\ \hline 4 & & \\ \hline \end{array}, s_1 s_2 s_3 s_4 \right\rangle \\
&\rightarrow [[[[S_1 \otimes S_2]_{1, s_{12}} \otimes S_3]_{\frac{3}{2}, s_{123}} \otimes S_4]_{1, s_{q^4}} \\
&= \sum_{s_1, s_2, s_3, s_4, s_{12}, s_{123}} C\left(\frac{1}{2}, s_1; \frac{1}{2}, s_2; 1, s_{12}\right) C\left(1, s_{12}; \frac{1}{2}, s_3; \frac{3}{2}, s_{123}\right) \\
&\quad \times C\left(\frac{3}{2}, s_{123}; \frac{1}{2}, s_4; 1, s_{q^4}\right) \chi_{s_1} \chi_{s_2} \chi_{s_3} \chi_{s_4} \\
\psi_{[22]_\lambda}^S(0, 0) &\rightarrow \left| \begin{array}{|c|c|} \hline 1 & 2 \\ \hline 3 & 4 \\ \hline \end{array}, s_1 s_2 s_3 s_4 \right\rangle \\
&\rightarrow [[[[S_1 \otimes S_2]_{1, s_{12}} \otimes S_3]_{\frac{1}{2}, s_{123}} \otimes S_4]_{0,0} \\
&= \sum_{s_1, s_2, s_3, s_4, s_{12}, s_{123}} C\left(\frac{1}{2}, s_1; \frac{1}{2}, s_2; 1, s_{12}\right) C\left(1, s_{12}; \frac{1}{2}, s_3; \frac{1}{2}, s_{123}\right) \\
&\quad \times C\left(\frac{1}{2}, s_{123}; \frac{1}{2}, s_4; 0, 0\right) \chi_{s_1} \chi_{s_2} \chi_{s_3} \chi_{s_4} \\
\psi_{[22]_\rho}^S(0, 0) &\rightarrow \left| \begin{array}{|c|c|} \hline 1 & 3 \\ \hline 2 & 4 \\ \hline \end{array}, s_1 s_2 s_3 s_4 \right\rangle \\
&\rightarrow [[[[S_1 \otimes S_2]_{0, s_{12}} \otimes S_3]_{\frac{1}{2}, s_{123}} \otimes S_4]_{0,0} \\
&= \sum_{s_1, s_2, s_3, s_4, s_{123}} C\left(\frac{1}{2}, s_1; \frac{1}{2}, s_2; 0, 0\right) C\left(0, 0; \frac{1}{2}, s_3; \frac{1}{2}, s_{123}\right) \\
&\quad \times C\left(\frac{1}{2}, s_{123}; \frac{1}{2}, s_4; 0, 0\right) \chi_{s_1} \chi_{s_2} \chi_{s_3} \chi_{s_4} \tag{E.1}
\end{aligned}$$

where C is the Clebsch-Gordan coefficients.

APPENDIX F

QUARK CORE RADIUS

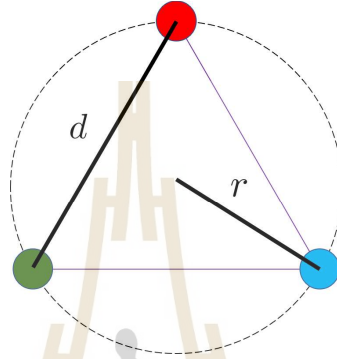


Figure F.1 Quark core radius.

A quark core radius is the average of the distance from the center of baryon mass to the position of quarks. In the Fig. F.1, the quark core radius (r) can be defined by the relation between the quark core radius and the average of distance between 2 quarks (d) which be written as

$$\begin{aligned}
 r &= \frac{1}{\sqrt{3}} d \\
 \langle r^2 \rangle &= \frac{1}{\sqrt{3}} \left(\frac{1}{3} \langle \Psi | ((r_1 - r_2)^2 + (r_1 - r_3)^2 + (r_2 - r_3)^2) | \Psi \rangle \right) \\
 &= \frac{1}{\sqrt{3}} \langle \Psi | (\lambda^2 + \rho^2) | \Psi \rangle
 \end{aligned} \tag{F.1}$$

where r_i are the position of the quark i .

CURRICULUM VITAE

NAME: Attaphon Kaewsnod **GENDER:** Male

NATIONALITY: Thai **DATE OF BIRTH:** June 10, 1988

EDUCATIONS:

- M.Sc. Department of Physics, Faculty of Science, Burapha University, Thailand, 2014.
- B.Sc. Department of Physics, Faculty of Science, Burapha University, Thailand, 2011.

PUBLICATIONS

- [1] S. Srisuphaphon, A. Kaewsnod, A. Limphirat, K. Khosonthongkee and Y. Yan, “**Role of pentaquark components in ϕ meson production proton-antiproton annihilation reactions**”, Phys. Rev. C **93**, no.2, 025201 (2016)
- [2] K. Xu, A. Kaewsnod, X. Liu, S. Srisuphaphon, A. Limphirat and Y. Yan, “**Complete basis for the pentaquark wave function in a group theory approach**”, Phys. Rev. C **100**, no.6, 065207 (2019)
- [3] K. Xu, A. Kaewsnod, Z. Zhao, X. Liu, S. Srisuphaphon, A. Limphirat and Y. Yan, “**Pentaquark components in low-lying baryon resonances**”, Phys. Rev. D **101**, no.7, 076025 (2020)